

*Experimental Investigation of the Mg-Al-Ca Ternary Phase  
Diagram*

Xiao Zhao Wang

A Thesis

in

the Department

of

Mechanical and Industrial Engineering

Presented in Partial Fulfillment of the Requirements  
for the Degree of Master of Applied Science (Mechanical Engineering) at  
Concordia University  
Montreal, Quebec, Canada

October 2005

© Xiao Zhao Wang, 2005

---



Library and  
Archives Canada

Bibliothèque et  
Archives Canada

Published Heritage  
Branch

Direction du  
Patrimoine de l'édition

395 Wellington Street  
Ottawa ON K1A 0N4  
Canada

395, rue Wellington  
Ottawa ON K1A 0N4  
Canada

*Your file* *Votre référence*  
*ISBN: 0-494-14315-0*  
*Our file* *Notre référence*  
*ISBN: 0-494-14315-0*

#### NOTICE:

The author has granted a non-exclusive license allowing Library and Archives Canada to reproduce, publish, archive, preserve, conserve, communicate to the public by telecommunication or on the Internet, loan, distribute and sell theses worldwide, for commercial or non-commercial purposes, in microform, paper, electronic and/or any other formats.

The author retains copyright ownership and moral rights in this thesis. Neither the thesis nor substantial extracts from it may be printed or otherwise reproduced without the author's permission.

#### AVIS:

L'auteur a accordé une licence non exclusive permettant à la Bibliothèque et Archives Canada de reproduire, publier, archiver, sauvegarder, conserver, transmettre au public par télécommunication ou par l'Internet, prêter, distribuer et vendre des thèses partout dans le monde, à des fins commerciales ou autres, sur support microforme, papier, électronique et/ou autres formats.

L'auteur conserve la propriété du droit d'auteur et des droits moraux qui protègent cette thèse. Ni la thèse ni des extraits substantiels de celle-ci ne doivent être imprimés ou autrement reproduits sans son autorisation.

---

In compliance with the Canadian Privacy Act some supporting forms may have been removed from this thesis.

Conformément à la loi canadienne sur la protection de la vie privée, quelques formulaires secondaires ont été enlevés de cette thèse.

While these forms may be included in the document page count, their removal does not represent any loss of content from the thesis.

Bien que ces formulaires aient inclus dans la pagination, il n'y aura aucun contenu manquant.

  
**Canada**

# ABSTRACT

## Experimental Investigation of the Mg-Al-Ca Ternary Phase Diagram

**Xiao Zhao Wang**

This work focuses on the experimental investigation of the ternary Mg-Al-Ca system using Differential Scanning Calorimetry (DSC), X-ray Diffraction (XRD) and metallographic techniques. Twenty one samples were chosen in the critical regions with the guidance of the phase diagrams developed by thermodynamic modeling.

The DSC has permitted real time measurement of the temperature and enthalpy of the phase transformations. The experimental results were compared with thermodynamic calculations using the phase assemblage diagrams and vertical sections.

The thermodynamic calculations are consistent with the experimental results in some samples, especially in the solidus temperature, whereas discrepancy was observed in several cases especially in the liquidus phase transformation temperature. This suggests that Mg-Al-Ca system should be reoptimised considering the new experimental findings. Nevertheless, the phases that were identified with the XRD and metallographic techniques show agreement with thermodynamic modeling. One of the invariant transformations predicted by thermodynamic modeling was verified experimentally and found to occur at 512°C and the composition is close to 10.8 at.% Ca 79.5 at.% Mg and 9.7 at.% Al.

In this study, a new phase region was found close to the Mg-Al side and a new ternary solid solution ( $\text{Mg}_2\text{Ca}$ ) was confirmed.

## ACKNOWLEDGEMENTS

I would like to thank everyone whose assistance has made this work possible. First, I would like to thank Dr. Medraj, my supervisor who offered me an opportunity to be a graduate student at Concordia University, and conduct research under his guidance. His advice and encouragement have been invaluable, as is the environment he provided to make this research possible.

I would like to thank Dr. Essadiqi of CANMET-MTL, Ottawa and Dr. Muntasar of Department of Chemistry, Concordia University for their kind help in conducting the experimental work

I would also like to thank the members of Dr. Medraj's research group, particularly MD Anwar Parvez for his kind help and cooperation. In addition, the author would like to acknowledge the financial assistance provided by the Natural Science and Engineering Research Council (NSERC) that made this research possible.

I would like to thank my wife, Xiao Feng Zhang, for her invaluable support, and for her constant love without which this thesis would not have been completed.

# TABLE OF CONTENTS

LIST OF FIGURES .....	vii
LIST OF TABLES.....	xiii
LIST OF ABBREVIATIONS.....	xv
CHAPTER 1.....	1
Introduction.....	1
1.1 Introduction.....	1
1.2 Thesis organization.....	3
CHAPTER 2.....	4
Literature review.....	4
2.1 Experimental Survey and Thermal Analysis Principles.....	4
2.1.1 Experimental Survey.....	4
2.1.2 DSC principle.....	6
2.1.3 Determination of phase diagram using DSC curve.....	8
2.2 Ternary system Mg-Al-Ca .....	10
2.3 Mg-Al Phase Diagram.....	16
2.4 Mg-Ca Phase Diagram.....	19
2.5 Al-Ca phase diagram.....	20
CHAPTER 3.....	23
The Objectives of this Study.....	23
CHAPTER 4.....	24
Experimental Procedures.....	24
4.1 Alloy Preparation.....	24
4.2 Differential Scanning Calorimetry.....	27
4.2.1 Procedure and Analysis.....	27
4.2.2 Calibration of the DSC instrument.....	30
4.3 X-ray powder diffraction.....	30
4.4 Metallographic technique .....	33
CHAPTER 5.....	34
Result and Discussions.....	34

5.1 Thermodynamic calculations.....	35
5.2 Samples in the Mg- Al <sub>2</sub> Ca - $\gamma$ phase field.....	35
5.2.1 Results and discussion of sample 1.....	35
5.2.2 New ternary phase observed in samples 2, 3 and 4.....	42
5.2.3 Results and discussion of sample 5.....	52
5.3 Samples in Mg-Al <sub>2</sub> Ca-Mg <sub>2</sub> Ca field.....	56
5.3.1 Samples 6, 7, 8 and 9 results and discussion.....	56
5.3.2 Investigation of the eutectic point in the Mg-rich corner.....	69
5.4 Samples in Al <sub>2</sub> Ca- $\gamma$ -Al triangle.....	84
5.5 Samples in Mg <sub>2</sub> Ca-Al <sub>2</sub> Ca-Al <sub>14</sub> Ca <sub>13</sub> phase field.....	94
5.6 Sample in Mg <sub>2</sub> Ca-Al <sub>14</sub> Ca <sub>13</sub> -Al <sub>3</sub> Ca <sub>8</sub> phase field.....	101
CHAPTER 6.....	104
Summary, Contributions and Suggestions.....	104
6.1 Summary.....	104
6.2 Contribution to the knowledge.....	106
6.3 Suggestion for future work.....	107
REFERENCES.....	109
APPENDIX A.....	117
XRD Patterns Simulation.....	117
APPENDIX B.....	127
Metallographic technique.....	127

# LIST OF FIGURES

Figure 2-1	The principle of power compensated Differential Scanning Calorimeter Analysis [26]	7
Figure 2-2	The principle of heat flux Differential Scanning Calorimeter Analysis [26]	7
Figure 2-3	Different principle of DSC signal detection [26]	8
Figure 2-4	Phase diagram for a binary system of immiscible solids and their completely miscible liquids [26]	9
Figure 2-5	DSC curve for the slow cooling of a molten mixture of composition $X_a$ initially at temperature $T_a$ [26]	9
Figure 2-6	Projection of the liquidus surface of the magnesium-rich region of the Mg-Al-Ca system [17]	11
Figure 2-7	Vertical section of the Mg-Al-Ca system at 4.5 wt% Al	12
Figure 2-8	Vertical section of the Mg-Al-Ca system at 8.5 wt% Al	12
Figure 2-9	Vertical section of the Mg-Al-Ca system at 16 wt %Al	13
Figure 2-10	The calculated liquidus surface including isotherms and four DTA samples	14
Figure 2-11	The calculated vertical section $\text{CaMg}_2\text{-Al}_2\text{Ca}$ with DTA signals from the alloy $\text{Al}_{36.67}\text{Ca}_{33.33}\text{Mg}_{30}$	14
Figure 2-12	The calculated vertical section at constant 20 at% Ca with DTA signals from alloy $\text{Al}_{20}\text{Ca}_{20}\text{Mg}_{60}$	15
Figure 2-13	The calculated vertical section at constant 15 at% Mg with DTA signals from alloy $\text{Al}_{15}\text{Ca}_{70}\text{Mg}_{15}$ and $\text{Al}_{45}\text{Ca}_{40}\text{Mg}_{15}$	15
Figure 2-14	The Al-Mg phase diagram from Murray [43]	17
Figure 2-15	The Al-Mg phase diagram from Saunders work [44]	18
Figure 2-16	The calculated and Assesses Mg-Ca Phase Diagram with Experimental points [52]	20
Figure 2-17	The calculated Al-Ca phase diagram and experimental DTA data	21
Figure 2-18	The calculated Al-Ca phase diagram using random solution model, compared with experimental data	22
Figure 4-1	The distribution of investigated compositions in mole fraction	25
Figure 4-2	Setaram Differential Scanning Calorimeter	28
Figure 4-3	The thermal cycles used during DSC experiments	28

Figure 4-4	Demonstration of DSC spectra with sample 3	29
Figure 4-5	The DSC spectrum of pure Mg	30
Figure 4-6	X-ray Diffractometer configurations	31
Figure 4-7	The simulated XRD pattern for $Al_2Ca$	32
Figure 5-1	Isothermal section at 25°C showing the studied sample	34
Figure 5-2	DSC spectra of sample 1 (20.43/44.79/34.78 Ca/Mg/Al wt%)	36
Figure 5-3	The calculated vertical section at constant 35.4 at.% Al with DSC signals from cooling curve of sample 1	37
Figure 5-5	Phase assemblage diagram of sample 1 (20.43/44.79/34.78 Ca/Mg/Al wt%)	38
Figure 5-5	XRD pattern of sample 1 (20.43/44.79/34.78 Ca/Mg/Al wt%)	40
Figure 5-6	Micrograph of sample 1 1000X (20.43/44.79/34.78 Ca/Mg/Al wt%)	41
Figure 5-7	DSC spectra of sample 2 (3.59/78.84/17.57 Ca/Mg/Al wt%)	43
Figure 5-8	Phase assemblage diagram of sample 2 (3.59/78.84/17.57 Ca/Mg/Al wt%)	44
Figure 5-9	The calculated vertical section at constant 2.3 at% Ca with DSC signals from cooling curve of sample 2	44
Figure 5-10	DSC spectra of sample 3 (2.50/69.79/27.71 Ca/Mg/Al wt%)	45
Figure 5-11	Phase assemblage of sample 3 (2.50/69.79/27.71 Ca/Mg/Al wt%)	46
Figure 5-12	The calculated vertical section at constant 1.6 at.% Ca with DSC signals from cooling curve of sample 3	47
Figure 5-13	DSC spectra of sample 4 (7.09/72.16/20.75 Ca/Mg/Al wt%)	47
Figure 5-14	Phase assemblage of sample 4 (7.09/72.16/20.75 Ca/Mg/Al wt%)	48
Figure 5-15	The calculated vertical section at constant 7.09 wt% Ca with DSC signals from cooling curve of sample 4	48
Figure 5-16	XRD pattern of sample 2 (3.59/78.84/17.57 Ca/Mg/Al wt%)	49
Figure 5-17	XRD pattern of sample 3 (2.50/69.79/27.71 Ca/Mg/Al wt%)	49
Figure 5-18	Micrograph of sample 2, 500x (3.59/78.84/17.57 Ca/Mg/Al wt%)	50
Figure 5-19	Micrograph of sample 3, 500X (2.50/69.79/27.71 Ca/Mg/Al wt%)	50
Figure 5-20	XRD pattern of sample 4 (7.09/72.16/20.75 Ca/Mg/Al wt%)	52
Figure 5-21	Optical micrograph of sample 4 1000X (7.09/72.16/20.75	52



	Ca/Mg/Al wt%)	
Figure 5-22	DSC spectrum of sample 5 (2.66/92.17/5.17 Ca/Mg/Al wt%)	53
Figure 5-23	Phase assemblage of sample 5 (2.66/92.17/5.17 Ca/Mg/Al wt%)	53
Figure 5-24	The calculated vertical section at constant 1.7at.% Ca with DSC signals from cooling curve of sample 5	54
Figure 5-25	XRD pattern of Sample 5 (2.66/92.17/5.17 Ca/Mg/Al wt%)	54
Figure 5-26	Optical micrograph of sample 5, 500X (2.66/92.17/5.17 Ca/Mg/Al wt%)	55
Figure 5-27	XRD pattern of sample 6 (32.68/36.30/31.02 Ca/Mg/Al wt%)	57
Figure 5-28	Optical microscope of sample 6, 500X (32.68/36.30/31.02 Ca/Mg/Al wt%)	57
Figure 5-29	Phase assemblage of sample 6 (32.68/36.30/31.02 Ca/Mg/Al wt%)	58
Figure 5-30	Optical micrograph of sample from Gröbner's work	58
Figure 5-31	XRD pattern of sample 7(35.62/58.07/6.30 Ca/Mg/Al wt%)	59
Figure 5-32	Optical micrograph of sample 7, 1000x (35.62/58.07/6.30 Ca/Mg/Al wt%)	60
Figure 5-33	Phase assemblage of sample 7 (35.62/58.07/6.30 Ca/Mg/Al wt%)	60
Figure 5-34	XRD pattern of sample 8 (26.16/52.30/21.54 Ca/Mg/Al wt%)	61
Figure 5-35	Optical micrograph of sample 8, 500X (26.16/52.30/21.54 Ca/Mg/Al wt%)	62
Figure 5-36	Phase assemblage of sample 8 (26.2/52.3/21.5 Ca/Mg/Al wt%)	62
Figure 5-37	DSC spectra of sample 6 (32.68/36.30/31.02 Ca/Mg/Al wt%)	63
Figure 5-38	DSC spectra of sample 7(35.62/58.07/6.30 Ca/Mg/Al wt%)	64
Figure 5-39	DSC spectra of sample 8 (26.16/52.30/21.54 Ca/Mg/Al wt%)	64
Figure 5-40	The calculated vertical section at constant 25.3 at.% Ca with DSC signals from cooling curve of samples 7 (LH) and 6 (RH)	65
Figure 5-41	The calculated vertical section at constant 18.1 at% Ca with DSC signals from cooling curve of sample 8	66
Figure 5-42	XRD pattern of sample 9 (42.32/42.29/15.39 Ca/Mg/Al wt%)	67
Figure 5-43	Phase assemblage of sample 9 (42.32/42.29/15.39 Ca/Mg/Al wt%)	67
Figure 5-44	DSC spectrum of sample 9 (42.32/42.29/15.39 Ca/Mg/Al wt%)	68
Figure 5-45	The calculated vertical section at constant 16.9 at% Al with DSC signals from cooling curve of sample 9	68

Figure 5-46	Phase assemblage of sample 10 (16.44/73.61/9.95 Ca/Mg/Al wt%)	69
Figure 5-47	DSC spectra of sample 10 (16.44/73.61/9.95 Ca/Mg/Al wt%)	70
Figure 5-48	The calculated vertical section at constant 9.9 wt% Ca with DSC signals from cooling curve of sample 10 and sample 11	70
Figure 5-49	Optical micrograph of sample 10, 1000X (16.44/73.61/9.95 Ca/Mg/Al wt%)	71
Figure 5-50	XRD pattern of sample 10 (16.44/73.61/9.95 Ca/Mg/Al wt%)	71
Figure 5-51	XRD pattern of sample 11 (12.65/77.46/9.89 Ca/Mg/Al wt%)	73
Figure 5-52	Phase assemblage of sample 11 (12.65/77.46/9.89 Ca/Mg/Al wt%)	73
Figure 5-53	Optical microscope of sample 11 1000X (12.65/77.46/9.89 Ca/Mg/Al wt%)	74
Figure 5-54	(Mg) dendrite of sample 11 100X (12.65/77.46/9.89 Ca/Mg/Al wt%)	74
Figure 5-55	The calculated vertical section at constant 82 at% Mg with DSC signals from cooling curve of sample 11, 13 and 2	75
Figure 5-56	DSC spectra of sample 11	75
Figure 5-57	XRD pattern of sample 12 (19.32/62.65/18.04 Ca/Mg/Al wt%)	77
Figure 5-58	Phase assemblage of sample 12 (19.32/62.65/18.04 Ca/Mg/Al wt%)	78
Figure 5-59	Optical microscope of sample 12, 500X (19.32/62.65/18.04 Ca/Mg/Al wt%)	78
Figure 5-60	Optical microscope of sample 12, 1000X (19.32/62.65/18.04 Ca/Mg/Al wt%)	79
Figure 5-61	DSC spectra of sample 12 (19.32/62.65/18.04 Ca/Mg/Al wt%)	79
Figure 5-62	The calculated vertical section at constant 69 at% Mg with DSC signals from cooling curve of sample 7 and 12	80
Figure 5-63	XRD pattern of sample 13 (21.69/75.38/2.94 Ca/Mg/Al wt%)	82
Figure 5-64	Phase Assemblage of sample 13 (21.69/75.38/2.94 Ca/Mg/Al wt%)	82
Figure 5-65	Optical microscope of sample 13, 1000X (21.69/75.38/2.94 Ca/Mg/Al wt%)	83
Figure 5-66	DSC spectra of sample 13 (21.69/75.38/2.94 Ca/Mg/Al wt%)	83
Figure 5-67	XRD pattern of sample 14 (19.12/7.91/72.97 Ca/Mg/Al wt%)	85
Figure 5-68	XRD pattern of sample 15 (11.67/22.04/66.29 Ca/Mg/Al wt%)	85

Figure 5-69	Phase assemblage of sample 14 (19.12/7.91/72.97 Ca/Mg/Al wt%)	86
Figure 5-70	Phase assemblage of sample 15 (11.67/22.04/66.29 Ca/Mg/Al wt%)	86
Figure 5-71	DSC spectra of sample 14 (19.12/7.91/72.97 Ca/Mg/Al wt%)	87
Figure 5-72	DSC spectra of sample 15 (11.67/22.04/66.29 Ca/Mg/Al wt%)	87
Figure 5-73	The calculated vertical section at constant 19.1 wt% Ca with DSC signals from cooling curve of sample 14	88
Figure 5-74	The calculated vertical section at constant 8 at% Ca with DSC signals from cooling curve of sample 15	88
Figure 5-75	DSC spectra of sample 16 (15.68/33.28/51.04 Ca/Mg/Al wt%)	90
Figure 5-76	The calculated vertical section at constant 38.5 at% Mg with DSC signals from cooling curve of sample 16	90
Figure 5-77	XRD pattern of sample 16 (15.68/33.28/51.04 Ca/Mg/Al wt%)	91
Figure 5-78	Phase assemblage of sample 16 (15.68/33.28/51.04 Ca/Mg/Al wt%)	91
Figure 5-79	XRD pattern of sample 17 (22.81/15.31/61.88 Ca/Mg/Al wt%)	92
Figure 5-80	Phase assemblage diagram of sample 17 (22.81/15.31/61.88 Ca/Mg/Al wt%)	92
Figure 5-81	DSC spectra of sample 17 (22.81/15.31/61.88 Ca/Mg/Al wt%)	93
Figure 5-82	Calculated vertical section at constant 18 at% Mg with DSC signals from cooling curve of sample 17	93
Figure 5-83	XRD pattern of sample 18 (44.30/23.76/31.94 Ca/Mg/Al wt%)	95
Figure 5-84	XRD pattern of sample 19 (46.73/13.00/40.27 Ca/Mg/Al wt%)	95
Figure 5-85	XRD pattern of sample 20 (47.47/22.42/30.11 Ca/Mg/Al wt%)	96
Figure 5-86	Phase assemblage of sample 18 (44.30/23.76/31.94 Ca/Mg/Al wt%)	96
Figure 5-87	Phase assemblage of sample 19 (46.73/13.00/40.27 Ca/Mg/Al wt%)	97
Figure 5-88	Phase assemblage of sample 20 (47.47/22.42/30.11 Ca/Mg/Al wt%)	97
Figure 5-89	DSC spectra of sample 20 (47.47/22.42/30.11 Ca/Mg/Al wt%)	98
Figure 5-90	DSC spectra of sample 18 (44.30/23.76/31.94 Ca/Mg/Al wt%)	98
Figure 5-91	DSC spectra of sample 19 (46.73/13.00/40.27 Ca/Mg/Al wt%)	99
Figure 5-92	The calculated vertical section at constant 36.5 at% Ca with DSC signals from cooling curve of sample 19 and 20	99

Figure 5-93	The calculated vertical section at constant 31.9 wt% Al with the DSC signals from cooling curve of sample 18	100
Figure 5-94	DSC spectra of sample 21 (59.39/15.78/24.83 Ca/Mg/Al wt%)	101
Figure 5-95	Phase assemblage of sample 21 (59.39/15.78/24.83 Ca/Mg/Al wt%)	102
Figure 5-96	Calculated vertical section at constant 24.8 wt% Al with DSC signals from cooling curve of sample 21	102
Figure A-1	Calculated XRD diffraction pattern for $\text{Al}_2\text{Ca}$	117
Figure A-2	Calculated XRD diffraction pattern for $\text{Mg}_2\text{Ca}$	118
Figure A-3	Calculated XRD diffraction pattern for $\gamma$	119
Figure A-4	Calculated XRD diffraction pattern for $\text{Al}_4\text{Ca}$	120
Figure A-5	Calculated XRD diffraction pattern for $\text{Al}_3\text{Ca}_8$ .	121
Figure A-6	Calculated XRD diffraction pattern for $\text{Al}_{14}\text{Ca}_{13}$	122
Figure A-7	Calculated XRD diffraction pattern for $\beta$	123
Figure A-8	Calculated XRD diffraction pattern for Al	124
Figure A-9	Calculated XRD diffraction pattern for Mg	125

# LIST OF TABLES

Table 2-1	Crystal structure of the stable Al-Mg phases	18
Table 2-2	Special points of the Assessed Mg-Ca Phase Diagram by [52]	20
Table 4-1	Samples in different phase fields	24
Table 4-2	Sample composition in wt. % percent (N: Nominal and A: Actual)	26
Table 4-3	Experimental conditions for the determination of thermophysical properties	28
Table 4-4	The crystal structure data of Al <sub>2</sub> Ca	32
Table 4-5	Atoms positions in the unit cell of Al <sub>2</sub> Ca	33
Table 5-1	The DSC measurements with thermodynamic calculation in phase field Mg-Al <sub>2</sub> Ca- $\gamma$ (c: denotes cooling and h: denotes heating)	40
Table 5-2	Summary of the phase identification for the samples in the Mg- Al <sub>2</sub> Ca - $\gamma$ phase field	42
Table 5-3	Summary of phase identifications for samples 17, 29 and 13 in (Mg)-Mg <sub>2</sub> Ca-Al <sub>2</sub> Ca phase field	63
Table 5-4	The DSC measurements with thermodynamic calculation in (Mg)-Mg <sub>2</sub> Ca-Al <sub>2</sub> Ca phase field for samples 17, 29 and 13 (c: denotes cooling and h: denotes heating)	65
Table 5-5	The DSC measurements with thermodynamic calculation for samples 3, 26, 28 and 9 in Mg-Mg <sub>2</sub> Ca-Al <sub>2</sub> Ca phase field (c: denotes cooling and h denotes heating)	76
Table 5-6	Comparison between XRD results and thermodynamic predictions for samples 3, 26, 28 and 9 in Mg-Al <sub>2</sub> Ca-Mg <sub>2</sub> Ca phase field	76
Table 5-7	DSC measurements and calculated transformation temperature in Al <sub>2</sub> Ca- $\gamma$ -Al region	89
Table 5-8	DSC measurements with thermodynamic analysis in Mg <sub>2</sub> Ca-Al <sub>2</sub> Ca-Al <sub>14</sub> Ca <sub>13</sub> field	100
Table 5-9	DSC measurements with thermodynamic analysis of in Mg <sub>2</sub> Ca-Al <sub>14</sub> Ca <sub>13</sub> -Al <sub>3</sub> Ca <sub>8</sub> phase field phase field	103
Table A-1	The crystal structure data of Al <sub>2</sub> Ca	117
Table A-2	Atoms positions in the unit cell of Al <sub>2</sub> Ca	117
Table A-3	Crystal Structure Data of Mg <sub>2</sub> Ca	118

Table A-4	Atoms positions in the unit cell of $Mg_2Ca$	118
Table A-5	Crystal Structure data of $\gamma$	119
Table A-6	Atoms positions in the unit cell of $\gamma$	119
Table A-7	The crystal structure data of $Al_4Ca$	120
Table A-8	Atoms positions in the unit cell of $Al_4Ca$	120
Table A-9	The crystal structure data of $Al_3Ca_8$	121
Table A-10	Atoms positions in the unit cell of $Al_3Ca_8$	121
Table A-11	The crystal structure data of $Al_{14}Ca_{13}$	122
Table A-12	Atoms positions in the unit cell of $Al_{14}Ca_{13}$	122
Table A-13	The crystal structure data of $Al_3Mg_2$	123
Table A-14	Atoms positions in the unit cell of $Al_3Mg_2$	123
Table A-15	The crystal structure data of Al	124
Table A-16	Atoms positions in the unit cell of Al	124
Table A-17	The crystal structure data of pure Magnesium	125
Table A-18	Atoms positions in the unit cell of pure Mg	125
Table A-19	Solid phases lattice parameter comparison	126

## **LIST OF ABBREVIATIONS**

DSC	Differential Scanning Calorimetry
DTA	Differential Thermal Analysis
XRD	X-ray Diffraction
TG	Thermogravimetry
SEM	Scanning Electron Microscopy
EDS	Energy Dispersive Spectroscopy
EDX	Energy Dispersive X-ray Spectrometer
ICP	Inductive Coupled Plasma

# CHAPTER 1

## *Introduction*

---

### **1.1 Introduction**

Magnesium is the eighth most abundant element in the earth's crust and the third most plentiful element dissolved in seawater. It is the lightest structural metal with a density of  $1.741\text{g/cm}^3$  compared with the Al ( $2.70\text{g/cm}^3$ ) and Fe ( $7.86\text{g/cm}^3$ ). Mg has the best strength to weight ratio of common structural metals, and it has exceptional die-casting characteristics. This makes magnesium alloys particularly attractive for transportation applications such as in the automotive and aircraft industries for weight reduction and higher fuel efficiency. Demand from the automotive industry is the main driver of a 7% annual growth rate in the world's magnesium consumption, which is currently quoted by the International Magnesium Association as 415,000 tonnes/year. The use of Mg alloys in the automotive and electronic industries together has reportedly increased by 350% over the past 10 years, and is expected to grow at 25% per year until 2008 [1-4].

This rapid growth has highlighted the need for a greater understanding of factors that influence the properties of magnesium alloys and industry's increasing demands for a wider range of magnesium alloys with lower thermal expansion, higher fatigue strength, higher creep strength, and better corrosion resistance [3,4]. The current use of Mg in automotive applications is limited to non-critical parts because of its restricted creep properties. Rare earths additions improve creep resistance of these alloys by forming



precipitates, but the main drawback of using rare earth elements in Mg-based alloys is their high cost [5].

A large amount of effort has been made to increase the service temperature of the Mg alloys [6-8, 10]. The addition of Ca element has been reported in recent years to replace the cost intensive rare earths metals. The improvement of creep resistance is attributed to the thermal stability and the interface coherency of the  $Mg_2Ca$  and  $Al_2Ca$  compounds. Calcium additions also protect the melt surface combined with less slag formation and additive loss. And the resulting alloys show lower secondary creep rates and higher tensile strength than AZ91 combined with comparable castability and good melt handling [5, 7, 9-12].

However, to date little effort has been made to construct the phase relationships of the Mg-Al-Ca system. The limited publications on this system mainly focus on the calculations without sufficient experimental work. And these calculations exhibited a considerable discrepancy among the published results and substantial disagreement with experimental data. These problems were inferred from the thermodynamic modeling of the Mg-Al-Ca ternary system which did not take account of ternary phases [13]. Moreover, the accuracy of the thermodynamic model which the calculations are based on depends on the reliability of the experimental data. Therefore, parallel to the calculation work, there is a great need for a sufficient and reliable experimental data for reoptimization of the system.

## 1.2 Thesis organization

The present chapter of introduction illustrates the significance of developing Mg-Al-Ca based alloys and puts forward the existing problems. As a result, there is a great need for experimental work.

In chapter 2 literature review, as a warm-up and preparation to the current study, it is necessary to know the previous work and the problems. Therefore, this chapter outlines the major past research work on the Mg-Al-Ca phase diagram, the phase species and the methodology of the thermal analysis as well as the binary subsystems Mg-Al, Mg-Ca and Al-Ca that contribute to the properties of the ternary system.

Chapter 3 illustrates the specific objectives of this work.

Chapter 4 Experimental determination describes the alloy preparation, the DSC parameter determination and the calibration and the interpretation of the DSC experimental results. An introduction of phase identification with XRD and metallography is also provided in this chapter.

Chapter 5 includes the results and discussion of samples on each studied phase field. It discusses the consistency of experimental results obtained from XRD, microscopy and the DSC. Then the experimental results were compared with the thermodynamic values.

The thesis ends with Chapter 6, which provides the summary of this work, contribution to the current knowledge and suggestions for the future work.

# CHAPTER 2

## *Literature review*

---

Past researchers have worked on different facets of this system. For this work to go one step further, it is necessary to know the merits and deficiencies of the previous work. This chapter outlines some past research work on the Mg-Al-Ca phase diagram, the latest reports of the phase species in the system, and the methodology of the thermal analysis used. The constituent binary systems are also addressed.

## **2.1 Experimental Survey and Thermal Analysis**

### **Principles**

#### **2.1.1 Experimental Survey**

To measure the phase transformation temperature, currently two thermal techniques are prevalent: Differential Thermal Analysis (DTA) and Differential Scanning Calorimetry (DSC).

DTA is a conventional thermal analysis means, but its major function is limited to the determination of phase transformation temperature. Gröbner *et al.* [5] used DTA to investigate the Mg-Al-Ca system. The pre-molten sample was placed in a tantalum crucible which was sealed under argon by welding to avoid oxidation and evaporation. The DTA provided transformation temperatures that were later compared with the thermodynamic calculations. Gröbner *et al.* [16] followed the same approach to study the

Al-Li-Si system and provided extremely important information for the analysis of the DTA results. Tkachenko *et al.* [17] used DTA to construct the isotherms on the projection of the liquidus surface in the Mg-Al-Ca system. They also determined the composition and temperature of some of the invariant points in the system.

Differential Scanning calorimetry (DSC) is the newest of the entrants in the high-temperature thermal-analysis derby, having been around for 20 years [18]. There are two types of DSC: power-compensated DSC and heat-flux DSC. The power-compensated DSC is used for low temperature measurement because radiation heat is lost at temperatures above 650°C making the stability and repeatability of the baseline signals increasingly unstable. Power-compensated DSC is not recommended above this temperature [18]. About 15 years ago, a new type of thermal analysis instrument was introduced, dubbed high-temperature DSC (HTDSC). It differs from the previous type in that it is a heat-flux DSC rather than a power-compensated unit. It can operate at 1500°C or higher, depending on the model [18].

Instances of the use of DSC as a thermal analysis tool have been reported in recent years. Graham *et al.* [19] investigated the extruded Al-Si-Mg alloys with different heat treatment conditions by DSC. The thermograms generated from the DSC showed the precipitation events clearly. The DSC was also used to heat the sample to a selected temperature to allow precipitates to develop to various stages for investigation by TEM. Inoue *et al.* [20] used DSC to measure the thermal stability of Al-Ca and Al-Ca-M (M = Mg, Zn, Fe, Co, Ni or Cu) alloys at a scanning rate of 0.67 K/s. They detected the precipitation temperature of Al and Al<sub>4</sub>Ca from the amorphous phase Al<sub>100-x</sub>Ca<sub>x</sub>. Mahendran *et al.* [21] investigated the binary LiCl-CaCl<sub>2</sub> system using DSC. The

formation of a compound of  $\text{LiCaCl}_3$  at  $439\pm 4^\circ\text{C}$  is discerned with the support of the DSC results. The DSC is also capable of directly measuring the enthalpy changes associated with other thermal events: melting, solid-state phase transitions, chemical reactions, and even allotropic change. [18, 22-24].

On account of the limitation of DTA and the multiple applications of DSC in thermal analysis, the Setaram high temperature heat flux DSC was chosen in this work. Further, this equipment was used in another research [25] to measure the heat capacity of phases in the Sr-Cu-O system. Their results showed good agreement with literature values.

### **2.1.2 DSC principle**

Differential scanning calorimetry can determine the variation in the heat flow given out or taken in by a sample when it undergoes temperature scanning in a controlled atmosphere. With heating or cooling, any transformation taking place in a material is accompanied by an exchange of heat; DSC enables the temperature of this transformation to be determined and the heat from it to be quantified. As mentioned earlier, there are two kinds of DSC, power-compensated DSC and heat-flux DSC.

Power-compensated DSC principle is shown in Figure 2-1 schematically. The temperature difference is controlling the electrical power supplied to the sample and reference in order to keep them at the same temperature. The peak area directly corresponds to the heat consumed or produced by the sample. The difference in heat flow to or from a sample and to or from a reference is monitored as a function of temperature or time, while the sample is subjected to a controlled temperature program.

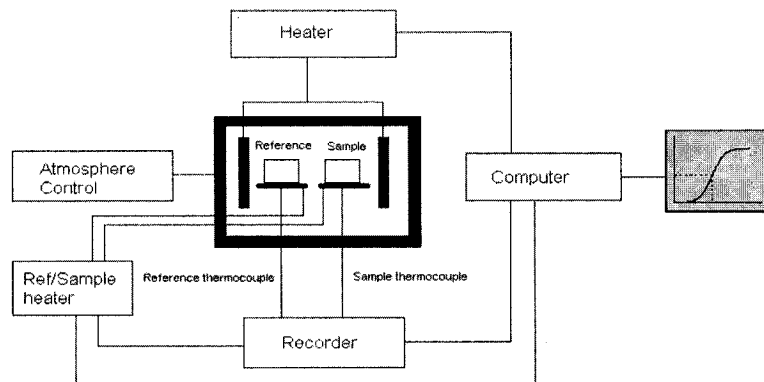


Figure 2-1: Schematic diagram of the power-compensated DSC [26]

A schematic diagram of a heat flux DSC is shown in Figure 2-2. A single heater heats a block containing both sample and reference pans. Thermocouples mounted under the pans measure the temperature of each as the block heats, thereby measuring the difference in heat flow from the crucibles. This gives a signal proportional to the difference in heat capacities between the sample and reference [18, 26].

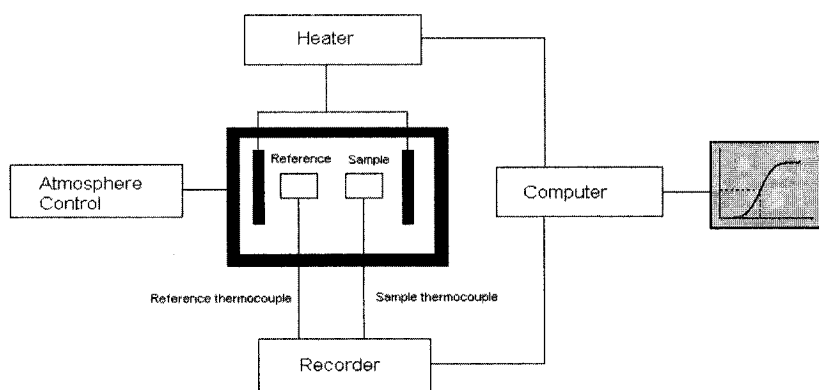


Figure 2-2: Schematic diagram of heat flux DSC [26]

The configuration and the signal detection in the two kinds of DSC are schematically compared in Figure 2-3.

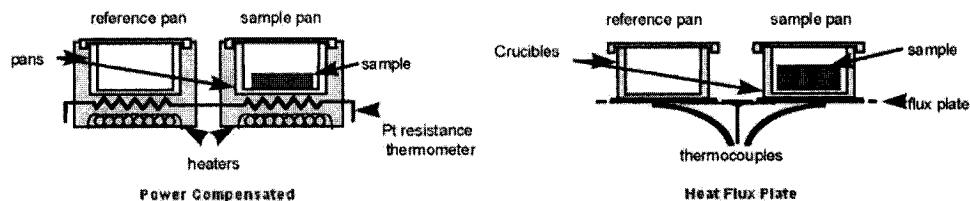


Figure 2-3: Different techniques of DSC signal detection [26]

### 2.1.3 Determination of phase diagram using DSC curve

A DSC record of the slow cooling of a molten mixture of composition  $X_a$  (mole fraction) initially at temperature  $T_a$ , as shown in Figures 2-4 and 2-5, would show no deviation from the baseline until temperature  $T_b$  when solid B begins to crystallize in an exothermic process. This exotherm is not sharp but tails off as crystallization becomes complete as can be seen in Figure 2-5. The area under this exotherm will depend upon the amount of B presents in the sample. As the temperature of the mixture falls further, the eutectic temperature,  $T_e$ , is reached and solid A crystallizes in a sharp exotherm. If the composition had been chosen to be that corresponding to point E, the DSC record would have shown only a single sharp exotherm as the eutectic composition solidifies [18, 26, 27].

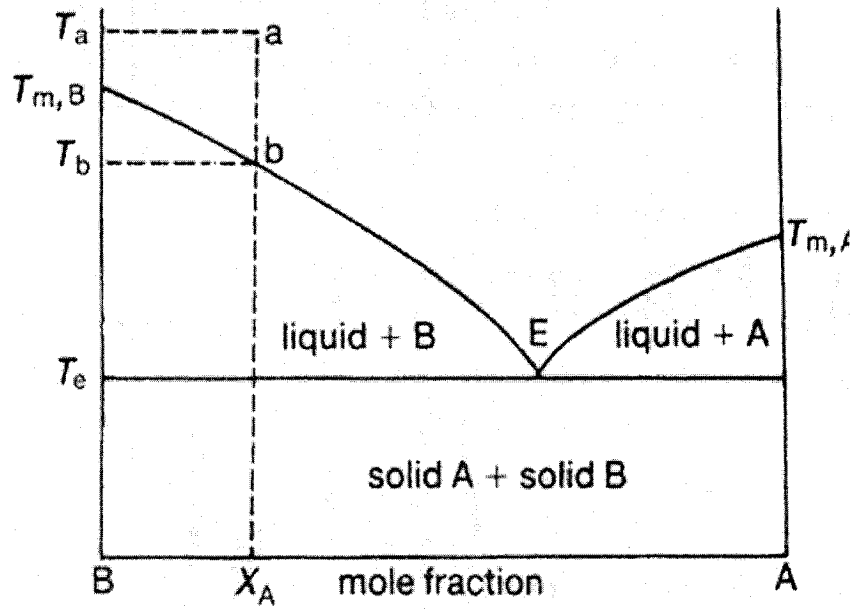


Figure 2-4: Phase diagram for a binary system of immiscible solids and their completely miscible liquids [26]

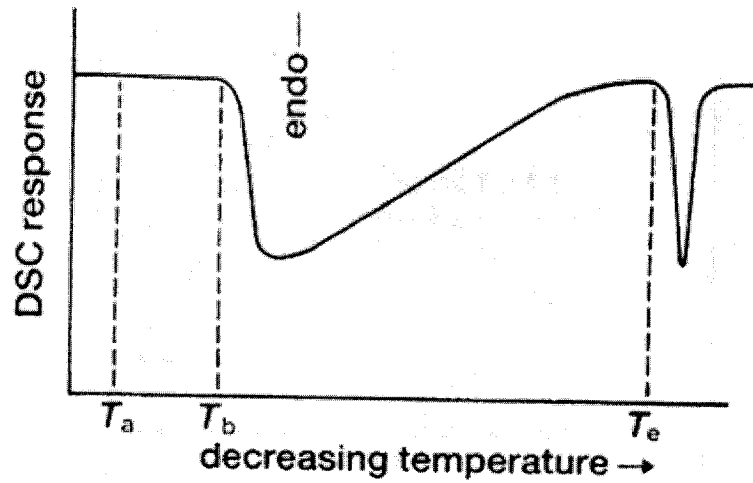


Figure 2-5: DSC curve for the slow cooling of a molten mixture of composition  $X_A$  initially at temperature  $T_a$  [26]



## 2.2 Ternary system Mg-Al-Ca

To date, there are some research publications on the Mg-Al-Ca system. However, many publications only deal with part of the system [17, 28-30]. Few of them involved experimental data, but the number of the samples is not enough especially in the Mg rich corner [5, 13, 17, 30].

Tkachenko *et al* [17] studied the phase equilibria in the Mg-Al-Ca system in the composition range 50-100 wt% Mg using DTA, XRD and microscopic analysis. The projection of the liquidus surface on the concentration triangle can be seen in the Figure 2-6. They determined that additions of Al and Ca decrease the liquidus temperature of magnesium alloys from 650°C to 438°C. The ternary eutectic occurs at the composition 18.2 wt% Ca, 72 wt% Mg and 9.2 wt% Al, and at temperature 510°C according to the reaction  $Le = (Mg) + Mg_2Ca + Al_2Ca$ . The quasibinary eutectic,  $e3 = (Mg) + Al_2Ca$ , happens at 535°C, which agrees with the results reported by Dow Chemical Co. [29]. The peritectic point at P in this figure was calculated corresponding to the transformation  $L + Al_2Ca = (Mg) + Mg_{17}Al_{12}$  and occurs at 470°C as shown in Figure 2-6.

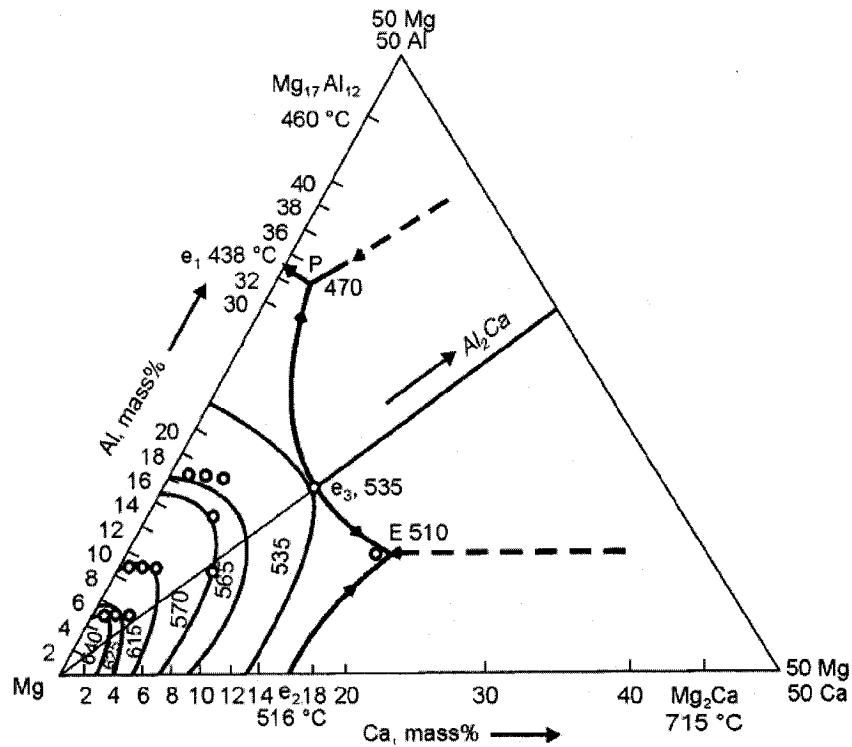


Figure 2-6: Projection of the liquidus surface of the magnesium-rich region of the Mg-Al-Ca system [17]

They labeled the DTA results on the vertical section at the concentrations 4.5, 8.5 and 16 wt% Al in Figures 2-7 to 2-9 [17]. The specimens were heated and cooled at the rate of 80°C/min. But they did not illustrate the corresponding DTA spectra and also did not mention whether the signal was obtained from the heating or the cooling curves. Actually, this heating or cooling rate is much higher than the usual 5°C/min. Therefore, the accuracy of the experimental results is doubtful.

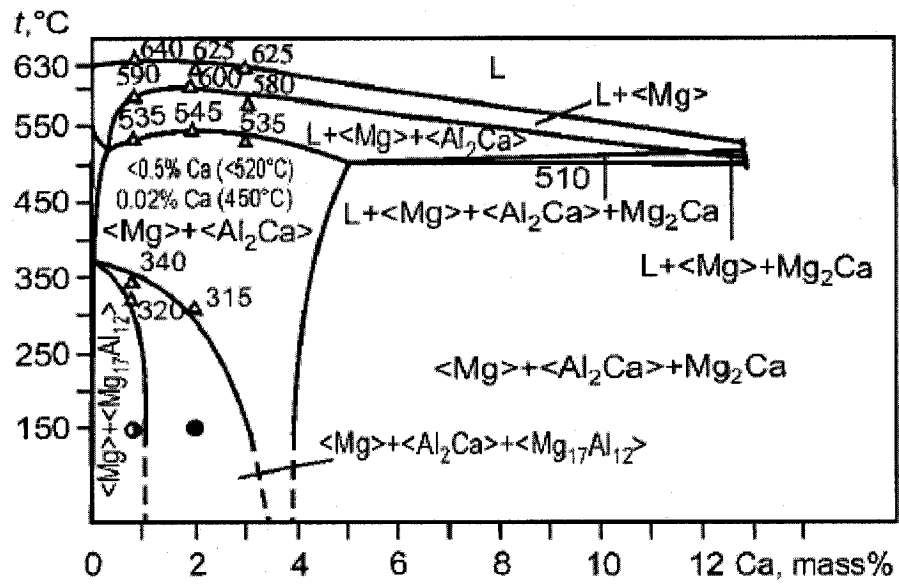


Figure 2-7: Vertical section of the Mg-Al-Ca system at 4.5 wt% Al [17]

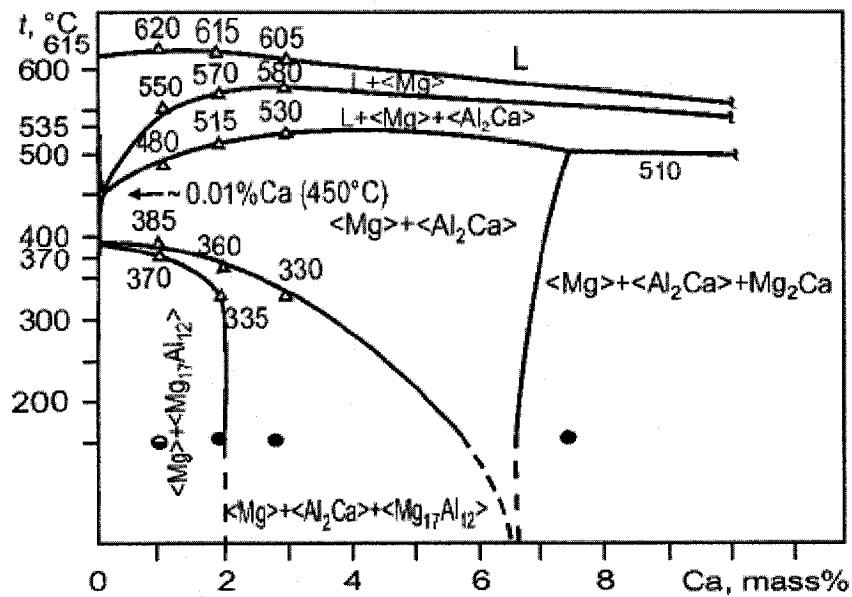


Figure 2-8: Vertical section of the Mg-Al-Ca system at 8.5 wt% Al [17]

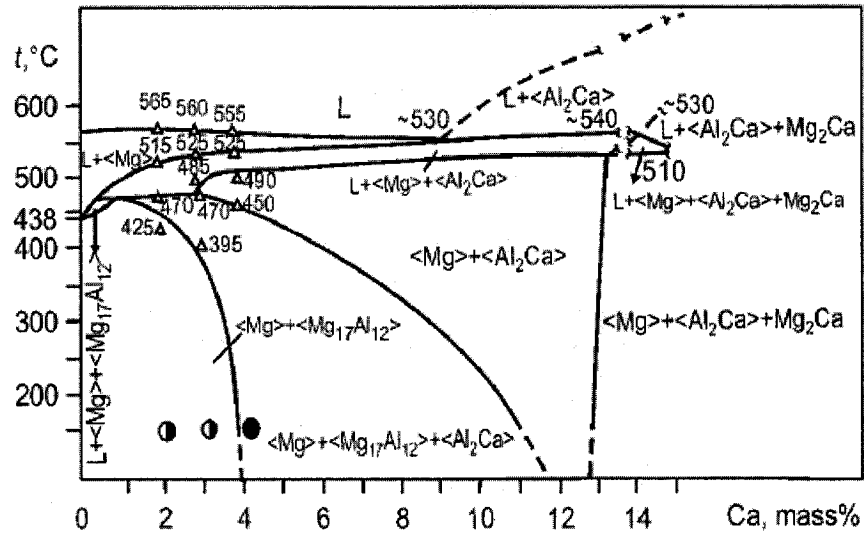


Figure 2-9: Vertical section of the Mg-Al-Ca system at 16 wt %Al [17]

In the work of Gröbner *et al.* [5], thermodynamic calculation of the ternary Mg-Al-Ca phase diagram was performed based on the three binary subsystems. The resulting liquidus is shown in Figure 2-10. It shows that the phase diagram projection is dominated by the highly stable phases  $Mg_2Ca$  and  $Al_2Ca$ . The four alloys investigated by DTA are marked by open circles shown in this diagram. The vertical sections of these four alloys with DTA measurements are shown in the Figures 2-11 to 2-13. They mentioned that the DTA signals are obtained either from the peak maximum point on the heating spectra or from the onset point on the cooling spectra [5]. The choice of using the measurements from either heating or cooling curves leads to inconsistency in the results as for the same phase transformation the cooling signal may differ from its heating signal by up to 30°C. Moreover, they did not mention how they match the DTA signals with the calculated boundaries. For example, in Figure 2-11 there are three DTA measurements but only two

phase boundaries. They match arbitrarily the two upper measurements with the calculated phase transformation boundaries without justification.

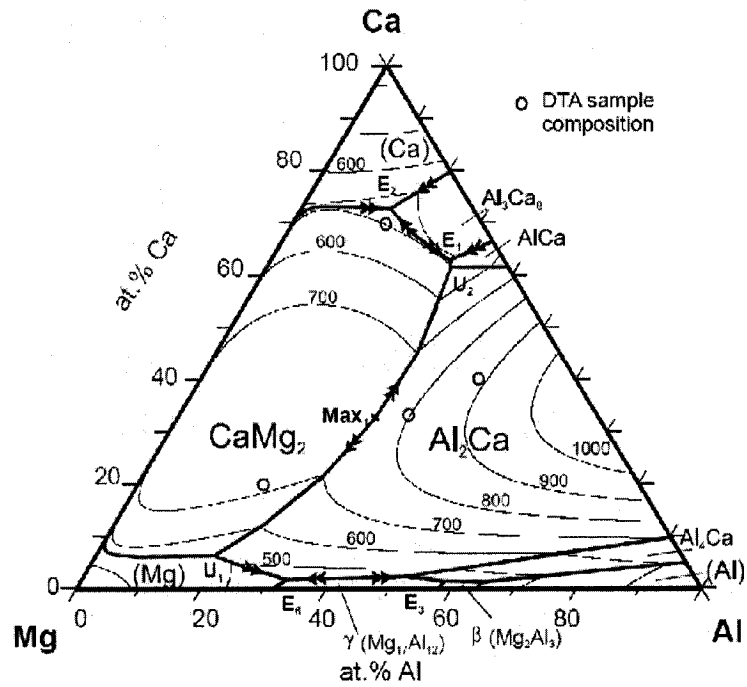


Figure 2-10: The calculated liquidus surface including isotherms and four DTA samples [5]

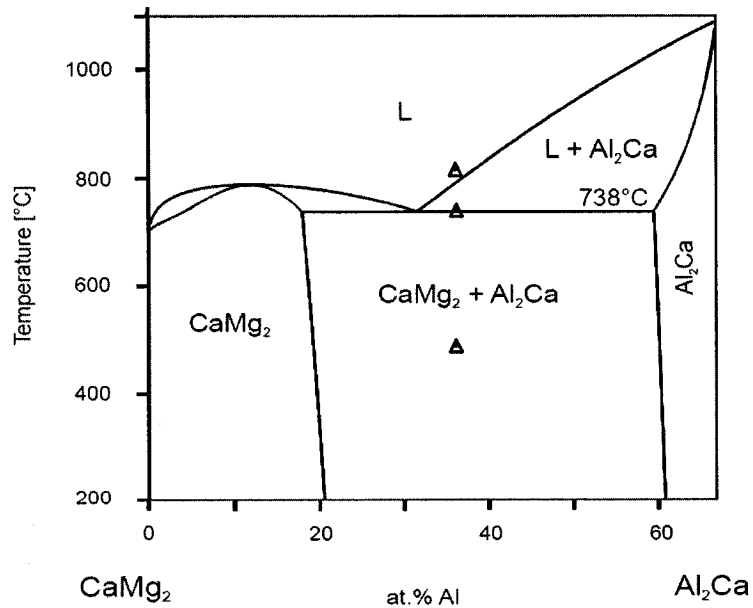


Figure 2-11: The calculated vertical section  $\text{CaMg}_2\text{-Al}_2\text{Ca}$  with DTA signals from the alloy  $\text{Al}_{36.67}\text{Ca}_{33.33}\text{Mg}_{30}$  [5]

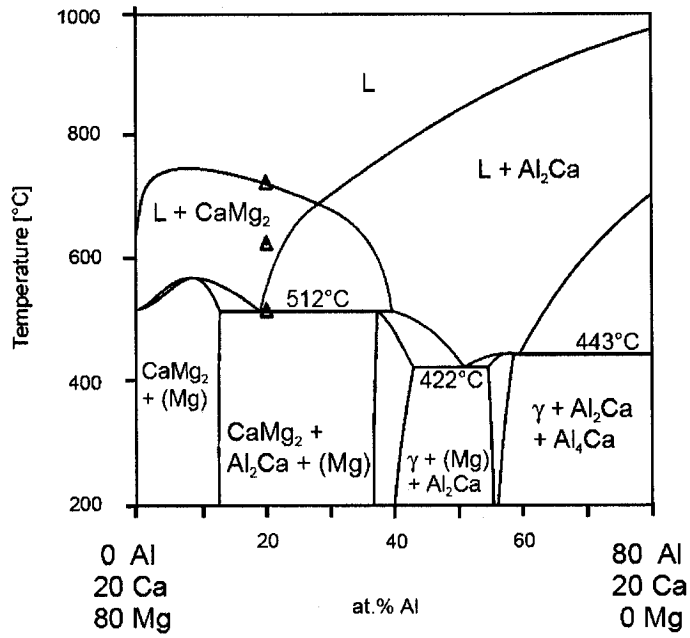


Figure 2-12: The calculated vertical section at constant 20 at.% Ca with DTA signals from alloy  $Al_{20}Ca_{20}Mg_{60}$  [5]

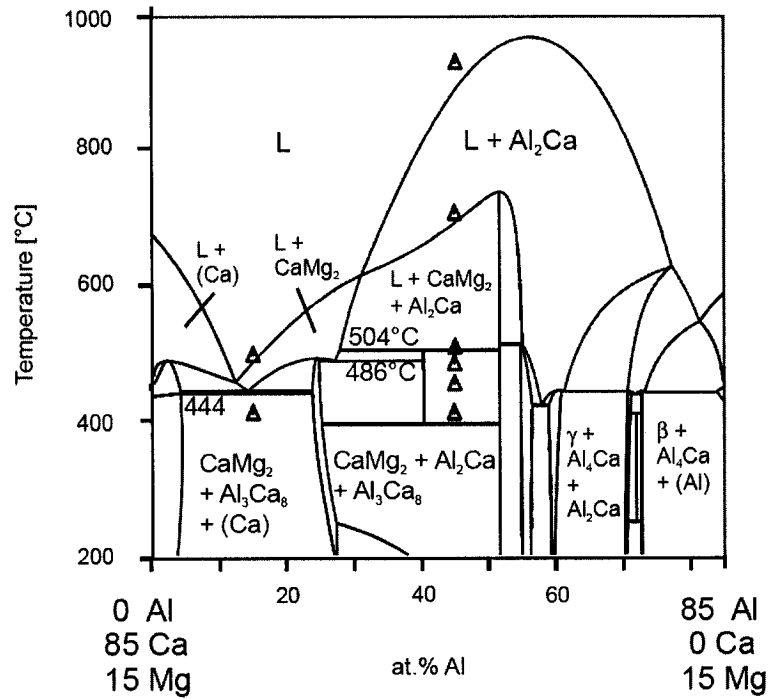


Figure 2-13: The calculated vertical section at constant 15 at.% Mg with DTA signals from alloy  $Al_{15}Ca_{70}Mg_{15}$  and  $Al_{45}Ca_{40}Mg_{15}$  [5]

Korey *et al.* [13] built the Mg-Al-Ca ternary thermodynamic model by combining the data of the three binary systems Al-Mg, Ca-Mg and Al-Ca. They assumed no ternary solubility and no ternary interactions in the system due to lack of experimental data. Therefore a discrepancy of the calculated phase diagram based on their modeling is expected.

In the Mg-Al-Ca ternary system, the binary subsystems, Mg-Al, Mg-Ca and Al-Ca, contribute to the properties of the ternary system, therefore they will be discussed in the following sections.

## 2.3 Mg-Al Phase Diagram

The Mg-Al system is of particular importance to the aluminum industry and has been explored in several experimental studies. There have been numerous reports on the Mg-Al phase diagram [31-37], and the crystal structures of the phases [32, 33, 38, 39]. However, phase diagram compilation showed numerous disagreements [40-42] mainly in the middle range of concentration.

Murray [43] reviewed and optimized the Mg-Al phase diagram based on the work prior to 1982 and published the optimized phase diagram shown in Figure 2-14. He indicated that R ( $\text{Al}_{30}\text{Mg}_{23}$ ) phase has a composition of 42 at.% Mg.  $\zeta$  ( $\text{Al}_{49}\text{Mg}_{32}$ ) phase was considered in a later optimization instead of R phase [44]. The existence of the  $\zeta$  phase and the temperature range of the R phase had been conflicting.

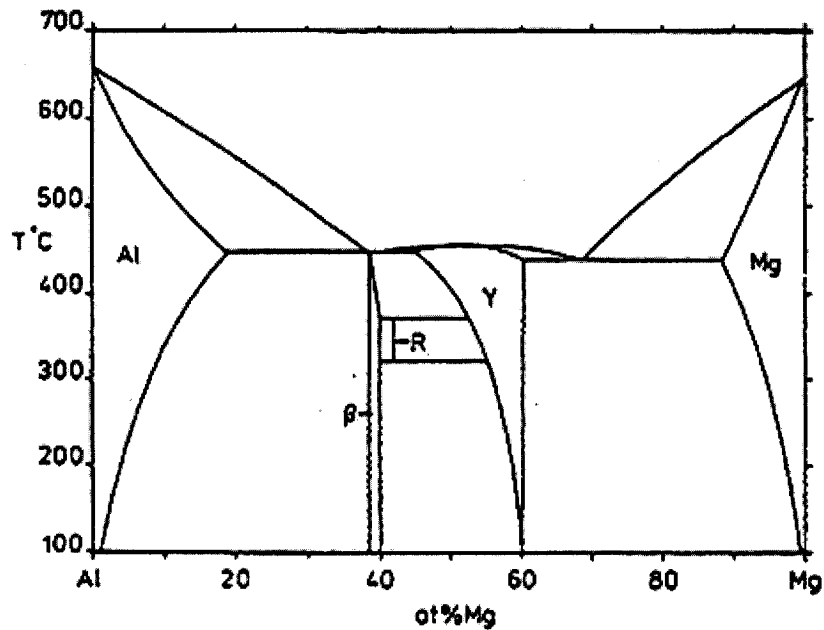


Figure 2-14: The Al-Mg phase diagram from Murray [12]

Saunders [44] reviewed the work on the Mg-Al system prior to 1989 and he questioned the existence of R phase. But he was certain about the existence of two intermediate compounds  $\beta$  ( $\text{Al}_{140}\text{Mg}_{89}$ ) and  $\gamma$ . He carried out a thermodynamic assessment on Mg-Al system based on the results of Schurmann and Geissier [45]. Saunders [44] modeled the  $\gamma$  phase which has  $\alpha$ -Mn structure by a sublattice model with 4 sublattices. However, the greatest disagreement between Saunders and Murray concerns the solubility range of the  $\gamma$  phase. His calculated Al-Mg phase diagram is shown in Figure 2-15.



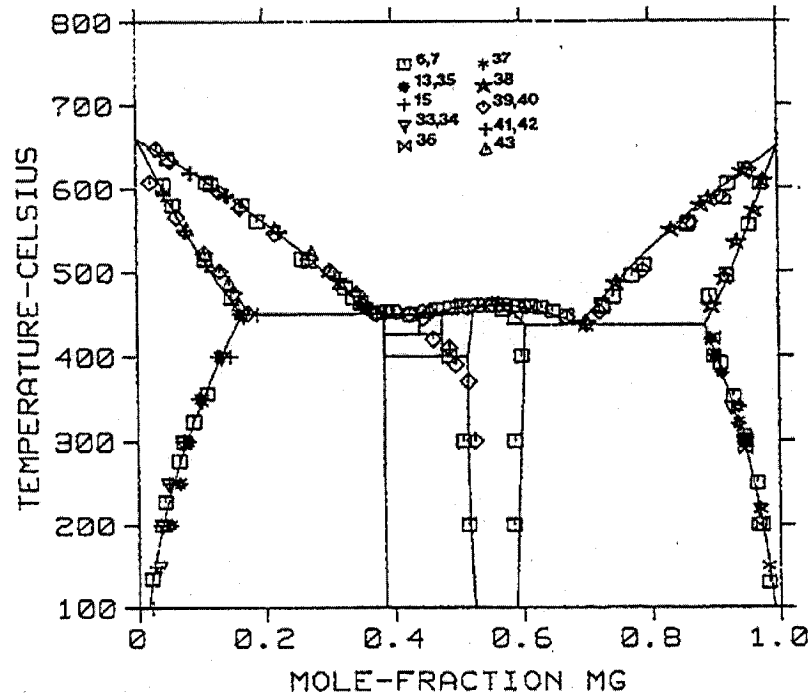


Figure 2-15: The Al-Mg phase diagram from Saunders work [44]

Later another experimental investigation was made by Liang *et al.* [46] where the R phase was found to be stable and the  $\zeta$  phase is suggested to be metastable. The crystal structures of all the stable phases based on Liang *et al.*'s study are shown in Table 2-1.

Table 2-1: Crystal structure of the stable Al-Mg phases

Phase	Space group	Prototype	Reference
fcc-Al	Fm-3m	Cu	
$\beta$ -Al <sub>140</sub> Mg <sub>89</sub>	Fd-3m	Cd <sub>2</sub> Na	[46]
$\epsilon$ -Al <sub>30</sub> Mg <sub>23</sub>	R-3	Co <sub>5</sub> Cr <sub>2</sub> Mo <sub>3</sub>	[38]
$\gamma$ -Mg <sub>17</sub> Al <sub>12</sub>	I-43m	$\alpha$ -Mn	[32]
hcp-Mg	P6 <sub>3</sub> /mmc	Mg	

## 2.4 Mg-Ca Phase Diagram

The liquidus has been explored in several experimental studies throughout the entire composition range [47-51]. The measurement of the liquidus temperature by Klemm and Dinkelacker [50] agrees well with [49]. Klemm and Dinkelacher [50] reported an eutectic point in the Ca-rich corner at 73 at.% Ca, around a temperature of 445°C. Nayeb-Hashemi *et al.* [52] collected all the phase diagram information together with crystallographic data [53, 54]. Then they assessed and calculated the Mg-Ca phase diagram. Their results are presented in Figure 2-16 and Table 2-2, which showed the agreement with the experimental results obtained by other researchers.

The melting point of Mg<sub>2</sub>Ca was determined as 715°C [56]. Kremann and Wostall reported that Mg<sub>2</sub>Ca has a very narrow range of homogeneity [56] with  $a = 6.23\text{\AA}$ ,  $c = 10.12\text{\AA}$  and  $c/a = 1.62$ .

The solid solubility of Ca in Mg was investigated by various methods. The results differ considerably. The solubility of Ca in solid Mg between 508 and 365°C is in the range of 0.58 to 0.95 at.% Ca [51, 53, 57, 59].

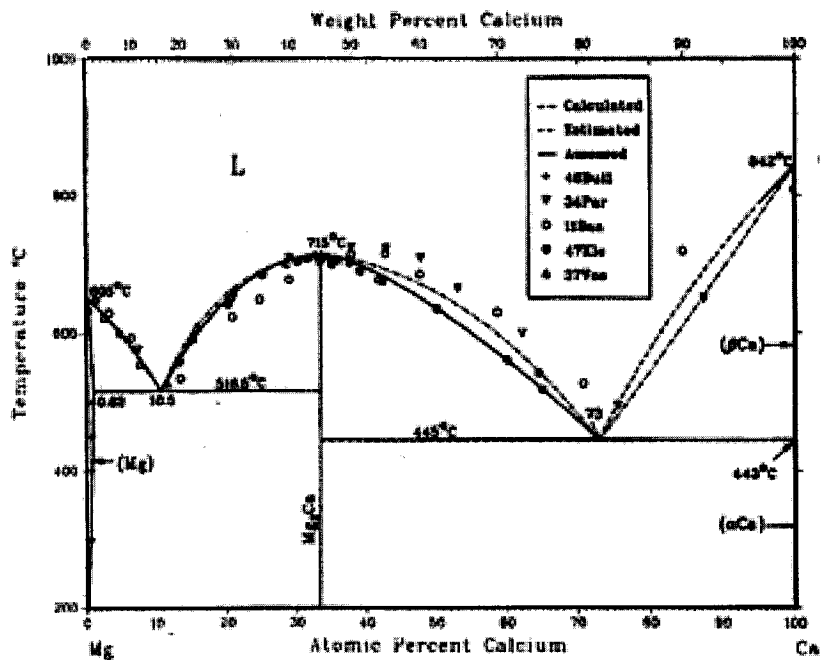


Figure 2-16: The calculated and assessed Mg-Ca Phase Diagram with Experimental points [52]

Table 2-2: Special points of the Assessed Mg-Ca Phase Diagram by [52]

Reaction	Compositions of the respective phases, at.% Ca			Temperature (°C)	Reaction Type
L = (Mg)		0		650	Congruent point
L = (Mg) + Mg <sub>2</sub> Ca	10.5	0.82	33.33	516.5	Eutectic
L = Mg <sub>2</sub> Ca + (αCa)	73	33.33	...	455	Eutectic
L = Mg <sub>2</sub> Ca	33.33			714	Congruent point
L = (βCa)	100			842	Congruent point
(βCa) = (αCa)	100			443	Allotropic

## 2.5 Al-Ca phase Diagram

Several experimental investigations were made on the Al-Ca system [60-63]. Matsuyama *et al.* [62] reported two intermetallic compounds: Al<sub>2</sub>Ca, which melts congruently at 1079°C and Al<sub>4</sub>Ca, which melts incongruently at 700°C. Recently, Kevorkov and Schmid-Fetzer [63] investigated the Al-Ca system experimentally and determined the

complete phase diagram using XRD, metallography, EDX as well as DTA. The binary diagram is shown in Figure 2-17. Two binary compounds  $\text{Al}_4\text{Ca}$  and  $\text{Al}_2\text{Ca}$  were confirmed. And two new compounds  $\text{AlCa}$  and  $\text{Al}_3\text{Ca}_8$  were found. But they did not report the crystal structure of  $\text{AlCa}$ . Nevertheless Huang and Cobett [64] reported the occurrence of a  $\text{Al}_{14}\text{Ca}_{13}$  compound with monoclinic structure instead of  $\text{AlCa}$ . Later on, Ozturk *et al.*[65] reoptimised the system with  $\text{Al}_{14}\text{Ca}_{13}$  intermetallic compound and reported the phase diagram shown in Figure 2-18.

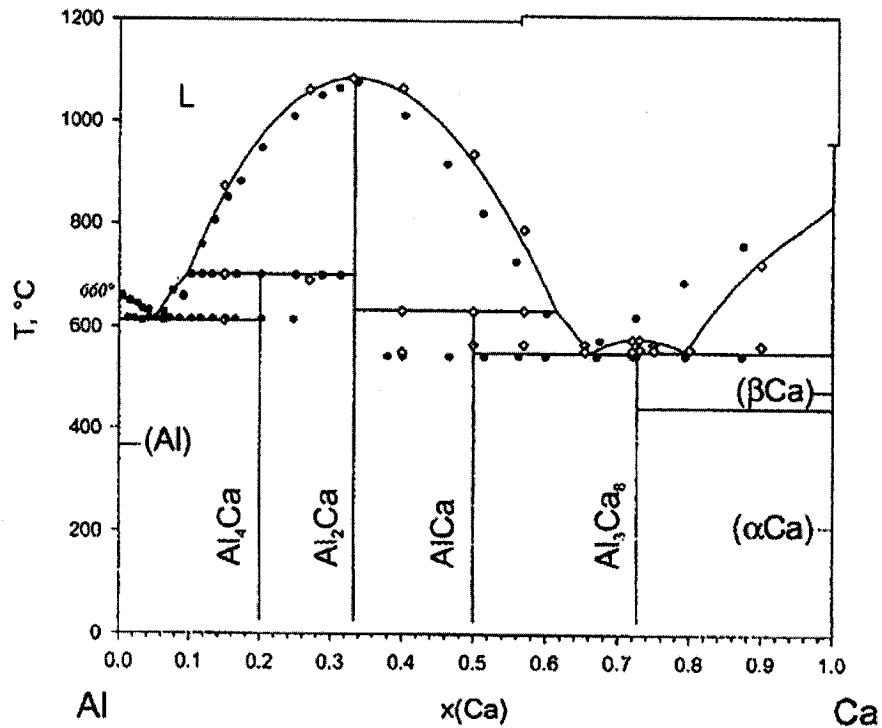


Figure 2-17: The calculated Al-Ca phase diagram and experimental DTA data [63]

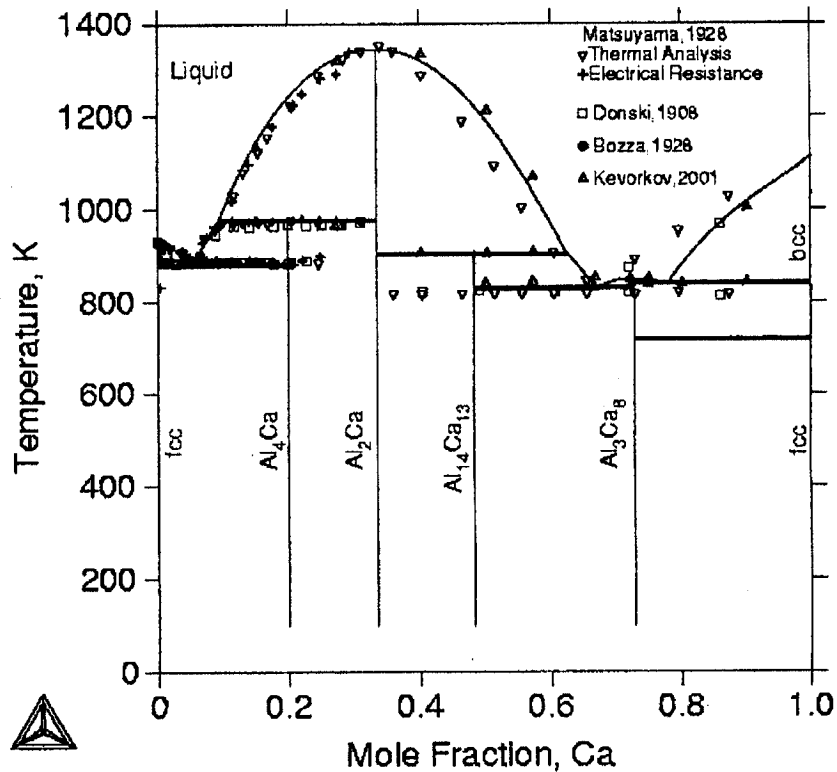


Figure 2-18: The calculated Al-Ca phase diagram using random solution model, compared with experimental data [65]

Analysis of the most recent publications [64-66] reveals that the stable phases in this system are: the liquid, Al-fcc, Ca-bcc, Ca-fcc and four intermetallic compounds:  $\text{Al}_4\text{Ca}$ ,  $\text{Al}_2\text{Ca}$ ,  $\text{Al}_{14}\text{Ca}_{13}$  and  $\text{Al}_3\text{Ca}_8$ .

The solubility of Ca at  $600^\circ\text{C}$  was found to be less than 0.03 at.% by Itkin *et al.* [67]. Kovorkov and Schmid-Fetzer [63] mentioned that, during XRD investigation of the Al and Ca-rich alloys, no deviation from the theoretical powder pattern were detected. Therefore the solubility regions of Ca in Al and Al in Ca are supposed to be negligible.

## CHAPTER 3

### *The Objectives of this Study*

---

The objective of this study is to carry out a systematic investigation on the ternary Mg-Al-Ca system using Differential Scanning Calorimetry (DSC), X-ray Diffraction (XRD) and metallography. Experimental results will be compared with the pertinent thermodynamic calculations. Specific objectives include:

- ✓ Verification of the solid phase transition, the liquidus and compound formation temperatures with the calculated ones based on the current thermodynamic modeling [14].
- ✓ Identification of the phases presented in the samples by XRD and comparing the results with thermodynamic predictions.
- ✓ Analysis of the morphology of the phases by metallographic technique.
- ✓ Calculation of the isothermal section, vertical sections and phase assemblage diagrams for the studied samples using the thermodynamic database developed by Islam [14] and with the aid of FactSage [15] computer program.
- ✓ Providing sufficient experimental data for the reoptimization of the Mg-Al-Ca system in future work.
- ✓ Developing an experimental methodology to verify the thermodynamic modeling.

# CHAPTER 4

## *Experimental Procedures*

---

### 4.1 Alloy Preparation

Twenty one samples were prepared based on thermodynamic calculations. These samples with their expected phase fields are listed in Table 4-1 and shown on the Gibbs triangle in Figure 4-1 in mole fractions.

Special attention was paid to the Mg-rich corner that is always a promising region for alloy development, shown by samples 2, 4, 5, 12 and 13. To verify the eutectic point in the Mg-rich corner, samples 10 to 13 were chosen based on the compositions predicted by thermodynamic modeling. Samples 9, 14 to 17 and 24 were chosen along or close to the phase boundaries in order to verify these calculated phase borderlines. Also, to compare with other experimental results from the literature, the composition of some samples, such as sample 6, were prepared.

*Table 4-1: Samples in different phase fields*

Group	Sample Nos.	Phase field
#1	1, 2,3,4,5	(Mg) + Al <sub>2</sub> Ca + $\gamma$
#2	6,7,8,9, 10,11,12,13	(Mg) + Al <sub>2</sub> Ca + Mg <sub>2</sub> Ca
#3	14,15,16,17	Al <sub>2</sub> Ca + $\gamma$ + Al
#4	18,19,20	Mg <sub>2</sub> Ca + Al <sub>2</sub> Ca + Al <sub>14</sub> Ca <sub>13</sub>
#5	21	Mg <sub>2</sub> Ca + Al <sub>2</sub> Ca + Al <sub>13</sub> Ca <sub>8</sub>

The Mg-Al-Ca alloys were prepared with magnesium of 99.8 wt%, aluminum of 99.9 wt. % and calcium of 99 wt. % at CANMET-MTL, Ottawa. The charge was melted in a graphite crucible in an induction-melting furnace under argon with 1% SF<sub>6</sub> to protect the melt from oxidation. The actual chemical composition was measured quantitatively by the Inductively Coupled Plasma (ICP) technique. Table 4-2 lists the actual and nominal compositions of the studied alloys.

It can be noticed that there is a difference between the nominal and actual compositions, which is due to the volatility of Ca. Nevertheless, the actual composition was used in the analysis during this work.

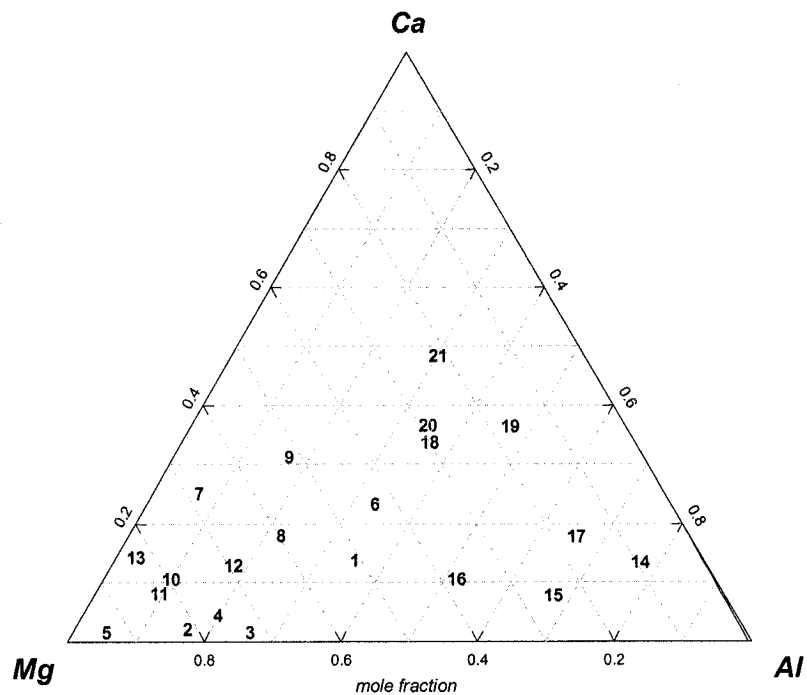


Figure 4-1: The distribution of investigated compositions in mole fractions



Table 4-2: Sample composition in wt. % percent  
(N: Nominal and A: Actual)

Sample No.		Ca	Mg	Al	Total
1	N	23.40	44.00	32.60	100.00
	A	20.43	44.79	34.78	100.00
2	N	4.50	78.00	17.50	100.00
	A	3.59	78.84	17.57	100.00
3	N	6.70	66.90	26.50	100.00
	A	2.50	69.79	27.71	100.00
4	N	10.30	69.70	20.00	100.00
	A	7.09	72.16	20.75	100.00
5	N	3.30	91.70	5.00	100.00
	A	2.66	92.17	5.17	100.00
6	N	34.50	37.60	27.90	100.00
	A	32.68	36.30	31.02	100.00
7	N	33.80	60.10	6.10	100.00
	A	35.62	58.07	6.30	100.00
8	N	28.60	52.10	19.30	100.00
	A	26.16	52.30	21.54	100.00
9	N	44.50	40.50	15.00	100.00
	A	42.32	42.29	15.39	100.00
10	N	19.90	70.40	9.70	100.00
	A	16.44	73.61	9.95	100.00
11	N	15.50	80.30	4.20	100.00
	A	12.65	77.46	9.89	100.00
12	N	23.20	62.90	14.00	100.00
	A	19.32	62.65	18.04	100.00
13	N	24.00	73.30	2.70	100.00
	A	21.69	75.38	2.94	100.00
14	N	20.90	7.70	71.40	100.00
	A	19.12	7.91	72.97	100.00
15	N	13.20	19.80	67.00	100.00
	A	11.67	22.04	66.29	100.00
16	N	16.20	32.70	51.10	100.00
	A	15.68	33.28	51.04	100.00
17	N	26.40	13.60	60.00	100.00
	A	22.81	15.31	61.88	100.00
18	N	43.70	23.90	32.40	100.00
	A	44.30	23.76	31.94	100.00
19	N	50.40	11.50	38.20	100.00
	A	46.73	13.00	40.27	100.00
20	N	43.40	15.80	40.90	100.00
	A	47.47	22.42	30.11	100.00
21	N	60.80	14.70	24.50	100.00
	A	59.39	15.78	24.83	100.00

## 4.2 Differential Scanning Calorimetry

### 4.2.1 Procedure and Analysis

A Setaram Setsys DSC-1200 instrument, shown in Figure 4-2, was used to detect the phase transformations and the invariant equilibrium temperatures of the bulk samples. This equipment operates based on the heat flux principle and is capable of reaching up to 1200°C. Endothermic reactions, which absorb heat, are denoted as downward pointing peaks; and exothermic reactions, which release heat, are denoted as upward pointing peaks in this work. The sample and reference cell unit were purged with high purity argon three times before the heating and cooling sessions in order to prevent sample oxidation.

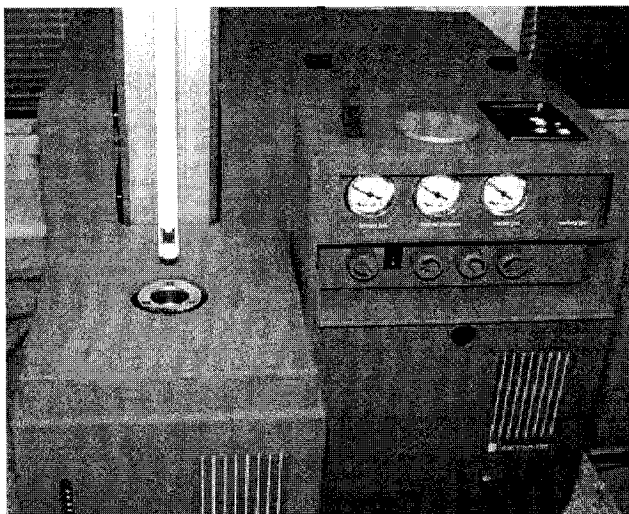


*Figure 4-2: Setaram Differential Scanning Calorimeter*

Determination of sample weight is taken into account, because smaller weight gives more sensitivity to phase transformation, but yields weak signals. Samples with 35 to 45 mg in mass were used.

The heating and cooling rates influence the results. The lower heating and cooling rate generate higher accuracy of the phase transformation temperature; however it will lead to more Mg evaporation. It was noticed that using 2°C /min rate did not provide better results than 5°C /min. Table 4-3 and Figure 4-3 show the experimental parameters of the DSC experiments used in this work.

The reproducibility was verified through comparing the thermal results of two or three heating and cooling cycles for each sample.

*Table 4-3: Experimental conditions for the determination of thermophysical properties*

Item	Conditions
Heating rate	5°C/min
Cooling rate	5°C/min
Temperature range	25~800°C
Atmosphere	Flowing argon, 1 atm.
Weight of sample	35-45 (mg)

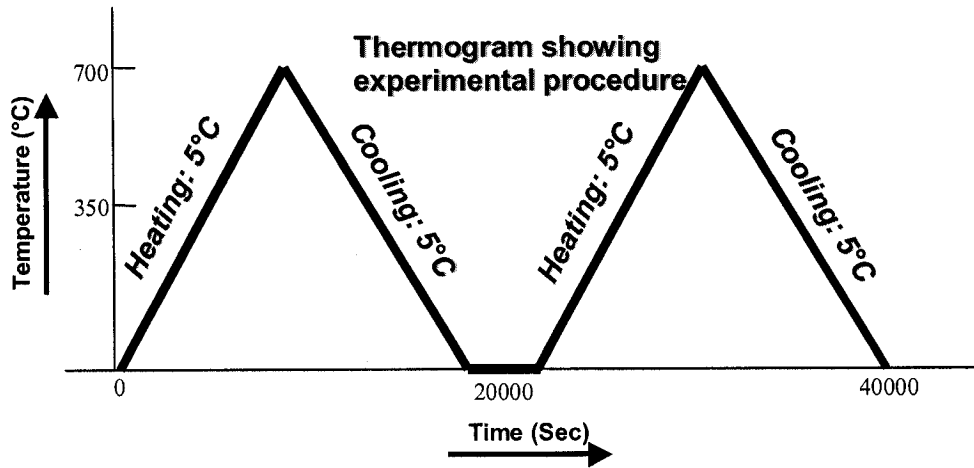


*Figure 4-3: The thermal cycles used during DSC experiments*

The phase transformation temperature was determined by the onset of peak in the cooling curve. The choice of determining the transformation temperatures based on the heating or cooling curves, and whether to choose the onset or the peak point are critical

issues for the reliability of the experimental data. Gröbner *et al* [5] used either the onset of heating or the peak point as the phase transformation temperature. The author believes that the results are not consistent if using the onset or peak point randomly. Secondly, the use of onset point of heating session is not practical. For example, in Figure 4-4, the second peak in the heating spectrum can not give an onset point clearly. However, the cooling spectrum gives a definite onset point. It can be explained that the grain nucleation accumulates a big energy, which comes from the enthalpy change during the phase transformation, in the course of supercooling. When this energy bursts out, it produces a distinct onset point in the DSC cooling spectrum.

The supercooling effect cause reading of measurements lower than the actual phase transformation temperature. To resolve this problem, the DSC instrument in this work was calibrated with pure Mg, and the reading of the onset of the peak was intentionally set to be equal to the known melting point, so it seems that the reading of onset in the cooling spectrum can be minimised.

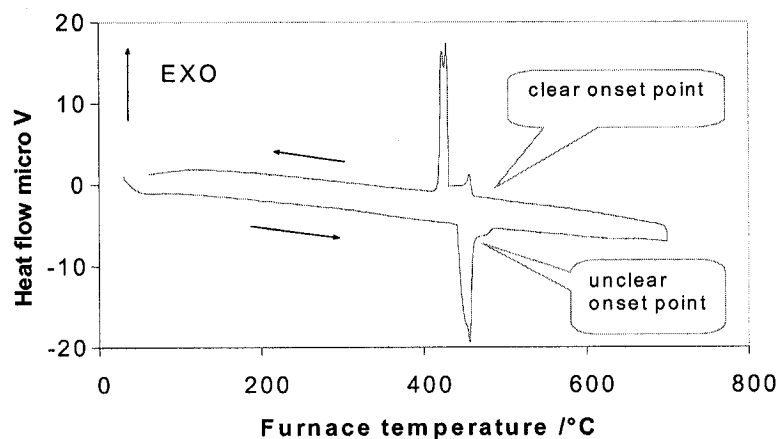
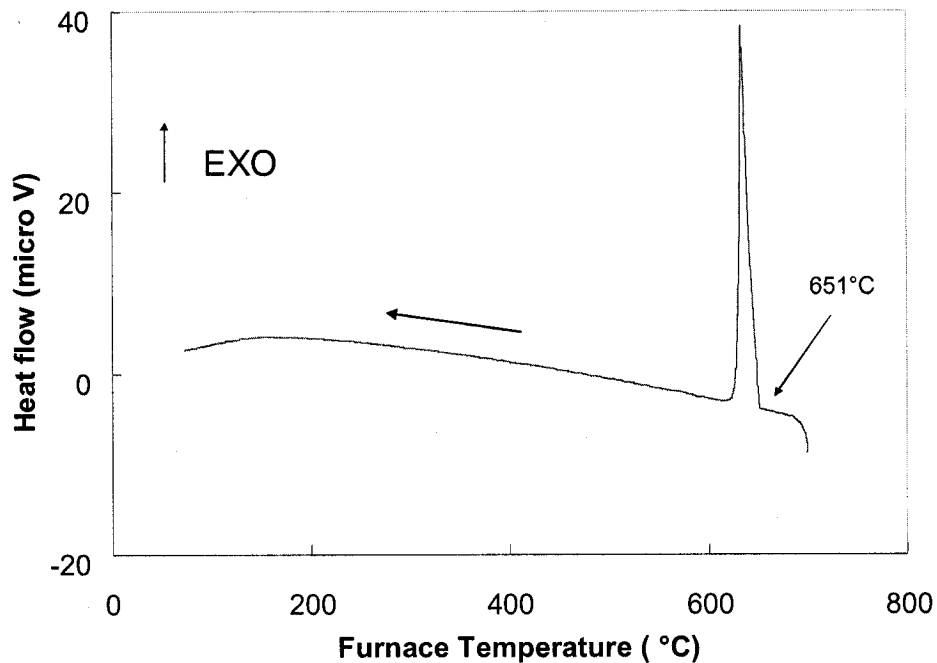


Figure 4-4: Demonstration of DSC spectra with sample 3

## 4.2.2 Calibration of the DSC instrument

The DSC was calibrated by using 40mg pure Mg sample with a 5°C/min. heating and cooling rates. The onset of the peak during cooling occurs at 651°C in Figure 4-5 . It is identical to the known melting point of Mg as 650±1°C [68].



*Figure 4-5: The DSC spectrum of pure Mg*

## 4.3 X-ray powder diffraction

A Philips X-ray diffractometer was used for phase identification. A schematic diagram of an X-ray diffractometer is shown in Figure 4-6. It can be seen that this instrument consists of three basic parts: a source of X-ray radiation, a specimen and the detector and counting equipment. This machine uses filtered  $\text{CuK}\alpha$  radiation, at an accelerating voltage of 40 kV ( $\pm 0.1\%$ ) and a beam current of 20 mA ( $\pm 0.1\%$ ). The intensity and  $2\theta$

data were acquired and stored using a personal computer. Each component wavelength of a polychromatic beam of radiation falling onto a single crystal will be diffracted at a discrete angle, in accordance with Bragg's law expressed by equation 4-1:

$$\sin 2\theta = \frac{\lambda}{2d} \quad \dots\dots\dots 4-1$$

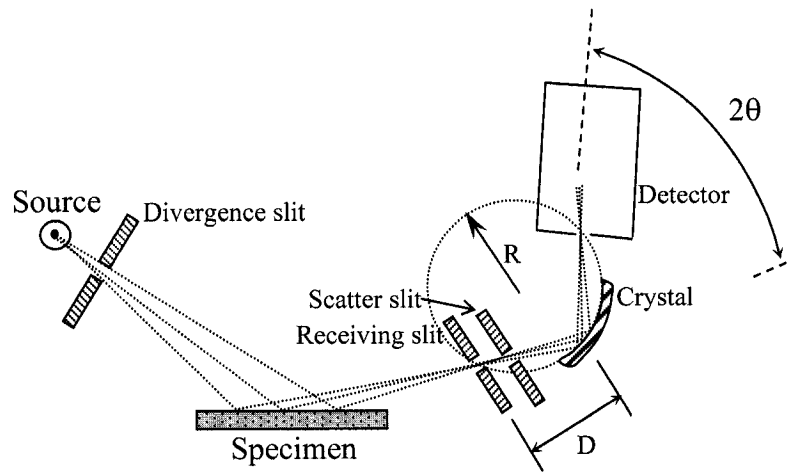


Figure 4- 6: X-ray Diffractometer configurations

The samples were powdered for the investigation by XRD to determine the phases present. The scanning step was 0.02° of 2θ diffraction angle and the exposure time was 1 second. The obtained diffraction patterns were analyzed by comparing with the simulated ones for each possible phase. The simulation of XRD patterns were calculated using Powdercell 2.4 [15].

According to Bragg's law, the peak positions, 2θ, depend on the wavelength used and the lattice spacing, d. Furthermore, any calculation of the intensity of a diffracted

beam depends on the structure factor, which is determined by the arrangement of atoms within a unit cell. In other words, the crystal structure and atom positions in the unit cell must be known in order to calculate an x-ray diffraction pattern. Those variables can be expressed as lattice parameters and Wyckoff position. Calculation of XRD pattern of  $Al_2Ca$  will be demonstrated here as an example and the other calculated XRD patterns are given in Appendix A. By applying the lattice parameters listed in Table 4-4 and Wyckoff positions in Table 4-5, the resultant XRD pattern is shown in Figure 4-7.

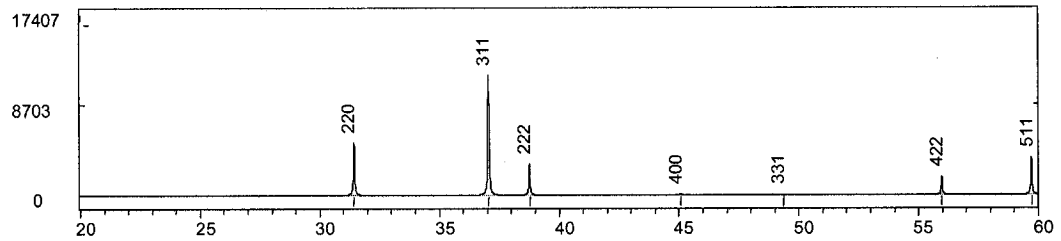


Figure 4-7: The simulated XRD pattern for  $Al_2Ca$

Table 4-4: The crystal structure data of  $Al_2Ca$  [69-71]

Structure	$Cu_2Mg$		
Spacegroup	Fd-3m		
Space number	227		
Lattice parameter (nm)	a	b	c
	0.8040	0.8040	0.8040
Angles	$\alpha$	$\beta$	$\gamma$
	90°	90°	90°
Atoms in unit cell	24		

Table 4-5: Atoms positions in the unit cell of  $Al_2Ca$  [69-71]

Atom	Wyckoff position	x	y	z
Ca	8a	0	0	0
Al	16d	5/8	5/8	5/8

In many cases, XRD peaks shift due to the dissolution of other elements which causes distortion of the crystal lattice. For example, the characteristic peaks of pure Mg at  $2\theta = 36.6^\circ$  shifts to  $37.12^\circ$ , when Mg dissolves 10 at.%. Likewise, the  $Al_2Ca$  is reported to dissolve 5 at.% Mg [5], so the lattice expands and the XRD peaks shift to smaller angles. The  $Mg_2Ca$  dissolves up to 22 at.% Al and form  $(Mg,Al)_2Ca$  solid solution, so the lattice parameters shrink and the XRD peaks shift to higher angles.

A comparison of lattice parameters of pure Mg, (Mg),  $Al_2Ca$ ,  $Mg_2Ca$  with their solid solution lattice parameters is shown in the Appendix A.

## 4.4 Metallographic technique

Optical microscopy was used to examine the microstructure; such as grain size, shape, distribution of the phases and inclusions that are present.

Usually 500X magnification is the minimum required to reveal clear phase morphology. Lower magnification pictures such as 100X are also acquired and used for comparing the relative amount of phases. Experience for preparation of metallographic samples is summarized in Appendix B.



# CHAPTER 5

## *Result and Discussions*

All the samples studied in this work are labelled on the 25°C isothermal section in Figure 5-1. The thermodynamic calculation in this work is based on the thermodynamic model for Mg-Al-Ca system established by Islam and Medraj [72]. This chapter will describe how to verify the thermodynamic model by investigating phase transformation temperatures, identifying the phases as well as the phase morphology using DSC, XRD and optical microscopy, respectively.

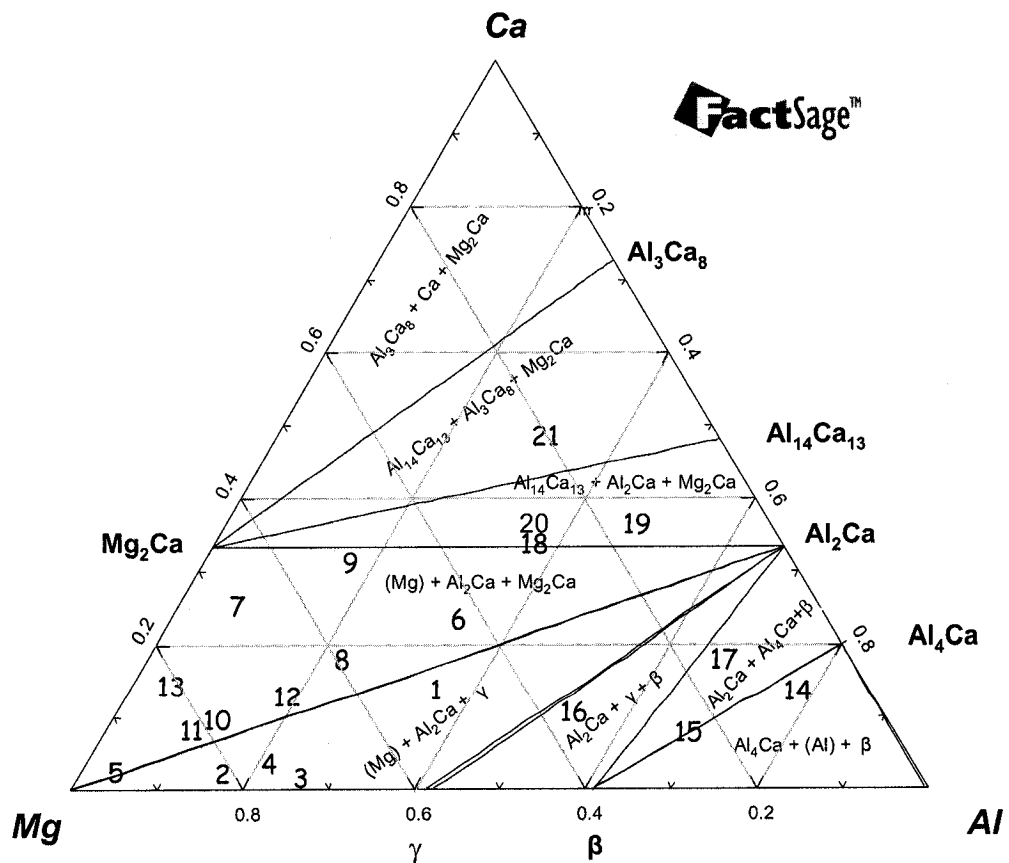


Figure 5-1: Isothermal section at 25°C showing the studied samples

## **5.1 Thermodynamic calculations**

Factsage 5.3 thermodynamic program [73] was used to calculate phase assemblage diagrams, vertical and isothermal sections of the ternary Mg-Al-Ca system. The phase assemblage diagram shows the phase transformation temperature during thermal session as well as the relative amount of each phase at any temperature. It can serve as guidance to understand the DSC pattern. The vertical section shows the sequence of the thermal events during heating or cooling. And the isothermal section presents the phases in equilibrium at the temperature in question.

## **5.2 Samples in the Mg- Al<sub>2</sub>Ca - $\gamma$ phase field**

Five samples 1 to 5 were studied in this region as shown in Figure 5-1. The experimental results of these samples will be discussed and compared with the thermodynamic predictions.

### **5.2.1 Results and discussion of sample 1**

The phase transformation temperatures are obtained from the cooling curve rather than the heating curve as discussed earlier in chapter 4. The DSC heating and cooling curves of sample 1 are shown in Figure 5-2. Two exotherms appear in the cooling curve at 442°C and 523°C. This corresponds to the two endotherms that appear in the heating spectrum at 472°C and 540°C. Another exothermic signal was revealed on the cooling curve at 750°C, but did not appear in the heating spectrum. It can be seen from this figure

that the peaks appear to be more distinct in the cooling than in the heating curve. This is common and is due to the supercooling effect that causes more grain nucleation and more energy accumulation. Therefore, in this study, the phase transformation temperatures are always acquired from the onset of the cooling curve.

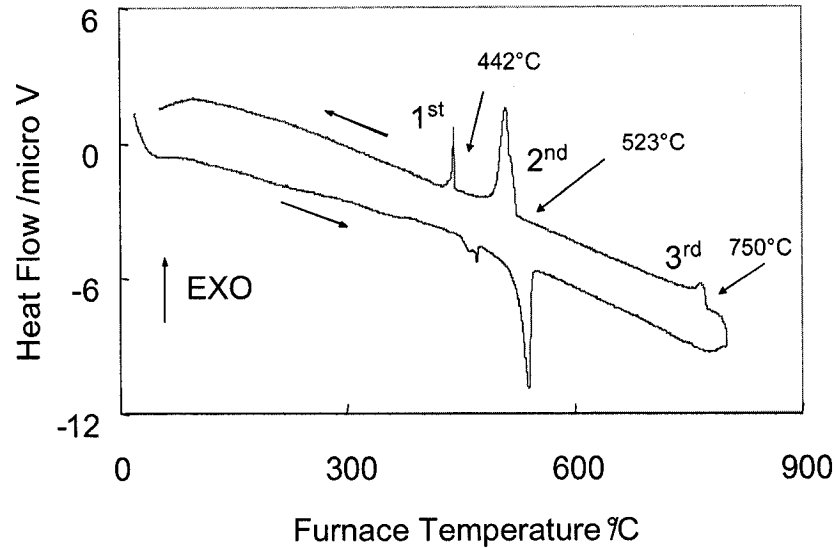


Figure 5-2: DSC spectra of sample 1 (20.43/44.79/34.78 Ca/Mg/Al wt%)

In many cases, not all of the phase transformations can be detected by the DSC. Therefore, it is very important to build a theory to link the observed DSC peaks with the right phase transformation. In the beginning of this work, the DSC results were explained by the relevant vertical sections. The slope rate of the phase boundary was used to analyze the matching of the DSC peaks. The more flat the boundary should be connected with the sharper peak and the steeper boundary corresponds to the weaker peak. In many cases, the slope was too steep where the peak was too weak to observe. For example, in the DSC pattern of sample 1, the three exotherms on the cooling curve correspond to the

three phase boundaries in the vertical section (Figure 5-3): L/L + Al<sub>2</sub>Ca /L + Al<sub>2</sub>Ca + (Mg)/ Al<sub>2</sub>Ca + (Mg) +  $\gamma$ . In this figure, the solid triangles are marked on the vertical section to represent the DSC results.

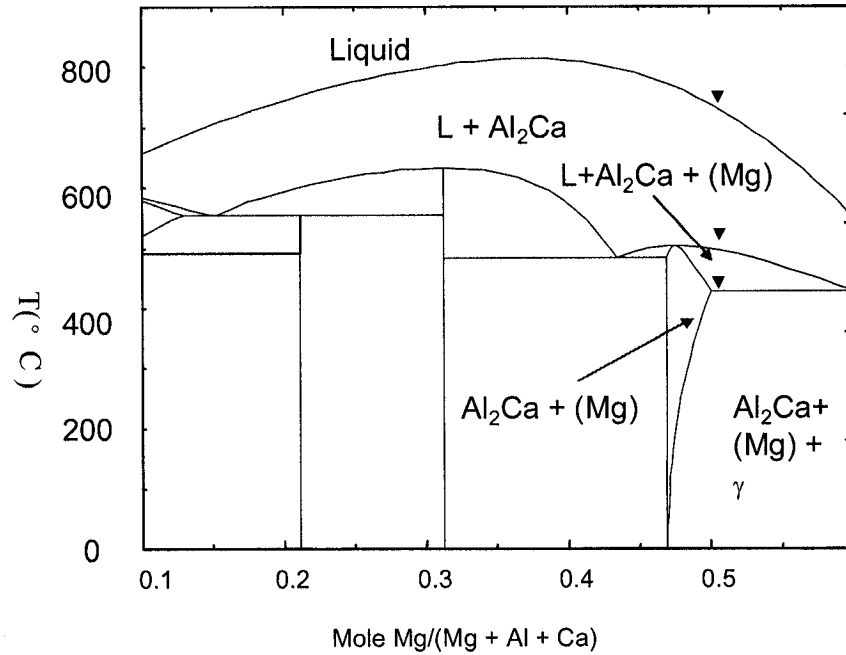


Figure 5-3: The calculated vertical section at constant 35.4 at.% Al with DSC signals from cooling curve of sample 1

But later on it was found that the phase assemblage diagram (Figure 5-4) shed more light on understanding the DSC peaks and correlating them to their phase transformations. The DSC peak pattern relies on the phase transformation rate, which can be revealed easier from the phase assemblage diagram. For example, the steeper the phase borderline between the liquid and a precipitating phase the higher the phase transformation rate and the narrower and sharper the DSC peaks will be.

There are three scenarios to correlate the phase assemblage diagram with the DSC peaks pattern. The first scenario is that the vertical phase borderline, indicating the

infinite phase transformation rate such as eutectic transformation, which is theoretically revealed with infinite sharp peak. The second extreme scenario is where there is no peak revealed on the DSC pattern which corresponds to a phase borderline with too low slope. The third scenario is between these two extremes. In this scenario, the steeper phase borderline in the phase assemblage diagram should be linked to the stronger peak on the DSC pattern and vice versa.

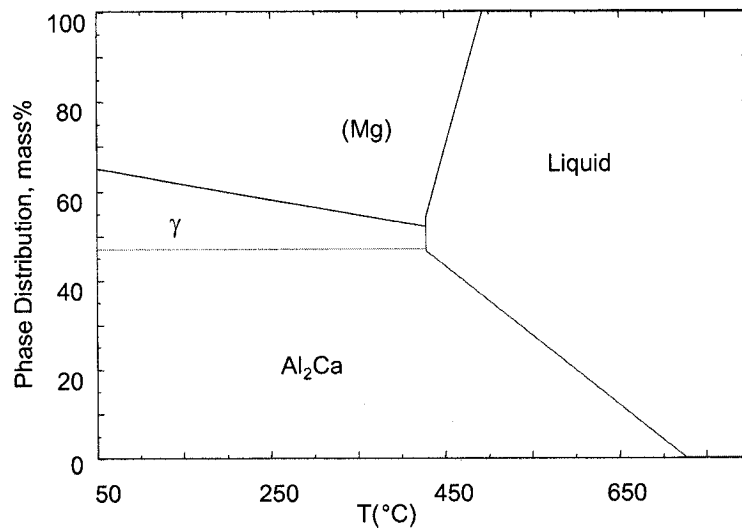


Figure 5-4: Phase assemblage diagram of sample 1  
(20.43/44.79/34.78 Ca/Mg/Al wt%)

Although the three scenarios are all related to the phase transformation rate, to facilitate the analysis process of each sample throughout this work, the reasoning for the first scenario is hereafter named the infinite phase change rate principle and for the third scenario is named the phase amount involvement principle. This name was given because steep borderline will cause more precipitation of the new phase per unit temperature drop during solidification. In another words, the steeper the phase borderline will cause more

involvement of a new phase. As a result, this amount of the new phase involvement causes a stronger heat flux in the DSC pan and is revealed by a stronger DSC peak.

The application of these principles is demonstrated in the DSC pattern interpretation of sample 1. The first peak at 442°C in Figure 5-2 is the sharpest; this is because of the infinite change rate of  $\gamma$  phase as indicated by the vertical borderline on the phase assemblage diagram shown in Figure 5-4. The formation of (Mg) during solidification process shown in Figure 5-4 leads to greater amount of nucleation during cooling, which causes higher system enthalpy change. This results in a stronger and broader second peak in the cooling curve at 523°C. This respects the phase amount involvement principle. After the first two peaks are determined, the right most third peak is nothing but the liquidus because the gentle phase transformation demonstrated by the low slope of the borderline between the liquid and  $\text{Al}_2\text{Ca}$  phases in Figure 5-4 predicts that only little heat flux would be generated between the sample pan and the reference pan in the DSC instrument, as a result, the third peak is relatively weak.

The DSC measurements and the calculations of sample 1 are summarized in Table 5-1. The discussion of the rest of the samples listed in the table will follow.

The XRD pattern of sample 1 in Figure 5-5 indicates that the phases that exist in sample 1 at room temperature are  $\text{Al}_2\text{Ca}$  and (Mg) and traces of  $\gamma$ . This is consistent with the micrograph shown in Figure 5-6. The strong peaks of  $\text{Al}_2\text{Ca}$  and (Mg) are due to their large amounts in the sample. Although  $\gamma$  peaks are not strong, it can be identified in the micrograph shown in Figure 5-6.

Table 5-1 The DSC measurements with thermodynamic calculation in the Mg-Al<sub>2</sub>Ca- $\gamma$  phase field (c: denotes cooling and h: denotes heating)

Sample	DSC Thermal Signals (°C)	Thermodynamic calculation based on the database reported in [14]	
		Temp.( °C)	Reactions or phase boundary
1	472h/442c	430	(Mg)* + Al <sub>2</sub> Ca + $\gamma$ / (Mg) + Al <sub>2</sub> Ca + L
	540h/523c	496	(Mg) + Al <sub>2</sub> Ca + L / Al <sub>2</sub> Ca + L
	750c	728	Al <sub>2</sub> Ca + L/L
2	442h/431c	427	(Mg) + Al <sub>2</sub> Ca + $\gamma$ / Al <sub>2</sub> Ca + (Mg) + L
	-	485	Al <sub>2</sub> Ca + (Mg)/ (Mg) + L
	556h /542 c	539	(Mg) + L /L
3	441h /431c	428	(Mg) + Al <sub>2</sub> Ca + $\gamma$ / Al <sub>2</sub> Ca + (Mg) + L
	-	450	Al <sub>2</sub> Ca + (Mg)/ (Mg) + L
	488h /460c	476	(Mg) + L /L
4	445c	428	(Mg) + Al <sub>2</sub> Ca + $\gamma$ / Al <sub>2</sub> Ca + (Mg) + L
	524c	494	Al <sub>2</sub> Ca + (Mg)/ (Mg) + L
	584c	502	(Mg) + L /L
5	-	195	(Mg) + Al <sub>2</sub> Ca + $\gamma$ / Al <sub>2</sub> Ca + (Mg)
	534 h/524c	501	Al <sub>2</sub> Ca + (Mg)/ (Mg) + L
	585 h/605c	616	(Mg) + L /L

\* Notation ( ) means solid solution.

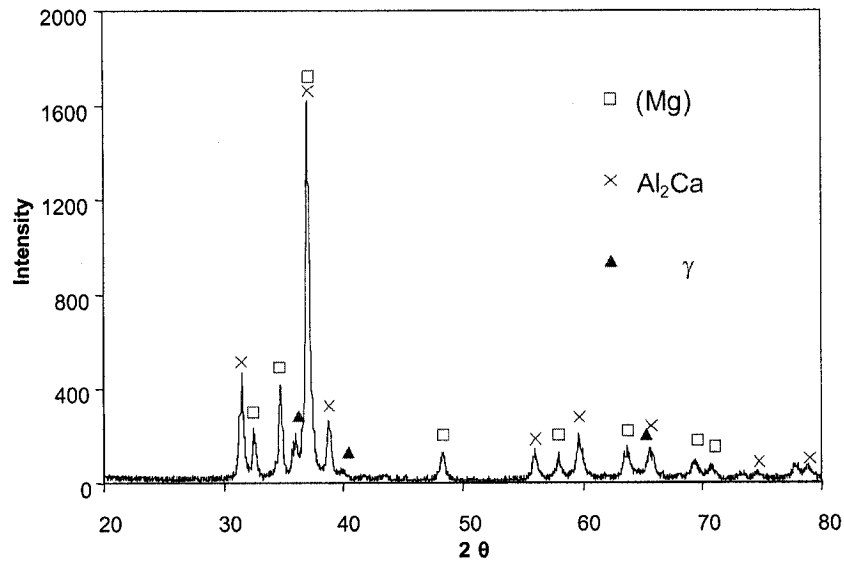
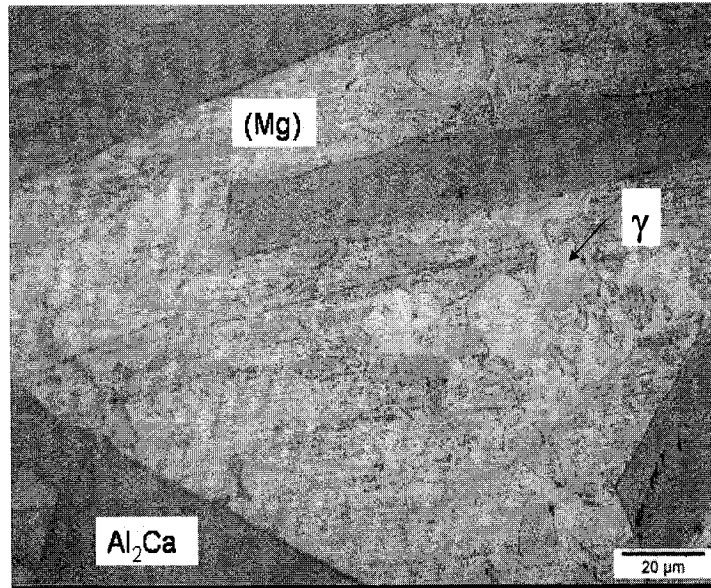


Figure 5-5: XRD pattern of sample 1 (20.43/44.79/34.78 Ca/Mg/Al wt%)



*Figure 5-6: Micrograph of sample 1 1000X  
(20.43/44.79/34.78 Ca/Mg/Al wt%.)*

It is worth mentioning that, in the XRD pattern of sample 1, the Mg peaks match the pattern of (Mg) with 10 at.% Al better than that of pure Mg, which indicates that Mg exists in the form of solid solution in this sample.

Figure 5-6 shows that the  $\gamma$  phase occurs around the plate-like  $\text{Al}_2\text{Ca}$  and within the (Mg) matrix. This is consistent with  $\gamma$  precipitation according to the phase transformation  $\text{L} + \text{Al}_2\text{Ca} + (\text{Mg}) / \text{Al}_2\text{Ca} + (\text{Mg}) + \gamma$ , indicated on the vertical section in Figure 5-4.

The morphology of the primary and secondary  $\text{Al}_2\text{Ca}$  is observed in the micrograph in Figure 5-6. Being compared with the vertical section in Figure 5-4, the massive plates is supposed to be the primary  $\text{Al}_2\text{Ca}$  phase according to  $\text{L} / \text{Al}_2\text{Ca} + \text{L}$



transformation; and the smaller islands are probably the secondary  $\text{Al}_2\text{Ca}$  phase yielded from  $\text{L} + \text{Al}_2\text{Ca} / \text{L} + \text{Al}_2\text{Ca} + (\text{Mg})$  transformation. In fact, the morphology of  $\text{Al}_2\text{Ca}$  is consistent in all the samples in this system.

The XRD pattern and micrograph results are also in agreement with the calculated phase assemblage diagram and isothermal section shown in Figures 5-4 and 5-1, respectively. The identified phases for the sample 1 and other samples to be discussed in this phase field are summarized in Table 5-2. This table compares the experimental findings of XRD and metallography with the thermodynamic calculations. Thus, DSC, XRD, morphology and volume fraction of metallographic results are in agreement with the thermodynamic model in this phase field for sample 1.

*Table 5-2: Summary of the phase identification for the samples  
in the Mg-  $\text{Al}_2\text{Ca}$  -  $\gamma$  phase field*

Sample	Identified phases by XRD	Thermodynamic calculation [14]
1	<b>(Mg) + <math>\text{Al}_2\text{Ca}</math> + <math>\gamma</math></b>	<b>(Mg) + <math>\text{Al}_2\text{Ca}</math> + <math>\gamma</math></b>
2	<b>(Mg) + <math>\gamma</math> + <math>\tau_1</math> (less strong peak)</b>	<b>(Mg) + <math>\gamma</math> + <math>\text{Al}_2\text{Ca}</math> (little)</b>
3	<b>(Mg) + <math>\gamma</math> + <math>\tau_1</math> (stronger peak)</b>	<b>(Mg) + <math>\gamma</math> + <math>\text{Al}_2\text{Ca}</math> (little)</b>
4	<b>(Mg) + <math>\text{Al}_2\text{Ca}</math> (strong peak) + <math>\gamma</math></b>	<b>(Mg) + <math>\text{Al}_2\text{Ca}</math> + <math>\gamma</math></b>
5	<b>(Mg) + <math>\text{Al}_2\text{Ca}</math></b>	<b>(Mg) + <math>\text{Al}_2\text{Ca}</math> + <math>\gamma</math> (little)</b>

Note: the bold font means the phases are with significant amount.

## 5.2.2 New ternary phase observed in the Mg-Al-Ca system

The discussion of the DSC results of samples 2, 3 and 4 has concurrently verified the invariant phase transformation temperature. The XRD and metallographic investigations suggest the existence of a new phase and delimit the composition range.

The DSC spectra of sample 2 are illustrated in Figure 5-7. Two peaks appear on the DSC pattern. The first peak, featuring a narrow and sharp peak at 431°C in the cooling session, indicates a eutectic transformation. The tail peak at 542°C represents a univariant reaction and its onset point corresponds to the liquidus. This finding can be correlated with the phase assemblage diagram in Figure 5-8. The narrow and sharp peak is caused by the infinite phase transformation indicated by the horizontal borderline in the vertical section (Figure 5-9) or the vertical borderline on the phase assemblage diagram. This can be interpreted with the infinite phase change rate principle. Correspondingly, the tailing peak represents the liquidus and is created by the formation of (Mg) rather than Al<sub>2</sub>Ca due to the phase amount involvement principle. The phase transformation temperatures detected by the DSC are labeled on the vertical section shown in Figure 5-9. The DSC measurements of sample 2 are in perfect agreement with the calculated phase diagram.

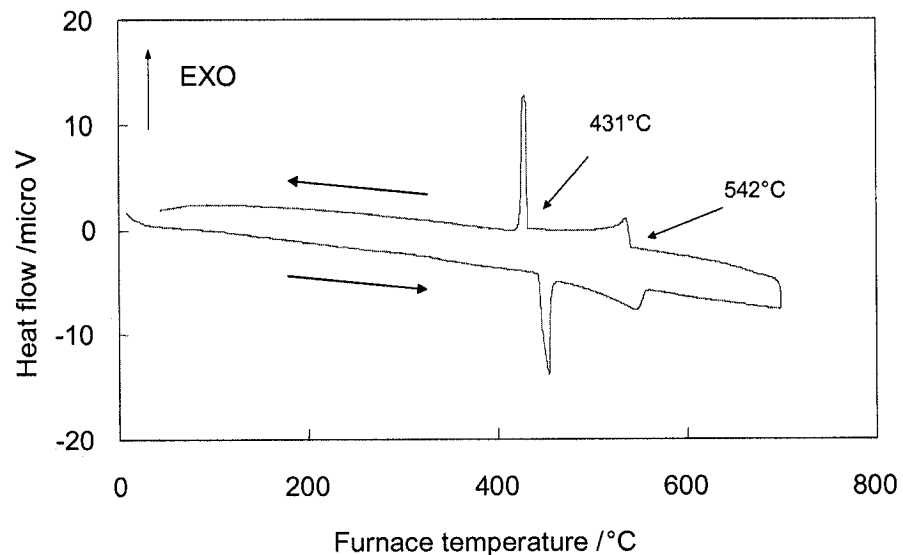


Figure 5-7: DSC spectra of sample 2 (3.59/78.84/17.57 Ca/Mg/Al wt%.)

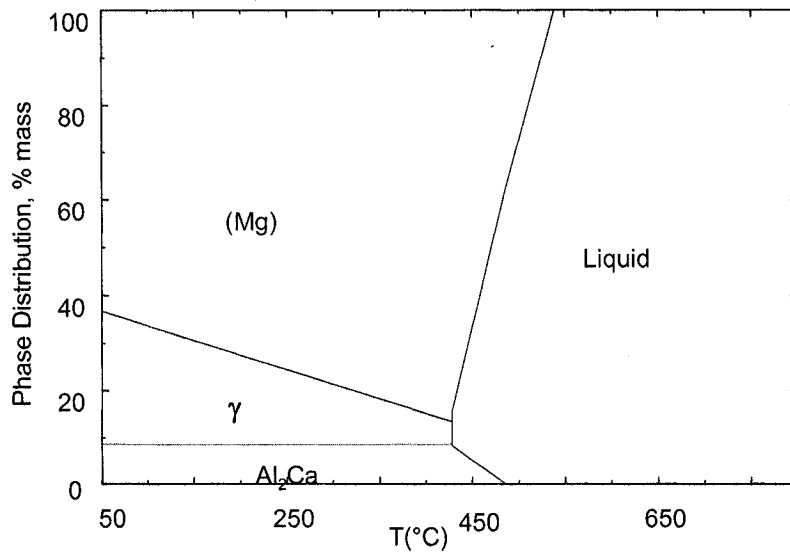


Figure 5-8: Phase assemblage diagram of sample 2 (3.59/78.84/17.57 Ca/Mg/Al wt%)

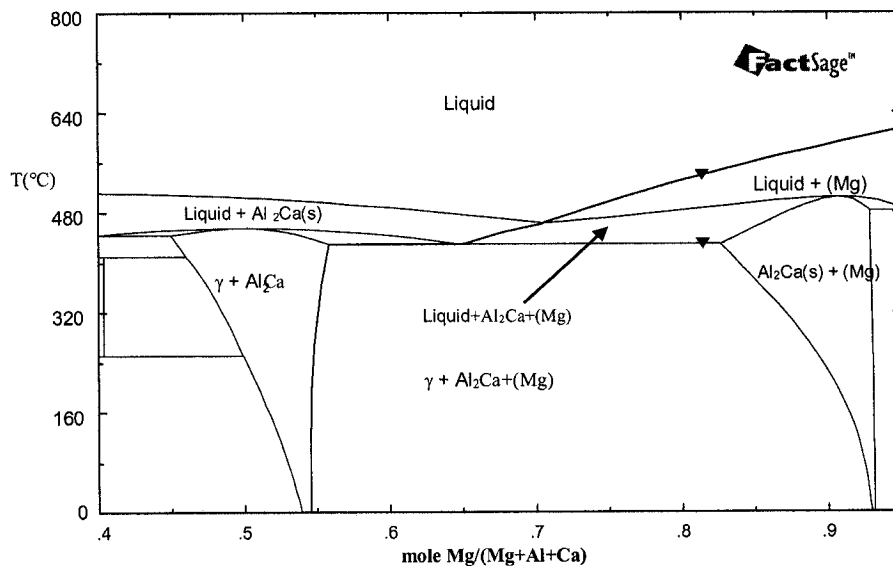


Figure 5-9: The calculated vertical section at constant 2.3 at.% Ca with DSC signals from cooling curve of sample 2

The DSC spectra of sample 3 are illustrated in Figure 5-10. The sharp and high peak at 431°C on the cooling curve corresponds to the eutectic transformation,

represented by  $L = (Mg) + \gamma + Al_2Ca$ , in the phase assemblage diagram (Figure 5-11) according to the infinite phase change rate principle. The onset at 460°C corresponds to the precipitation of (Mg) rather than  $Al_2Ca$  according to the phase amount involvement principle. The experimental results labeled on the vertical section in Figure 5-12 show consistency with the thermodynamic calculations for sample 3.

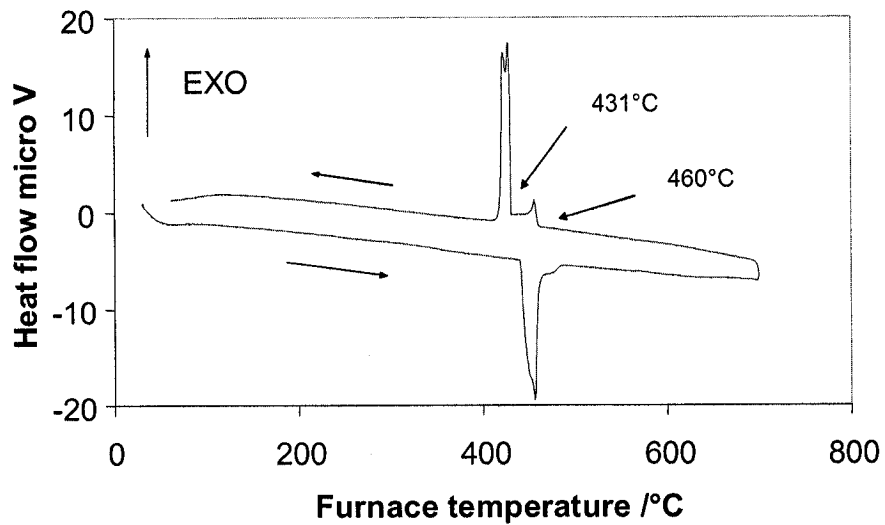


Figure 5-10: DSC spectra of sample 3 (2.50/69.79/27.71 Ca/Mg/Al wt%)

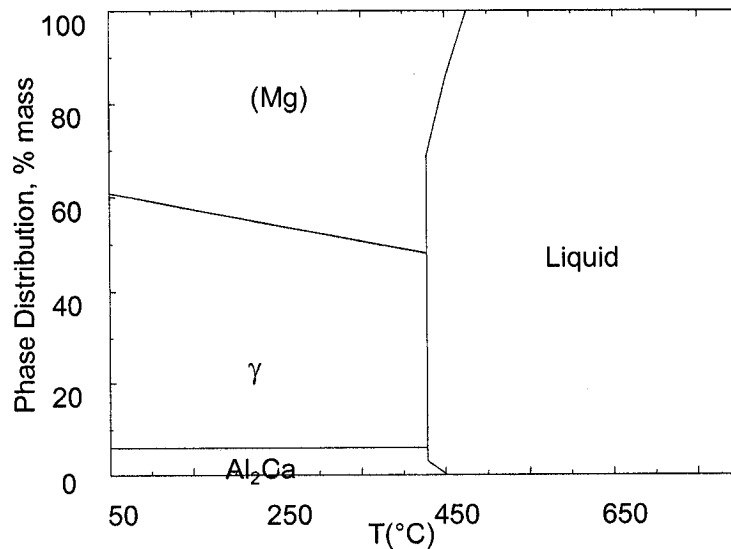


Figure 5-11: Phase assemblage of sample 3 (2.50/69.79/27.71 Ca/Mg/Al wt%)

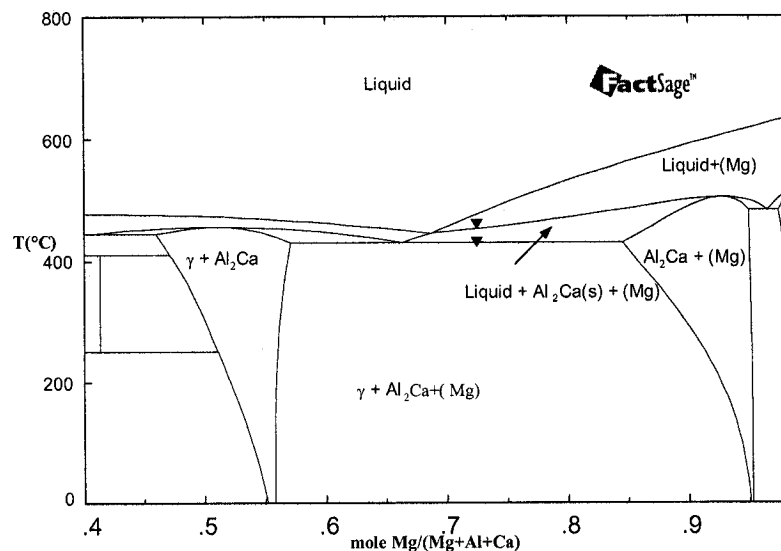


Figure 5-12: The calculated vertical section at constant 1.6 at.% Ca with DSC signals from cooling curve of sample 3.

Referring to the DSC spectra of sample 4 shown in Figure 5-13, the cooling profile shows four thermal events with the onset temperatures at 584, 524, 515, 445°C. Note that the peak at 515°C is partially overlapping with the peak at 524°C, and its temperature is estimated by extrapolation. The sharp peak at 445°C corresponds to an invariant transformation represented by vertical line in the phase assemblage diagram (Figure 5-14) according to the infinite phase change rate principle. The peak at 524°C corresponds to the liquidus according to the phase amount involvement principle. The peak detected in the cooling curve at 584°C is uncertain because of the weak signal. The DSC signals labeled on the vertical section (Figure 5-15) are in good agreement with thermodynamic modeling.

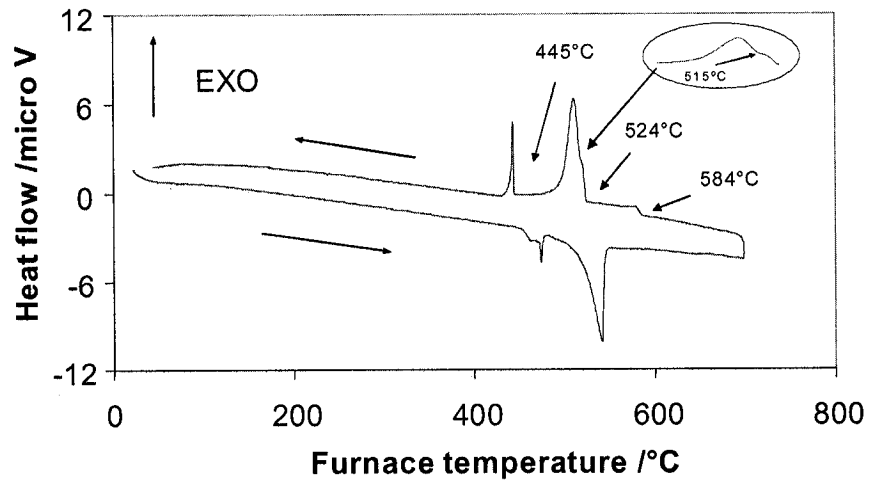


Figure 5-13: DSC spectra of sample 4 (7.09/72.16/20.75 Ca/Mg/Al wt%)

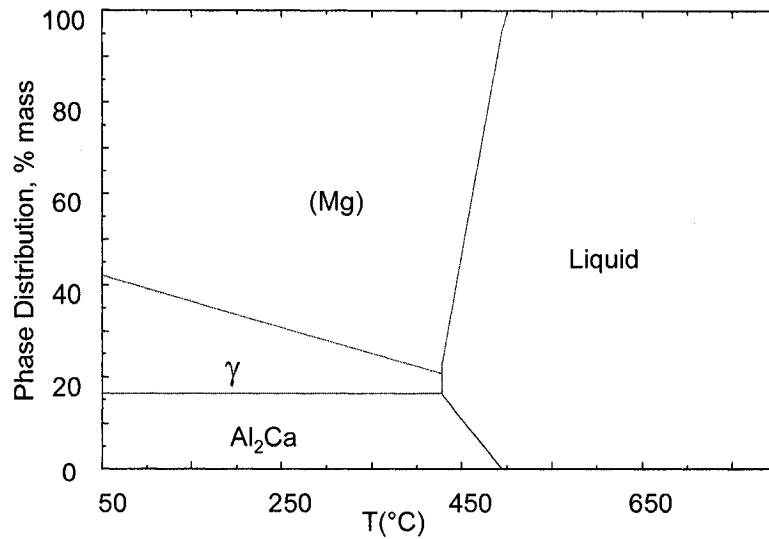


Figure 5-14: Phase assemblage of sample 4 (7.09/72.16/20.75 Ca/Mg/Al wt%)

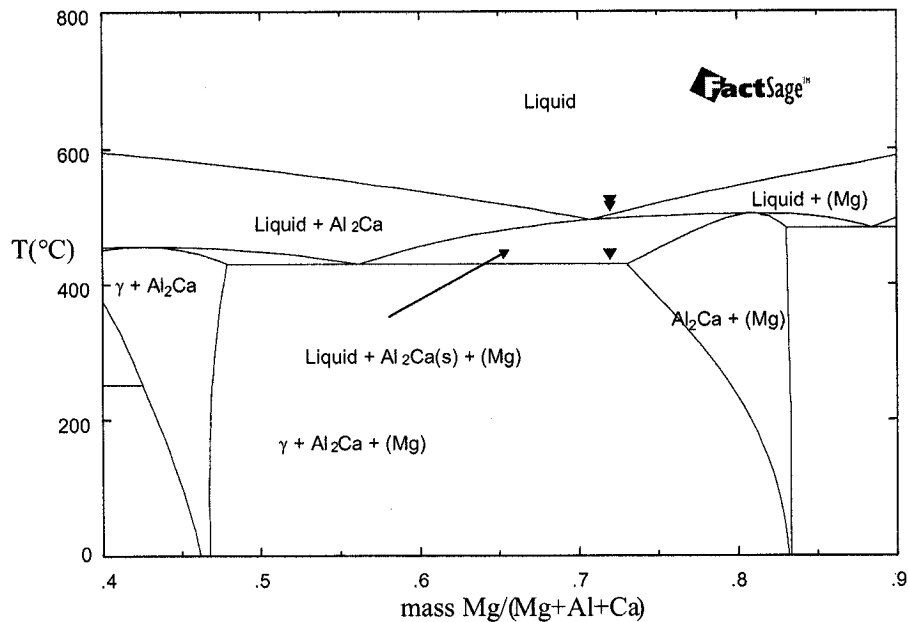


Figure 5-15: The calculated vertical section at constant 7.09 wt% Ca with DSC signals from cooling curve of sample 4

The DSC measurements with thermodynamic calculation of samples 2, 3 and 4 are summarized in Table 5-1.

The XRD patterns of sample 2 and 3 in Figure 5-16 and 5-17 show (Mg) and  $\gamma$  as expected. The  $\gamma$  amount in sample 3 is greater than in sample 2 as indicated by the higher intensity XRD peaks. This agrees with the thermodynamic modeling indicated by the isothermal section in Figure 5-1 since sample 3 is closer to  $\gamma$  than sample 2. The relative amount of  $\gamma$  phase contained in these two samples appears more obviously in the micrographs shown in Figures 5-18 and 5-19.

Analysis of the XRD pattern of sample 2 shows that peaks at 41.78, 33.9, 47.38, 60.64, and 62.14°, ranked according to peak intensity, do not belong to any known phase in the Mg-Al-Ca system. These peaks reoccur in the XRD pattern of the neighbor sample 3 in the same fashion. Therefore, the reproducibility suggests a probable new phase,

named  $\tau_1$  hereafter. However, these peaks did not appear in sample 4. The peaks' intensity in sample 3 is stronger than that in sample 2, suggesting that sample 3 is closer to the composition of this phase. Therefore, the distribution region of this new phase shall be determined around sample 2 and sample 3 but not reaching sample 4. A further work should be done in the future to determine the exact composition range and crystal structure of this phase.

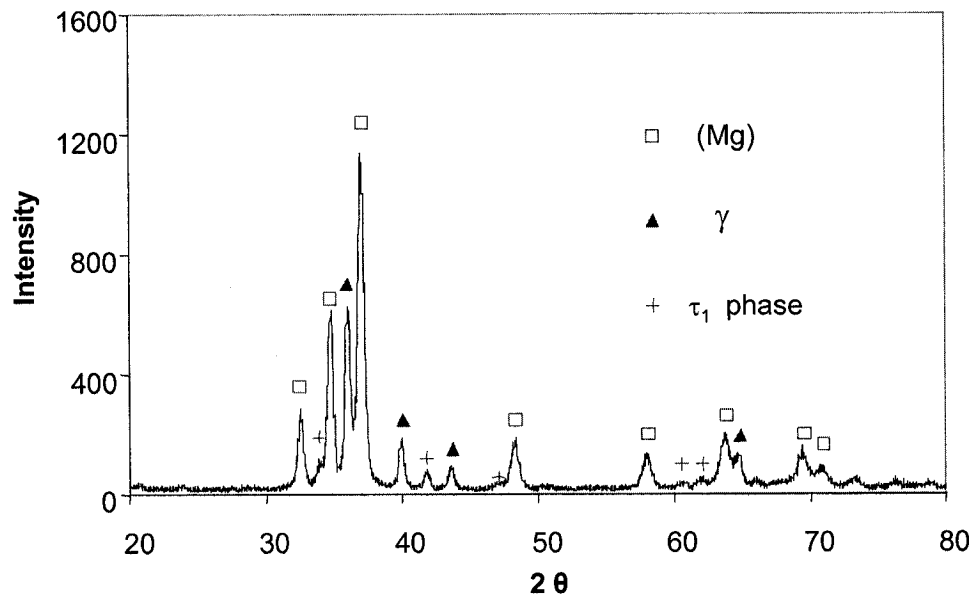


Figure 5-16: XRD pattern of sample 2 (3.59/78.84/17.57 Ca/Mg/Al wt%)

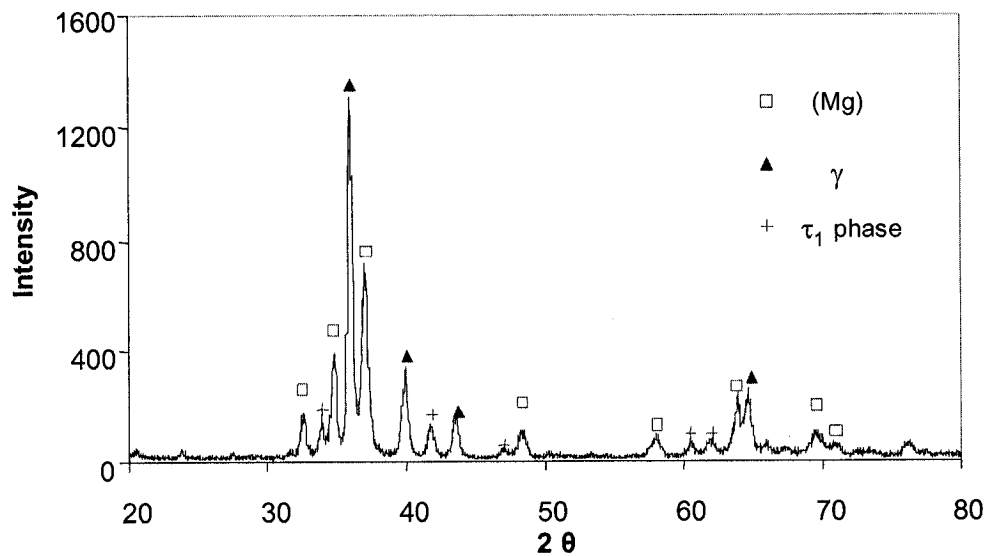


Figure 5-17: XRD pattern of sample 3 (2.50/69.79/27.71 Ca/Mg/Al wt%)



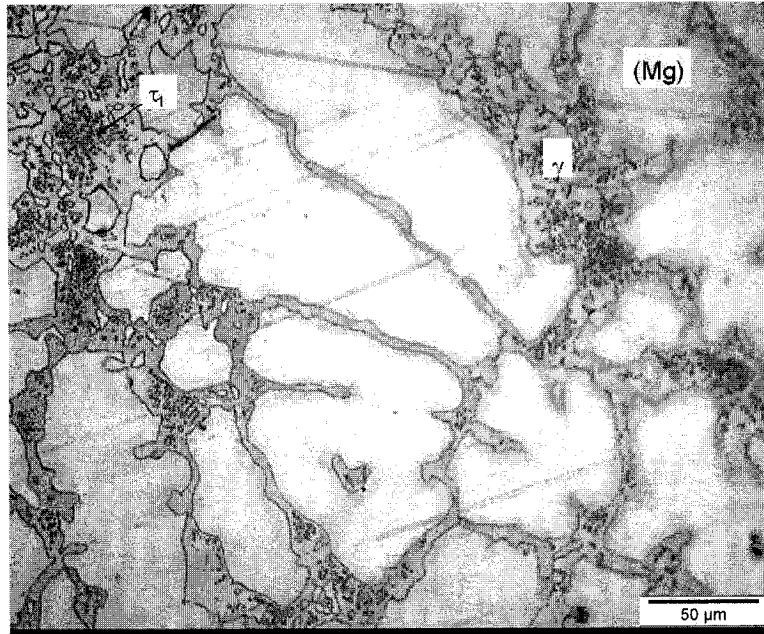


Figure 5-18: Micrograph of sample 2, 500x (3.59/78.84/17.57 Ca/Mg/Al wt%.)

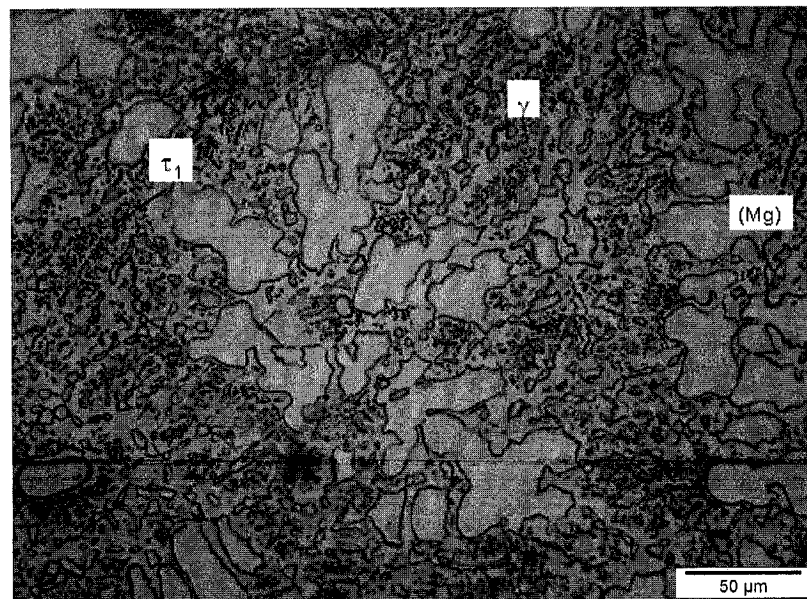


Figure 5-19: Micrograph of sample 3, 500X (2.50/69.79/27.71 Ca/Mg/Al wt%.)

The morphology of  $\tau_1$  phase is tentatively determined using Figures 5-18 and 5-19. Both micrographs show black spots embedded in the  $\gamma$  phase which are more numerous in sample 3 (Figure 5-19) than in sample 2 (Figure 5-18). This is in agreement with the XRD results of these two samples shown in Figures 5-16 and 5-17. Furthermore, these black spots were not observed in other samples like samples 1 and 4 in Figure 5-7 and 5-21 which are in the same phase field but a bit away from  $\tau_1$  area.

The XRD pattern of sample 4 in Figure 5-20 shows clearly the existence of (Mg),  $\text{Al}_2\text{Ca}$  and  $\gamma$ . This is in perfect agreement with the current thermodynamic model. The micrograph in Figure 5-21 also supports the existence of these phases and shows their pronounced amounts. The micrograph shows that the amount of  $\gamma$  phase in this sample is in between sample 2 and 3. This is in perfect agreement with their position in the isothermal section in Figure 5-1, and with the XRD peaks of  $\gamma$  phase in these samples.

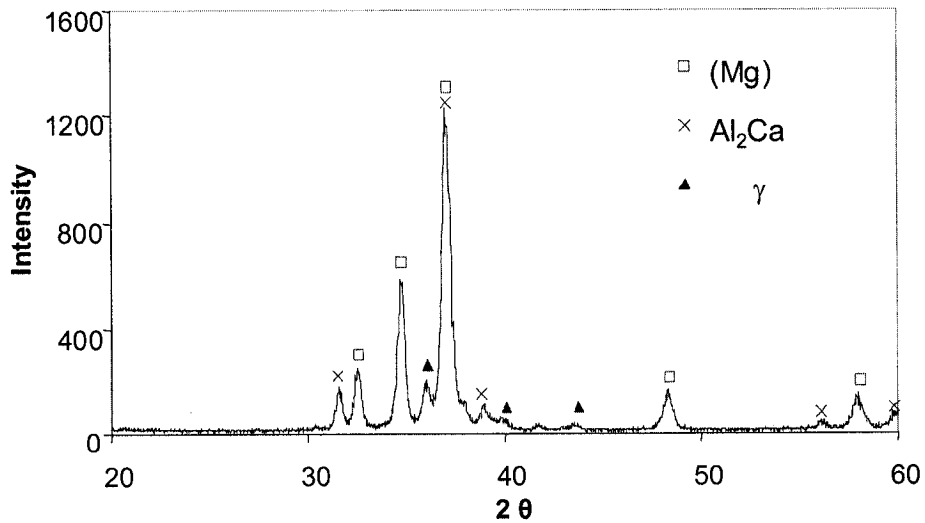
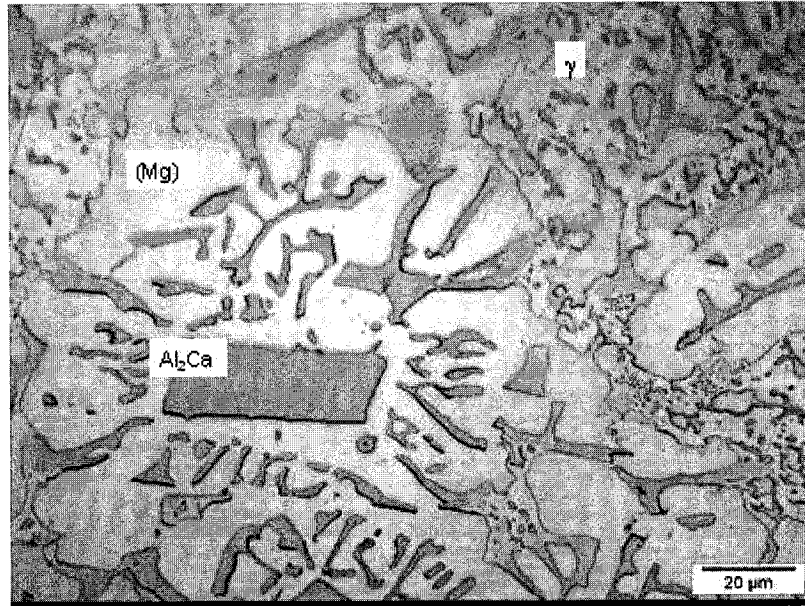


Figure 5-20: XRD pattern of sample 4 (7.09/72.16/20.75 Ca/Mg/Al wt%.)



*Figure 5-21: Optical micrograph of sample 4 1000X  
(7.09/72.16/20.75 Ca/Mg/Al wt%)*

The XRD results with thermodynamic calculations for samples 2, 3 and 4 are summarized in Table 5-2.

### **5.2.3 Results and discussion of sample 5**

Sample 5 is located in the Mg-rich corner. The DSC spectra are shown in Figure 5-22. Two exotherms are in agreement with the thermodynamic modeling. The peak at 524°C, sharp and narrow, corresponds to the transition  $L = (\text{Mg}) + \text{Al}_2\text{Ca}$  as can be seen in the phase assemblage diagram in Figure 5-23. The subsequent peak at 605°C is broader and tailing back to the baseline. Hence, it is interpreted as a univariant transformation corresponding to the liquidus that occurs according to  $L/L + (\text{Mg})$  in the vertical section in Figure 5-24.

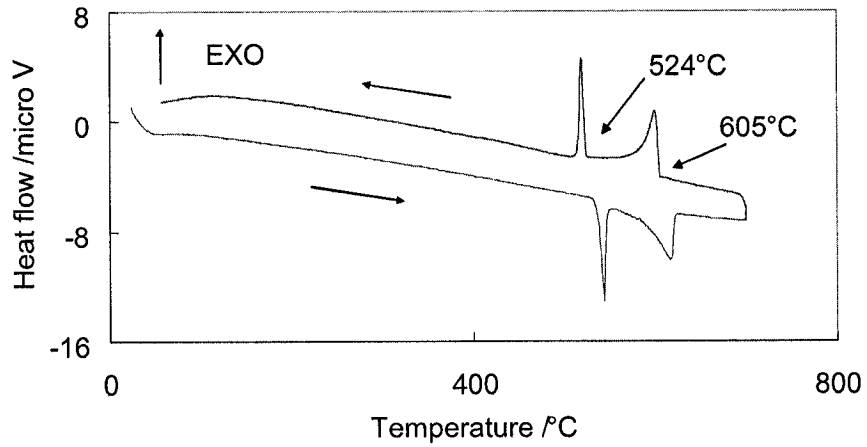


Figure 5-22: DSC spectrum of sample 5 (2.66/92.17/5.17 Ca/Mg/Al wt%)

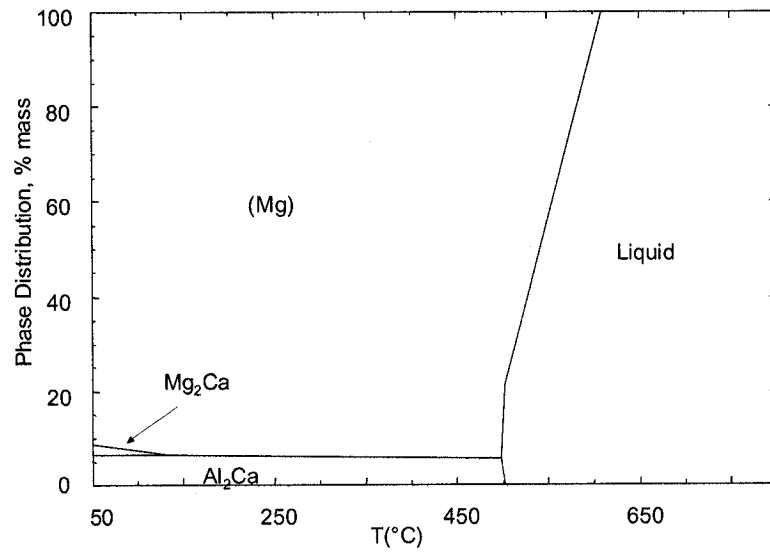


Figure 5-23: Phase assemblage of sample 5 (2.66/92.17/5.17 Ca/Mg/Al wt%)

The DSC measurements labeled on the vertical section in Figure 5-24 show an agreement with the thermodynamic model. The measurements are also summarized in Table 5-1.

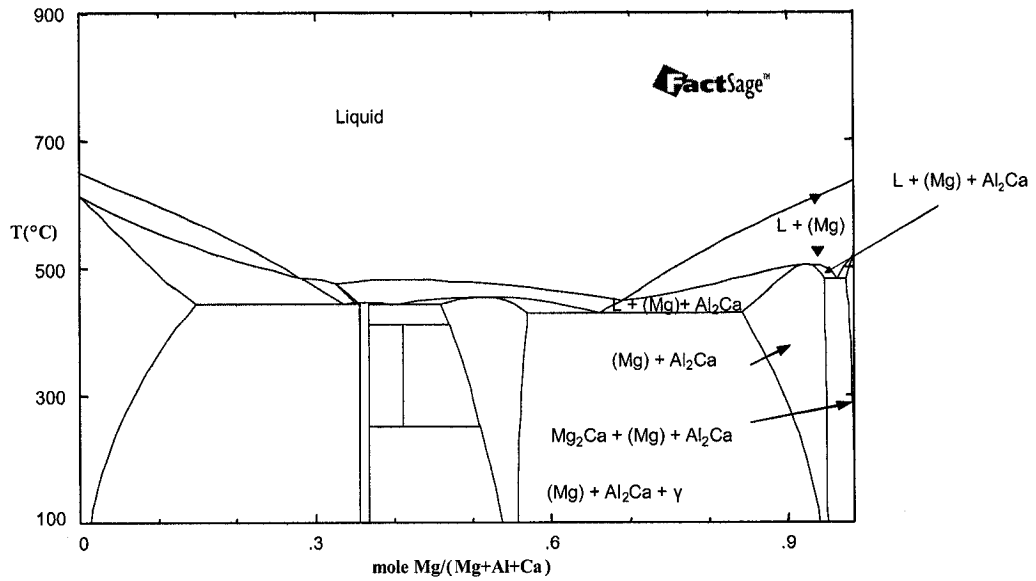


Figure 5-24: The calculated vertical section at constant 1.7at.% Ca with DSC signals from cooling curve of sample 5

The XRD pattern of sample 5 in Figure 5-25 showing stronger peaks for (Mg) than  $\text{Al}_2\text{Ca}$  suggests that (Mg) has greater relative amount than  $\text{Al}_2\text{Ca}$  in this sample. This is in agreement with the phase assemblage diagram shown in Figure 5-23. Also, it can be seen that  $\text{Mg}_2\text{Ca}$  was not detected in the XRD pattern due to its small relative amount.

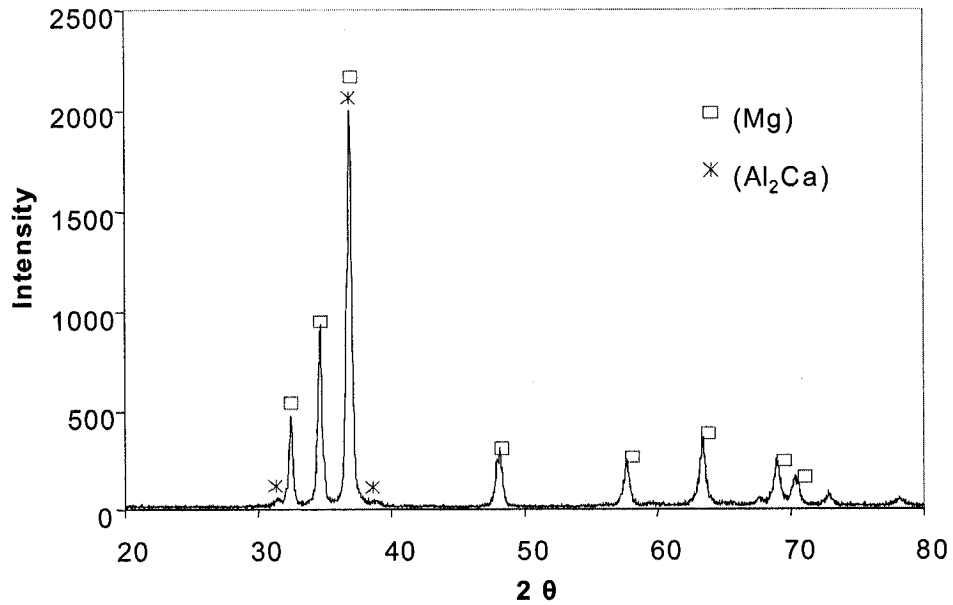
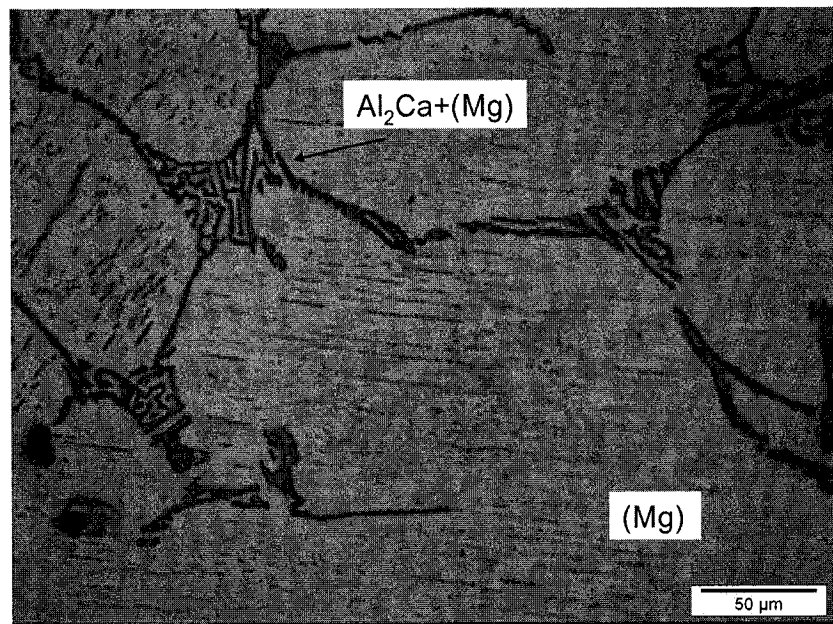


Figure 5-25: XRD pattern of Sample 5 (2.66/92.17/5.17 Ca/Mg/Al wt%.)

The sample's composition is close to GM-C alloy (4.5 wt% Al, 3 wt% Ca) which was studied by Korey *et. al.* [74] using XRD and EDS. They also confirmed the existence of  $\text{Al}_2\text{Ca}$ .

The micrograph of sample 5 in Figure 5-26 shows lamellar structure along the grain boundaries. This is in agreement with the transition  $L = (\text{Mg}) + \text{Al}_2\text{Ca}$  indicated in the phase assemblage diagram shown in Figure 5-23.



*Figure 5-26: Optical micrograph of sample 5, 500X  
(2.66/92.17/5.17 Ca/Mg/Al wt%.)*

## 5.3 Samples in the Mg-Al<sub>2</sub>Ca-Mg<sub>2</sub>Ca phase field

The eight samples chosen in the Mg-Al<sub>2</sub>Ca-Mg<sub>2</sub>Ca region and shown in Figure 5-1 will be discussed in this section.

### 5.3.1 Results and discussion of samples 6 to 9

Firstly, samples 6, 7 and 8 will be discussed together because they have common identified phases, then sample 9 will be discussed. XRD and microstructure results of these samples indicate that (Mg), Mg<sub>2</sub>Ca and Al<sub>2</sub>Ca phases exist in the three samples. These experimental results are coherent and in agreement with their calculated phase assemblage diagrams.

The XRD pattern of sample 6 shows strong peaks for Al<sub>2</sub>Ca but weak peaks for Mg<sub>2</sub>Ca in Figure 5-27. The micrograph of sample 6 in Figure 5-28 displays a large amount of plate-like Al<sub>2</sub>Ca. There is no distinct shape for Mg<sub>2</sub>Ca, and they are probably embedded in the lamellar structure during the invariant transformation that occurs according to  $L = (Mg) + Al_2Ca + Mg_2Ca$  at 480°C as can be seen in the phase assemblage diagram in Figure 5-29. The XRD results showing the relative intensity are consistent with the relative amount of phases shown in Figure 5-29. Further, the lamellar structure appears clearly in Figures 5-28, which is in consistent with the invariant transformation indicated in the phase assemblage. Nevertheless, in the XRD pattern of

sample 6 (Figure 5-27), three unknown peaks were observed and do not seem to belong to any of the phases in this sample.

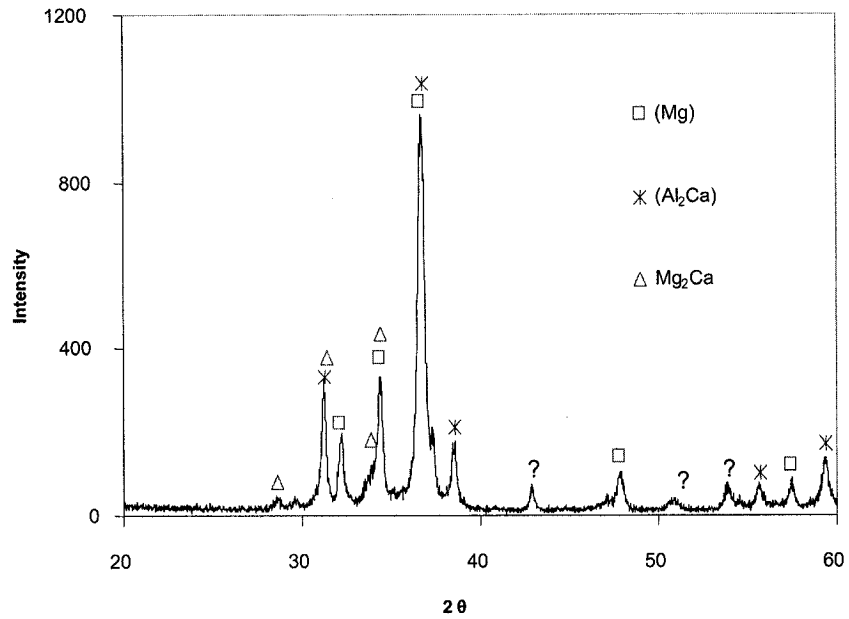


Figure 5-27: XRD pattern of sample 6 (32.68/36.30/31.02 Ca/Mg/Al wt%)

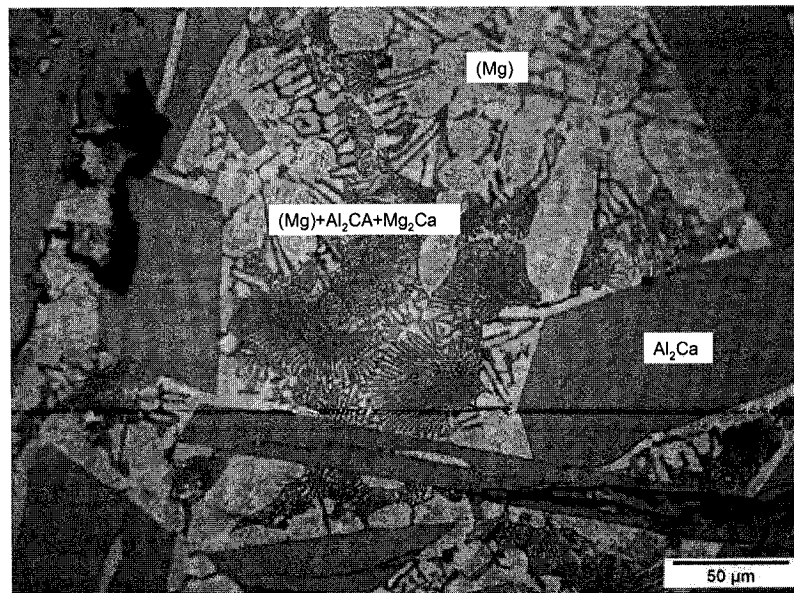


Figure 5-28: Optical microscope of sample 6, 500X  
(32.68/36.30/31.02 Ca/Mg/Al wt%)



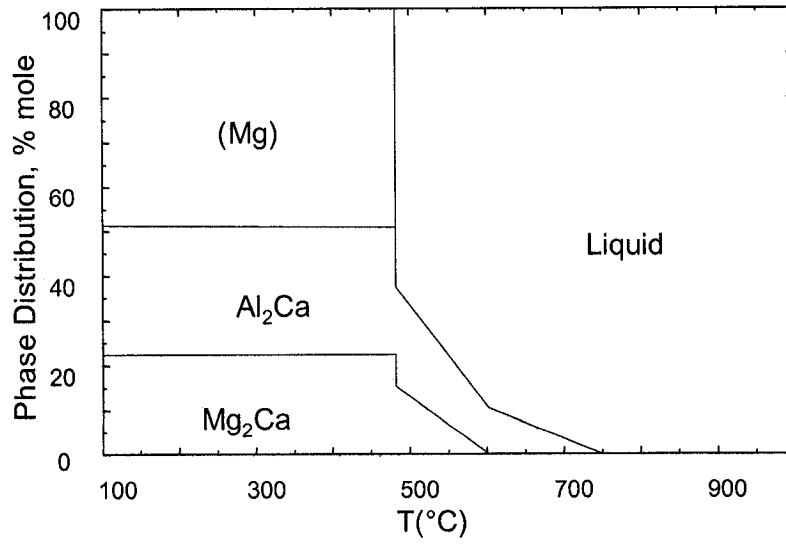


Figure 5-29: Phase assemblage of sample 6 (32.68/36.30/31.02 Ca/Mg/Al wt%.)

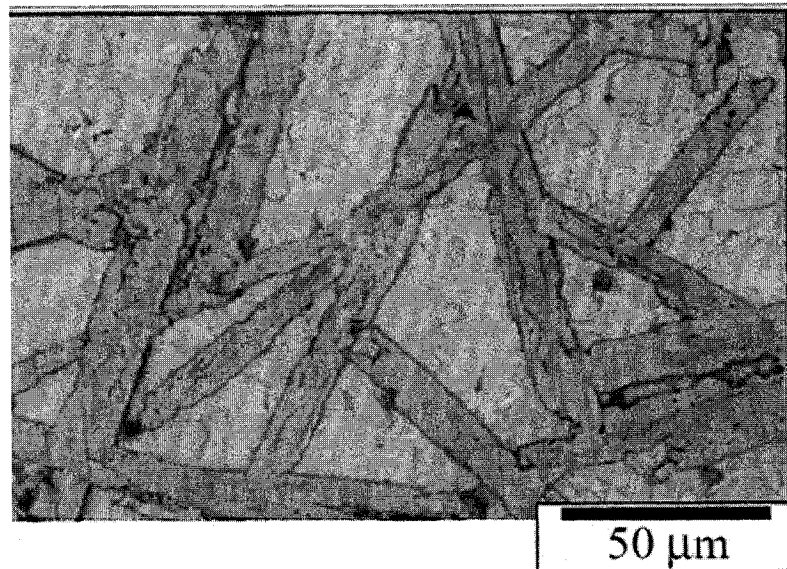


Figure 5-30: Optical micrograph of sample from Gröbner's work [5]

Grönbner *et al.* [5] reported a microstructure (Figure 5-30) of a sample with a chemical composition close to sample 6. It shows a similar micrograph to that of sample 6 in Figure 5-28.

The XRD pattern of sample 7 shows strong peaks for  $Mg_2Ca$  as can be seen in Figure 5-31, which is in contrast to only traces of  $Mg_2Ca$  in sample 6 revealed by Figure 5-27. The micrograph of sample 7 in Figure 5-32 shows several islands of  $Mg_2Ca$ , but no  $Al_2Ca$  plates. This suggests that  $Al_2Ca$  is embedded in the lamellar structure since most of the  $Al_2Ca$  precipitation occurs according to the eutectic reaction  $L = Al_2Ca + Mg_2Ca + (Mg)$  as can be seen in Figure 5-33.

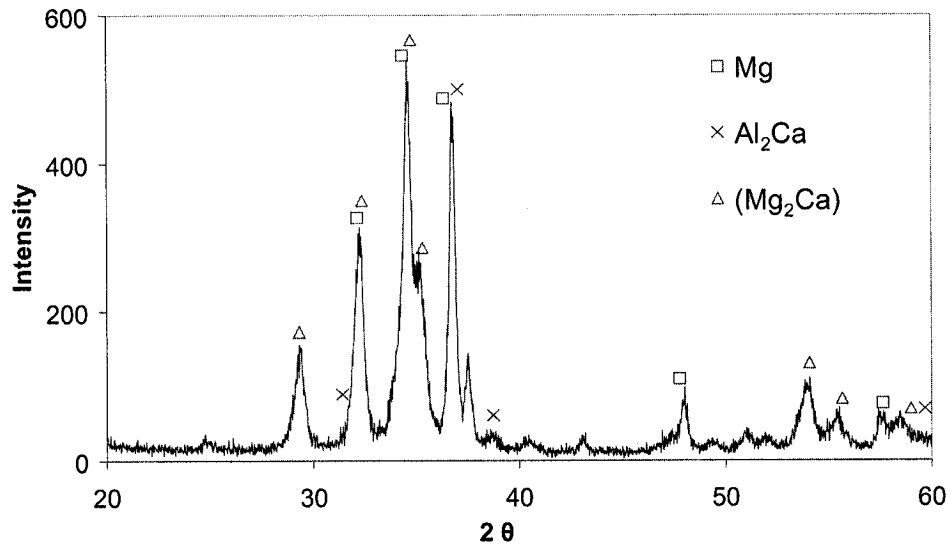


Figure 5-31: XRD pattern of sample 7 (35.62/58.07/6.30 Ca/Mg/Al wt%.)

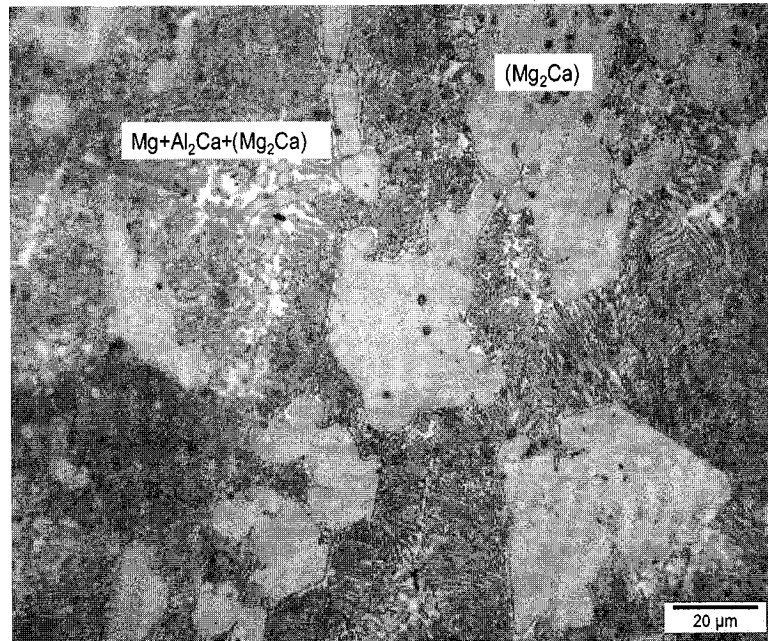


Figure 5-32: Optical micrograph of sample 7, 1000X  
(35.62/58.07/6.30 Ca/Mg/Al wt%)

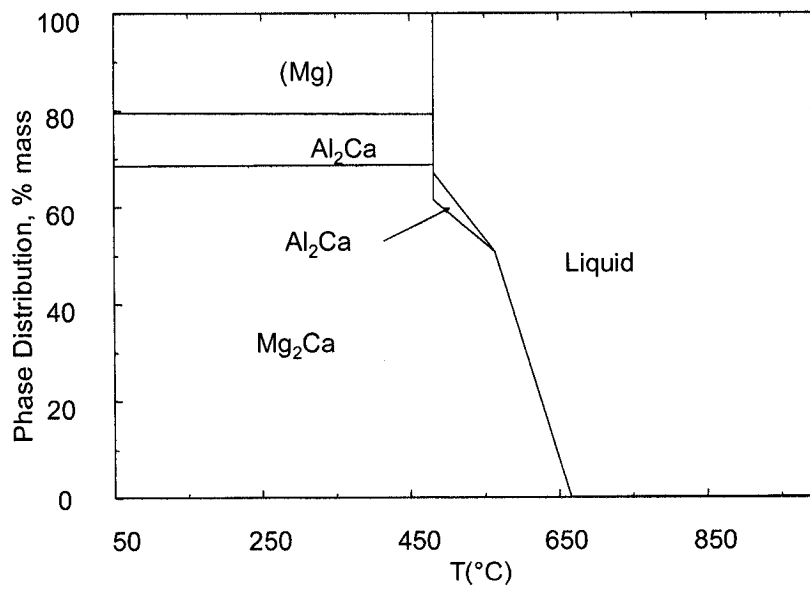


Figure 5-33: Phase assemblage of sample 7 (35.62/58.07/6.30  
Ca/Mg/Al wt%)

In sample 7, the XRD peaks are better matched with the (Mg<sub>2</sub>Ca) solid solution with 22 at.% Al than pure Mg<sub>2</sub>Ca. Therefore, it is confirmed that a ternary solid solution (Mg<sub>2</sub>Ca) exist in this sample.

The XRD pattern of sample 8 in Figure 5-34 shows (Mg), Al<sub>2</sub>Ca and Mg<sub>2</sub>Ca phases. The peaks' intensity of both Al<sub>2</sub>Ca and Mg<sub>2</sub>Ca in sample 8 falls between those of sample 6 and 7. This is expected because sample 8 is located between sample 7 and 6 as can be seen in Figure 5-1. Figure 5-35 presents the micrograph of sample 8 and shows Al<sub>2</sub>Ca clearly, but not Mg<sub>2</sub>Ca. Again, Mg<sub>2</sub>Ca is deemed to be embedded in the lamellar structure occurring due to the eutectic transformation.

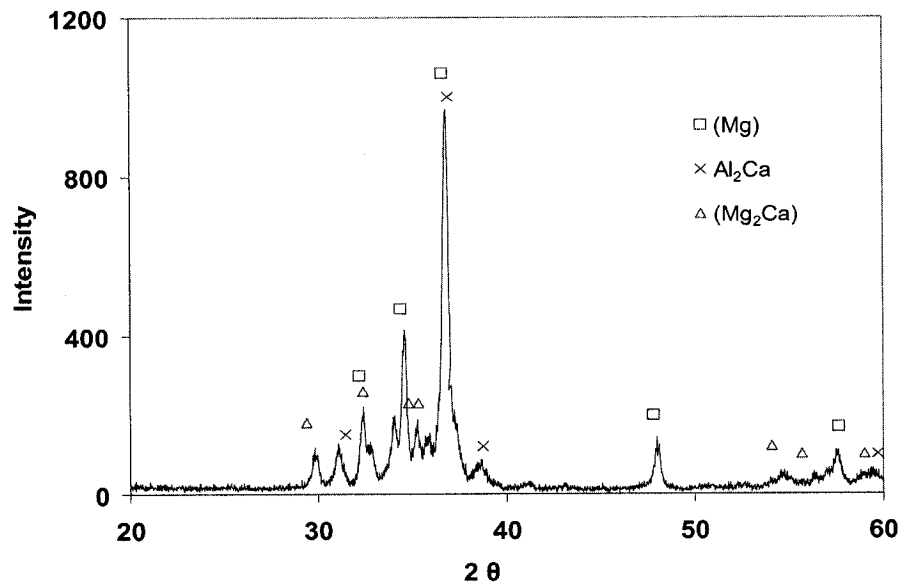


Figure 5-34: XRD pattern of sample 8 (26.16/52.30/21.54 Ca/Mg/Al wt%.)

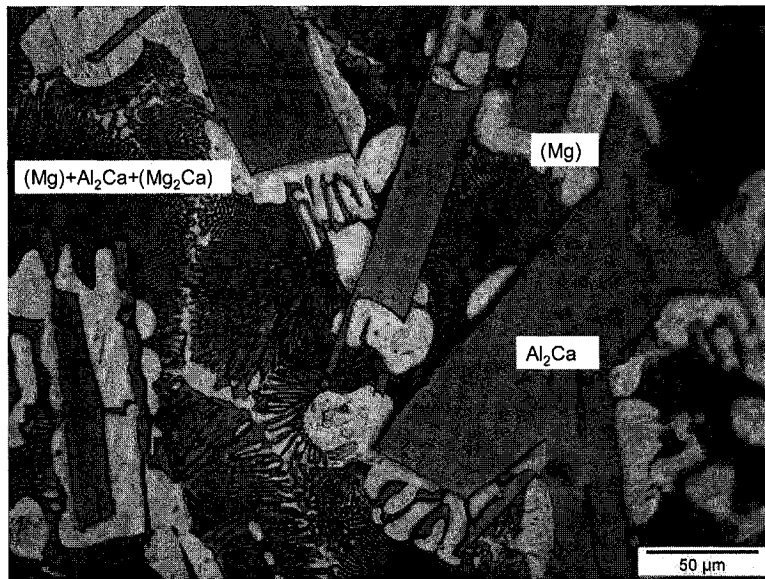


Figure 5-35: Optical micrograph of sample 8, 500X  
(26.16/52.30/21.54 Ca/Mg/Al wt%)

The XRD patterns and micrographs of sample 6, 7 and 8 show the existence of (Mg) with no doubt. This is consistent with their phase assemblage diagrams shown in Figures 5-29, 5-33 and 5-36. The identified and the calculated phases in these samples are summarized in Table 5-3 which suggests a perfect agreement except for  $Mg_2Ca$  being a solid solution rather than a pure compound in sample 7 and 8.

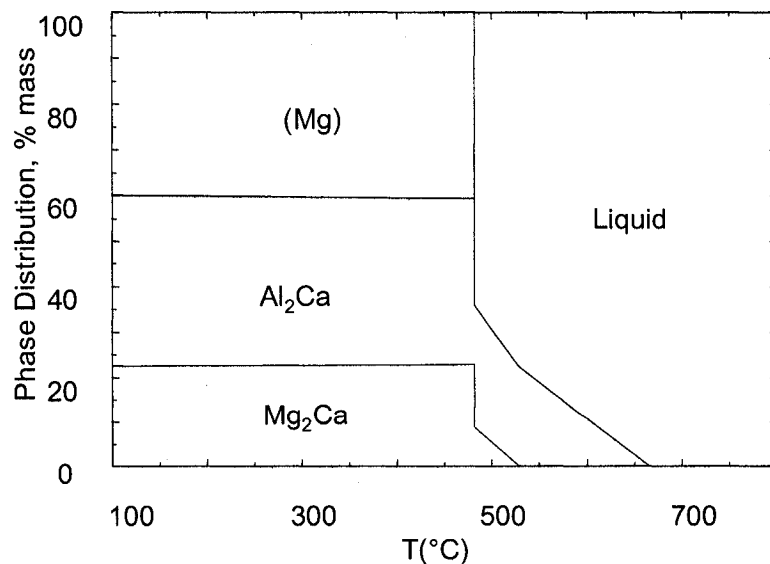


Figure 5-36: Phase assemblage of sample 8 (26.2/52.3/21.5  
Ca/Mg/Al wt%)

Table 5-3 Summary of phase identifications for samples 6, 7 and 8  
in (Mg)-Mg<sub>2</sub>Ca-Al<sub>2</sub>Ca phase field

Samples	Identified phases by XRD	Thermodynamic calculation [14]
6	(Al <sub>2</sub> Ca) + (Mg) + Mg <sub>2</sub> Ca	Al <sub>2</sub> Ca + (Mg) + Mg <sub>2</sub> Ca
7	(Mg <sub>2</sub> Ca) + (Mg) + Al <sub>2</sub> Ca	Al <sub>2</sub> Ca + (Mg) + Mg <sub>2</sub> Ca
8	(Mg) + (Mg <sub>2</sub> Ca) + Al <sub>2</sub> Ca	(Mg) + Mg <sub>2</sub> Ca + Al <sub>2</sub> Ca

The DSC results of samples 6, 7 and 8 are shown in Figures 5-37, 5-38 and 5-39, respectively. These diagrams display common features. The sharp and strong peaks occurring at 512, 514 and 519°C, respectively, correspond to the eutectic transformation according to the infinite phase change principle, and that can be expressed as  $L = (Mg) + Al_2Ca + Mg_2Ca$  according to their phase assemblage diagrams in Figure 5-29, 5-33 and 5-36. These DSC patterns also show that the liquidus temperatures are 772, 621°C for samples 6, and 7, respectively.

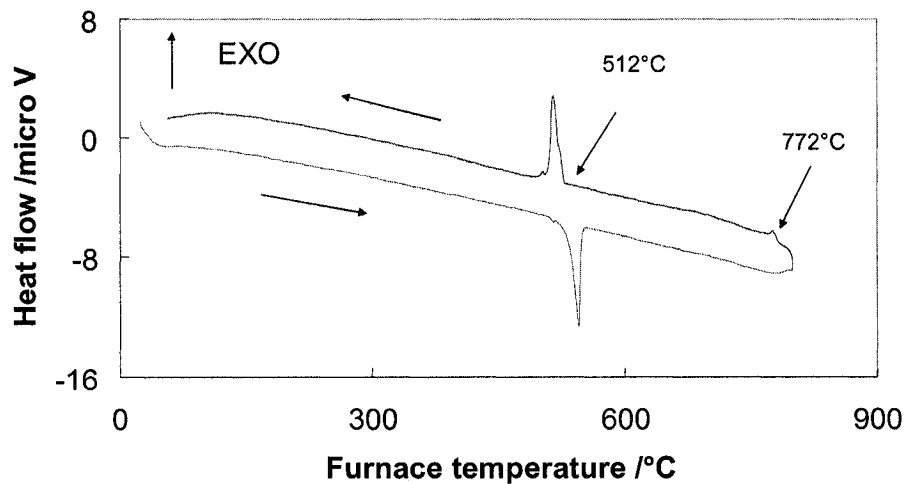


Figure 5-37: DSC spectra of sample 6 (32.68/36.30/31.02 Ca/Mg/Al wt%)

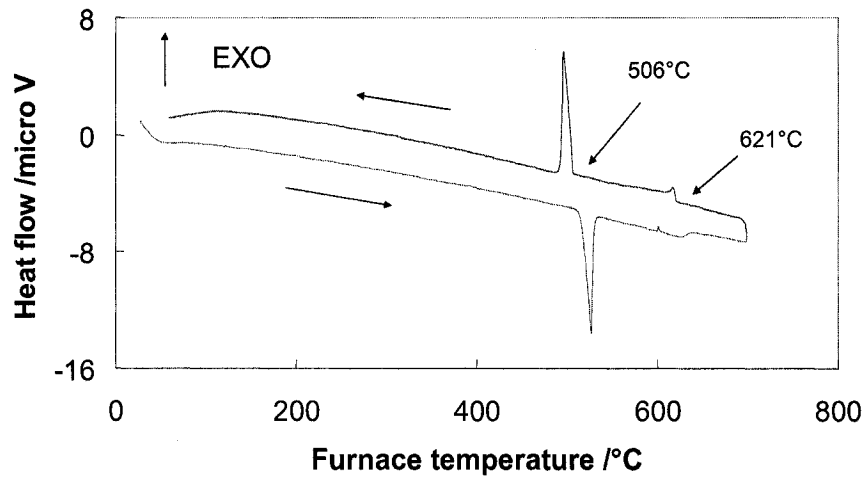


Figure 5-38: DSC spectra of sample 7 (35.62/58.07/6.30 Ca/Mg/Al wt%)

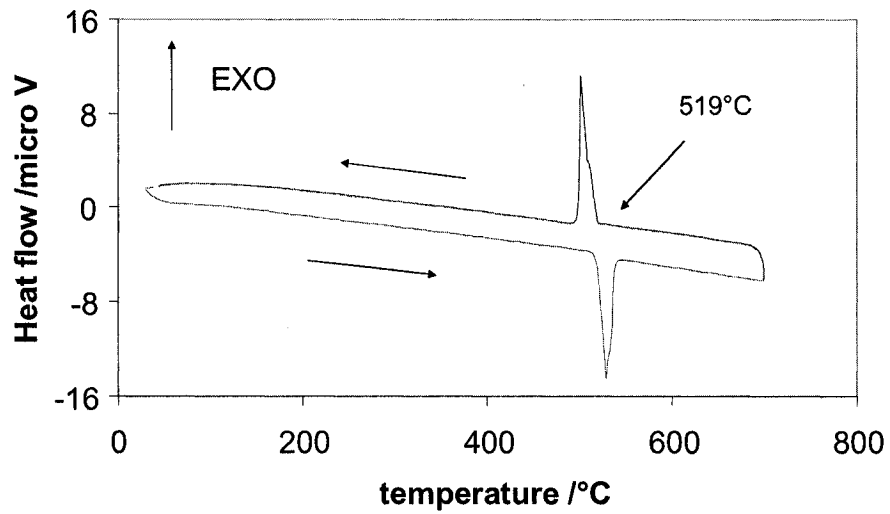


Figure 5-39: DSC spectra of sample 8 (26.16/52.30/21.54 Ca/Mg/Al wt%)

The DSC results of samples 6, 7 and 8 are summarized in Table 5-4, and labeled on the vertical sections in Figures 5-40 and 5-41, respectively. Agreement between the experimental results and thermodynamic calculations can be seen in these figures for

sample 6 and 7. The melting of sample 8 occurs at a higher temperature than 700°C and this is why it was not registered in the DSC spectra shown in Figure 5-39.

Table 5-4 The DSC measurements with thermodynamic calculation in (Mg)-Mg<sub>2</sub>Ca-Al<sub>2</sub>Ca phase field for samples 6, 7 and 8 (c: denotes cooling and h: denotes heating)

DSC measurements Sample	DSC Thermal Signals (°C)	Thermodynamic calculation based on the database reported in [14]	
		Temp.(°C)	Reactions or phase boundary
6	516h/512c	481	(Mg) + Al <sub>2</sub> Ca + Mg <sub>2</sub> Ca/Al <sub>2</sub> Ca + Mg <sub>2</sub> Ca + L
	-	600	Al <sub>2</sub> Ca + Mg <sub>2</sub> Ca + L/Al <sub>2</sub> Ca + L
	772c	748	Al <sub>2</sub> Ca/L
7	512h/506c	480	(Mg) + Al <sub>2</sub> Ca + Mg <sub>2</sub> Ca/Al <sub>2</sub> Ca + Mg <sub>2</sub> Ca + L
	-	569	Al <sub>2</sub> Ca + Mg <sub>2</sub> Ca + L/Al <sub>2</sub> Ca + L
	640h /621c	650	Al <sub>2</sub> Ca/L
8	514h/519 c	482	Al <sub>2</sub> Ca + (Mg) + Mg <sub>2</sub> Ca/L + Al <sub>2</sub> Ca + Mg <sub>2</sub> Ca
	-	631	L + Al <sub>2</sub> Ca + Mg <sub>2</sub> Ca/ L + Al <sub>2</sub> Ca
	-	666	L + Al <sub>2</sub> Ca/L

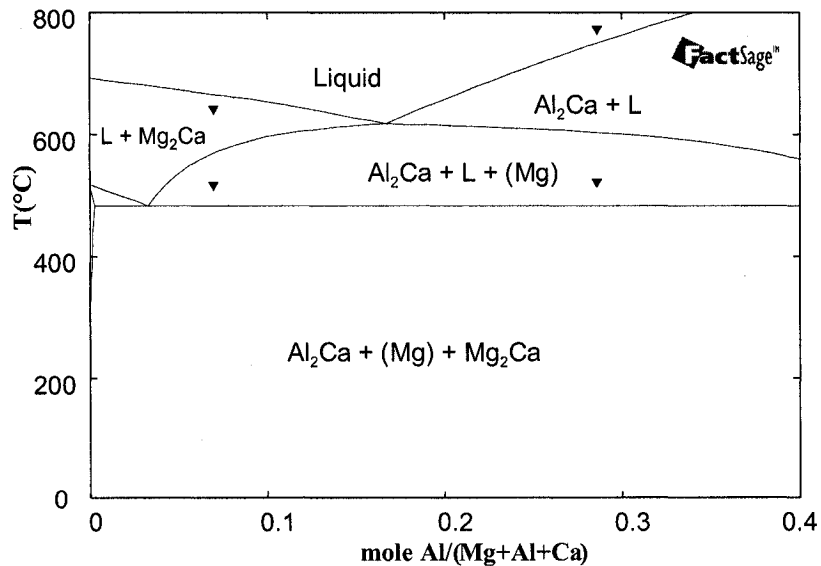


Figure 5-40: The calculated vertical section at constant 25.3 at.% Ca with DSC signals from cooling curve of samples 7 (left) and 6 (right)



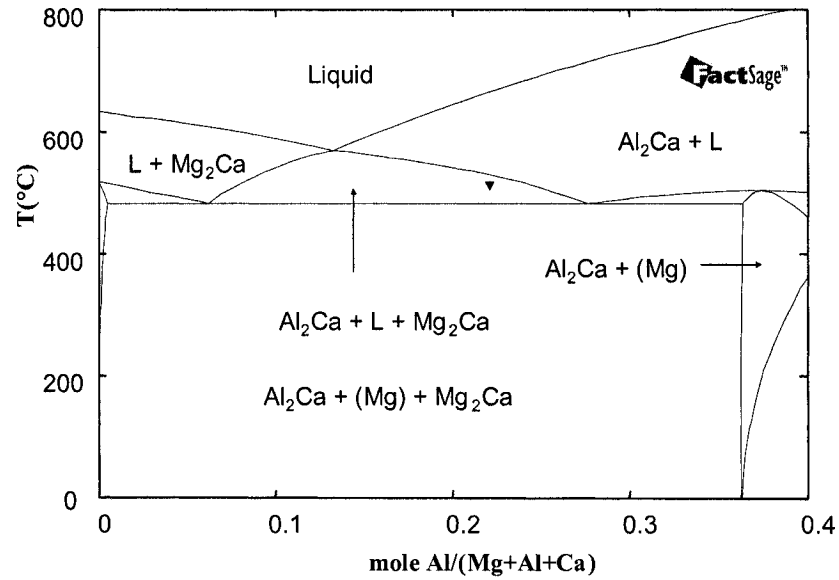


Figure 5-41: The calculated vertical section at constant 18.1 at.% Ca with DSC signals from cooling curve of sample 8

Sample 9 is close to the  $\text{Mg}_2\text{Ca}$ - $\text{Al}_2\text{Ca}$  borderline in Figure 5-1. The XRD pattern in Figure 5-42 reveals  $\text{Mg}_2\text{Ca}$ , (Mg) and  $\text{Al}_2\text{Ca}$ , which is in agreement with the phase assemblage diagram in Figure 5-43. Further, this figure shows the large relative amount of  $\text{Mg}_2\text{Ca}$ , which is reflected in the XRD pattern. In this Figure, the intensity is low in general, which resulted in higher background noise.

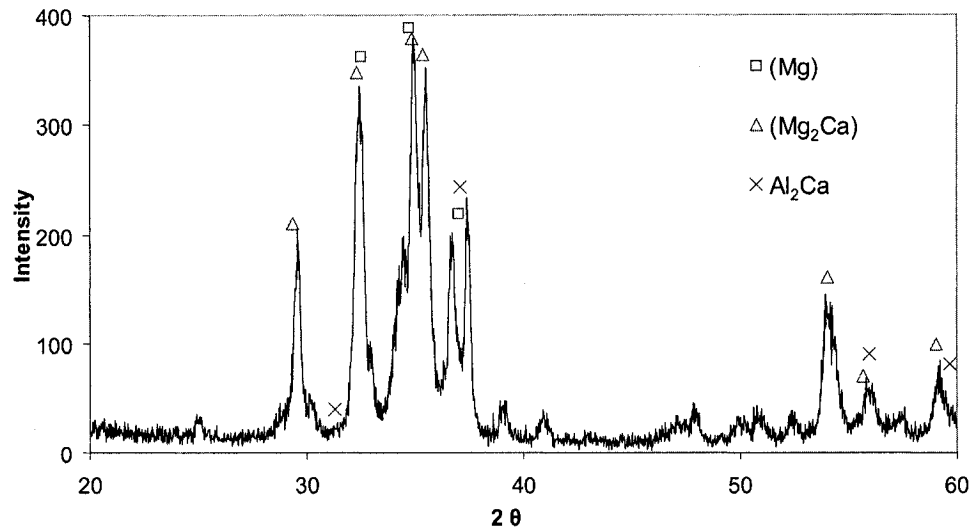


Figure 5-42: XRD pattern of sample 9 (42.32/42.29/15.39 Ca/Mg/Al wt%)

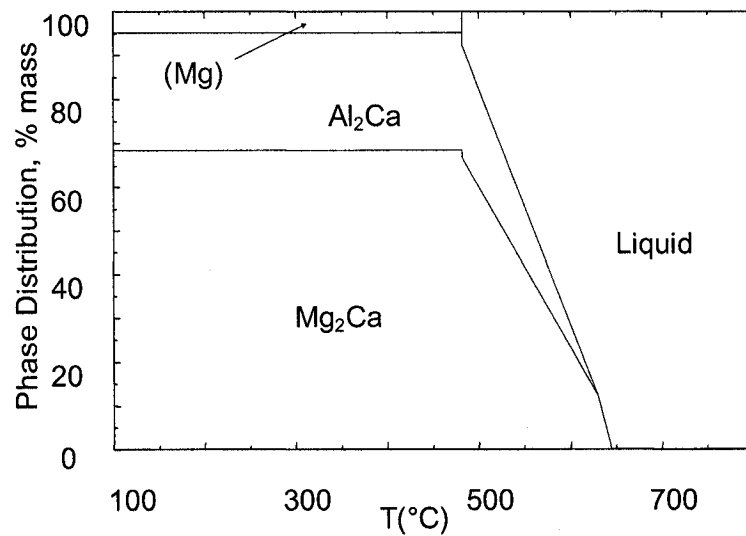


Figure 5-43: Phase assemblage of sample 9 (42.32/42.29/15.39 Ca/Mg/Al wt%)

The DSC curves of sample 9 in Figure 5-44 shows a single peak at 506°C. It corresponds to the transformation  $L + Al_2Ca + Mg_2Ca / (Mg) + Al_2Ca + Mg_2Ca$  that can be

seen in the phase assemblage diagram presented in Figure 5-43 and the vertical section in Figure 5-45. Melting of this sample was not observed by heating up to 700 °C.

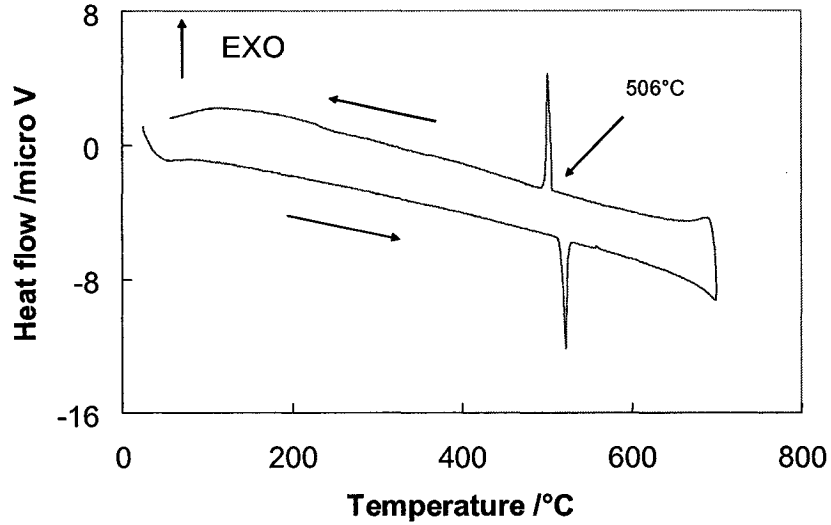


Figure 5-44: DSC spectrum of sample 9 (42.32/42.29/15.39 Ca/Mg/Al wt%)

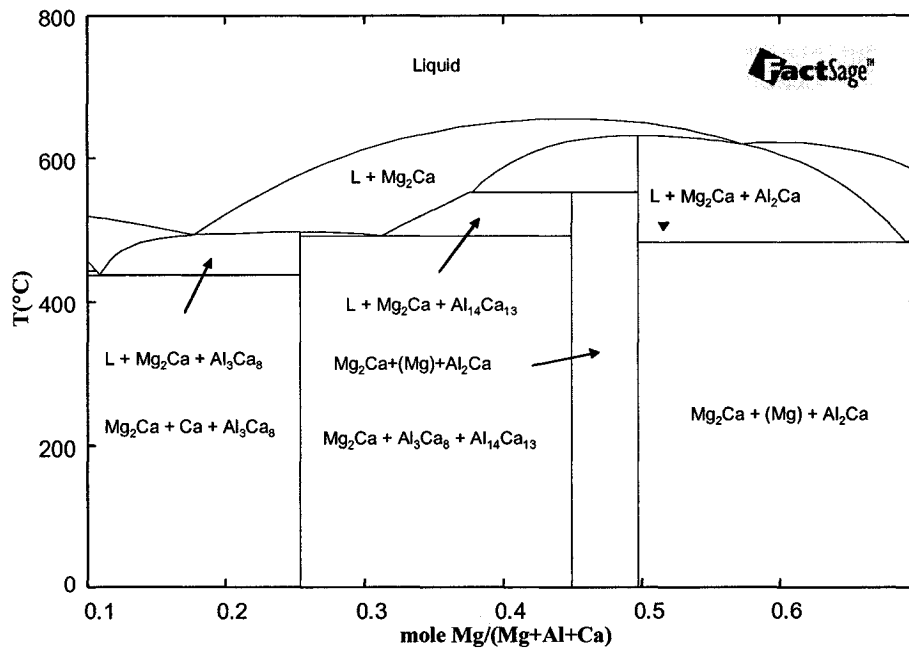


Figure 5-45: The calculated vertical section at constant 16.9 at. % Al with DSC signals from cooling curve of sample 9

### 5.3.2 Investigation of the eutectic point in the Mg-rich corner

One eutectic point in Mg-Mg<sub>2</sub>Ca-Al<sub>2</sub>Ca field can be investigated through examining samples 10 to 13.

Sample 10 was prepared with the calculated composition of the eutectic point predicted by thermodynamic modeling. The phase assemblage diagram in Figure 5-46 shows the eutectic transformation, i.e. liquid phase transforms into three phases simultaneously (L/(Mg) + Al<sub>2</sub>Ca + Mg<sub>2</sub>Ca) during cooling.

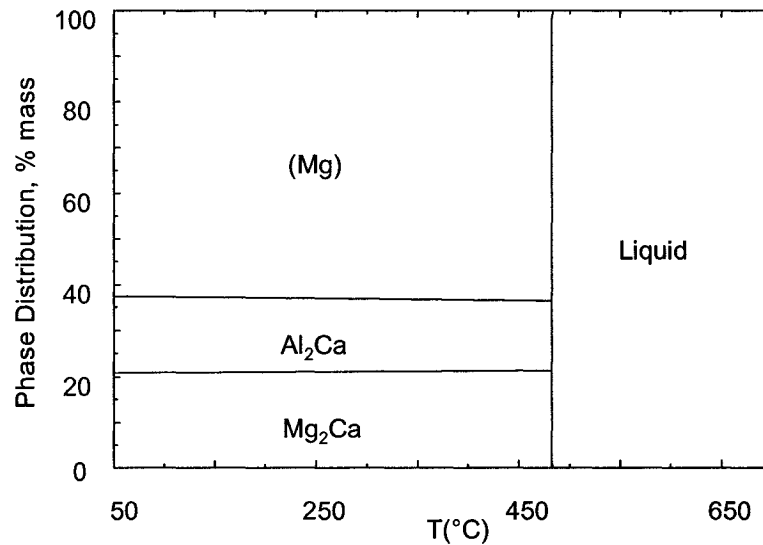


Figure 5-46: Phase assemblage of sample 10 (16.44/73.61/9.95 Ca/Mg/Al wt%)

The DSC spectra of sample 10 in Figure 5-47 shows a sharp, narrow and unique peak. This indicates the infinite heat transfer that occurs during an invariant transformation. If a lower heating/cooling rate and less mass sample are employed, it is expected to observe a narrower and sharper peak. This eutectic temperature was

measured as 512°C using the DSC, however the thermodynamic calculations show that this transformation is predicted at lower temperature of 483°C as can be seen in Figures 5-46 or 5-48. Labeling the DSC measurements of sample 10 along with sample 11 in Figure 5-48 shows the consistency of the experimental results. Additionally, the adjacent samples 11, 12 and 13 support this finding and will be discussed in this section.

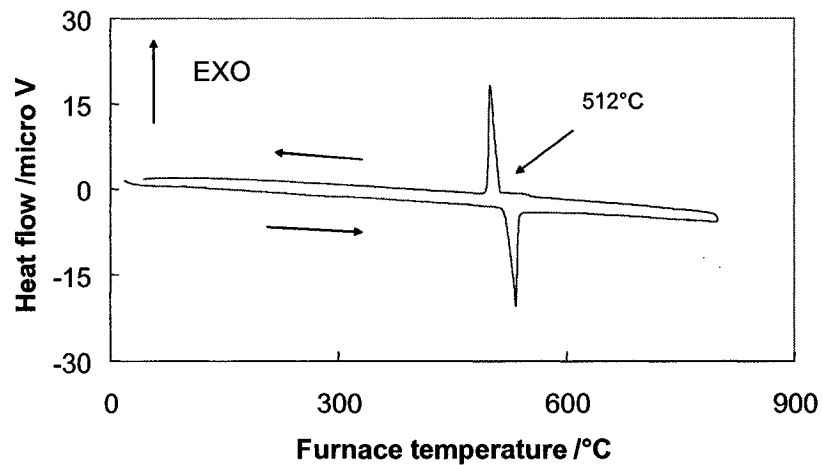


Figure 5-47: DSC spectra of sample 10 (16.44/73.61/9.95 Ca/Mg/Al wt%)

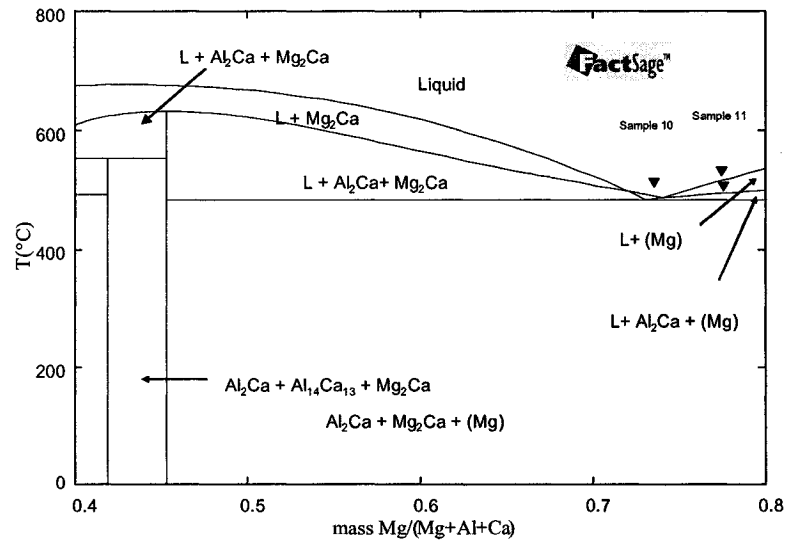


Figure 5-48: The calculated vertical section at constant 9.9 wt% Ca with DSC signals from cooling curve of sample 10 and sample 11

The optical micrograph of sample 10 in Figure 5-49 shows dominated typical lamellar eutectic feature and some plate-like precipitates. This indicates the sample is quite close to the eutectic composition.

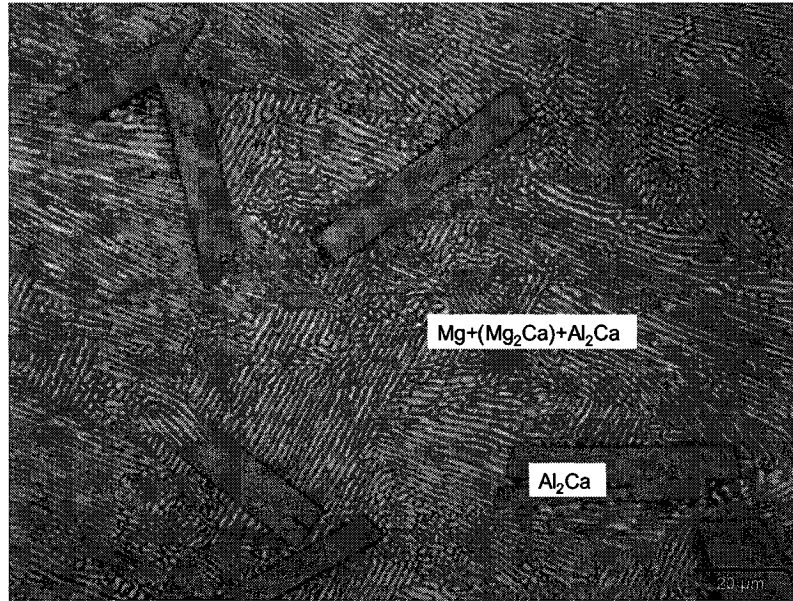


Figure 5-49: Optical micrograph of sample 10, 1000X (16.44/73.61/9.95 Ca/Mg/Al wt%.)

The XRD pattern in Figure 5-50 shows the coexistence of the (Mg),  $\text{Al}_2\text{Ca}$  and  $\text{Mg}_2\text{Ca}$  phases. This is in agreement with the phase assemblage shown in Figure 5-46.

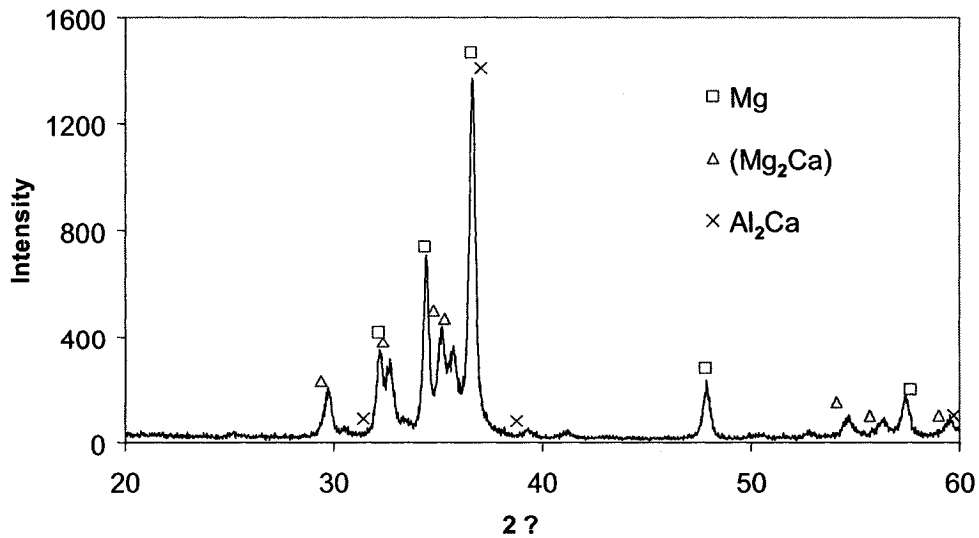


Figure 5-50: XRD pattern of sample 10 (16.44/73.61/9.95 Ca/Mg/Al wt%.)

Therefore, it is concluded that sample 10 has a eutectic temperature at 512°C. The sample composition 16.44 wt% Ca, 73.61 wt% Mg and 9.95 wt% Al (or 10.8 at.%Ca 79.5 at.%Mg and 9.7 at.%Al) is quite close to the eutectic composition in accord with the results of the DSC, XRD, microscope and thermodynamic modeling.

This eutectic composition and temperature was also reported by other researchers. Portnoi and Spektorova [75] reported that the eutectic was located at 9 at.% Al, 79 at.% Mg. The report on the Dow Chemical [76] confirmed the eutectic nature in Mg-Al<sub>2</sub>Ca section and placed the eutectic composition between 74 and 83 at.% Mg with a eutectic temperature of 535°C. The photomicrographs [76] of alloys with 74 and 83 at.% Mg support the occurrence of a eutectic at 78-79 at.% Mg. The results in this work are also quite close to what was found by Tkachenko *et al.* [17] who reported that the ternary eutectic L<sub>E</sub> = (Mg) + Mg<sub>2</sub>Ca + Al<sub>2</sub>Ca occurs at the composition 18.2 wt% Ca, 72 wt% Mg and 9.2 wt% Al (or 12.1 at.% Ca, 78.8 at.% Mg and 9.1 at.% Al), and at temperature 510°C.

The locations of samples 11, 12 and 13 are represented in Figure 5-1. The discussion of the experimental results of these samples along with sample 7 (discussed earlier) can further validate the accordance of this eutectic transformation.

The XRD pattern of sample 11 in Figure 5-51 displays the phases (Mg), (Mg<sub>2</sub>Ca) and Al<sub>2</sub>Ca. The identified phases are in agreement with the phase assemblage shown in Figure 5-52 except that the shift of (Mg) and (Mg<sub>2</sub>Ca) peaks indicating their existence in the form of solid solution.

The optical micrograph of sample 11 in Figure 5-53 is consistent with the solidification process illustrated by the calculated vertical section in Figure 5-55. The dendrites are primary (Mg) corresponding to the reaction  $L \rightarrow L + (Mg)$ . The interdendritic lamellae are composed of (Mg),  $(Mg_2Ca)$  and  $Al_2Ca$  that formed due to the eutectic reaction  $L \rightarrow (Mg) + Al_2Ca + (Mg_2Ca)$ . The dendrite morphology can be seen more clearly in Figure 5-54.

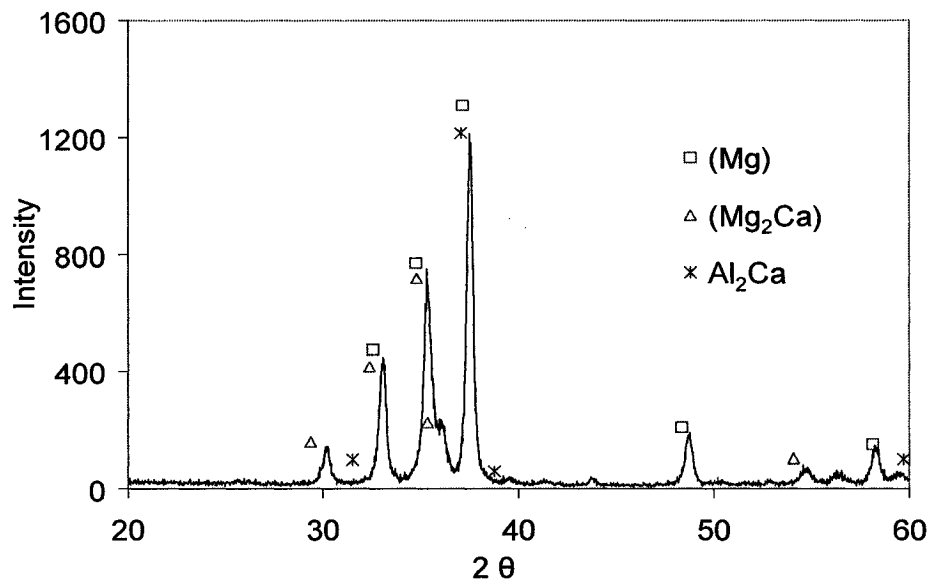


Figure 5-51: XRD pattern of sample 11 (12.65/77.46/9.89 Ca/Mg/Al wt%.)

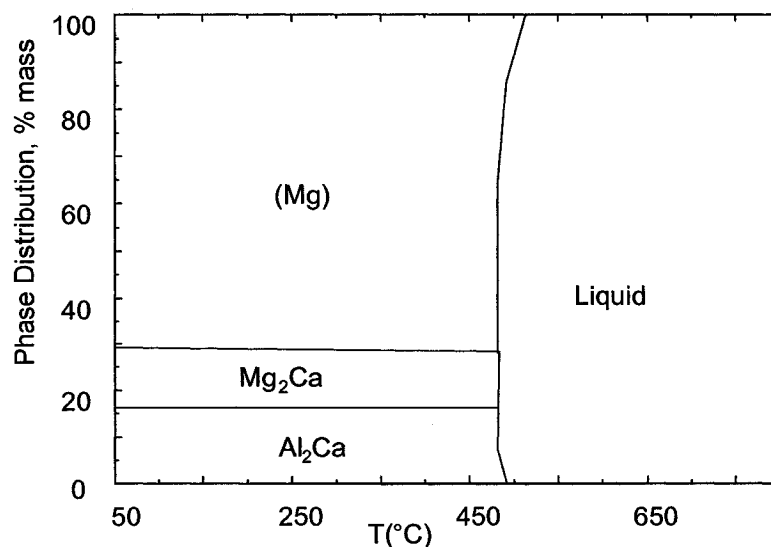


Figure 5-52: Phase assemblage of sample 11 (12.65/77.46/9.89 Ca/Mg/Al wt%.)



A similar statement was also reported by Suzuki *et al.* [77] and Pekguleryuz and Kaya [78]. It was stated that  $Mg_2Ca$  and/or  $Al_2Ca$  phases are expected to form in the interdendritic region.

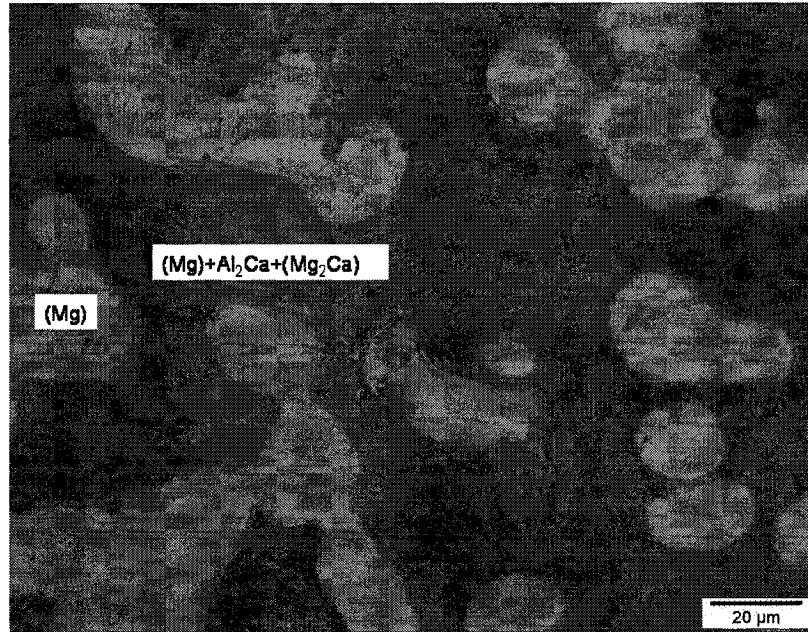


Figure 5-53: Optical microscope of sample 11 1000X (12.65/77.46/9.89 Ca/Mg/Al wt%.)



Figure 5-54: (Mg) dendrite of sample 11 100X (12.65/77.46/9.89 Ca/Mg/Al wt%.)

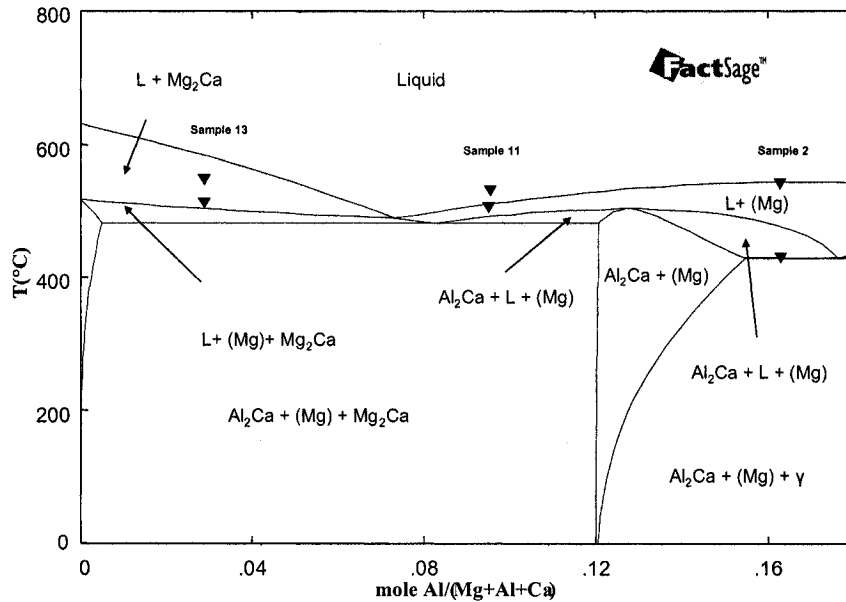


Figure 5-55: The calculated vertical section at constant 82 at.% Mg with DSC signals from cooling curve of sample 11, 13 and 2

The DSC results of sample 11 in Figure 5-56 is consistent with the calculated phase assemblage diagram in Figure 5-52 and vertical section in Figure 5-55. The sharp and narrow peak corresponds to the eutectic transformation at 506°C, according to the infinite phase change rate principle. The second small peak represents the liquidus point at 532°C, rather than the phase transformation by L + (Mg)/ L + (Mg) + Al<sub>2</sub>Ca, according to the phase amount involvement principle.

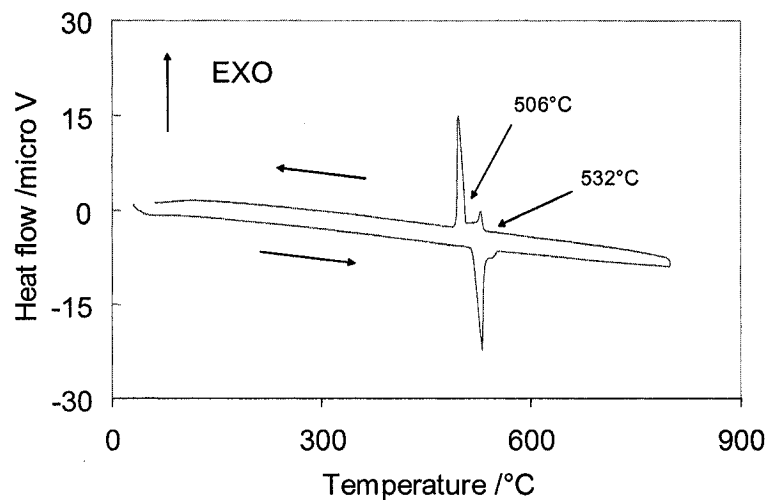


Figure 5-56: DSC spectra of sample 11

The DSC results of sample 11 and 13 are labeled on the vertical section shown in Figure 5-55. Similar values for the DSC measurements of the eutectic temperature were obtained for these two samples indicating the consistency of this work. Here the DSC results of sample 2, which was discussed earlier, are also labeled on the same diagram to give a more detailed comparison with the calculated phase diagram. The DSC measurements and the thermodynamic calculation of sample 11 are summarized in Table 5-5.

Table 5-5: The DSC measurements with thermodynamic calculation for samples 10, 11, 12 and 13 in Mg-Mg<sub>2</sub>Ca-Al<sub>2</sub>Ca phase field (c: denotes cooling and h: denotes heating)

Sample	DSC Thermal Signals (°C)	Thermodynamic calculation based on the database reported in [14]	
		Temp°C.	Reactions or phase boundary
10	516h/512c	480	L = (Mg) + Al <sub>2</sub> Ca + Mg <sub>2</sub> Ca
11	515h/506c	482	L + (Mg) + Al <sub>2</sub> Ca/ (Mg) + Al <sub>2</sub> Ca + Mg <sub>2</sub> Ca
	-	493	L + (Mg)/ L + (Mg) + Al <sub>2</sub> Ca
	545h/532c	512	L/L + (Mg)
12	516h/513c	481	(Mg) + Al <sub>2</sub> Ca + Mg <sub>2</sub> Ca/Al <sub>2</sub> Ca + Mg <sub>2</sub> Ca + L
	-	491	Al <sub>2</sub> Ca + Mg <sub>2</sub> Ca + L/Al <sub>2</sub> Ca + L
	678h/626c	587	Al <sub>2</sub> Ca/L
13	520h/513c	480	(Mg) + Al <sub>2</sub> Ca + Mg <sub>2</sub> Ca/ Mg <sub>2</sub> Ca + (Mg) + L
	-	502	Mg <sub>2</sub> Ca + (Mg) + L /Mg <sub>2</sub> Ca + L
	580/548c	572	Mg <sub>2</sub> Ca + L/L

Table 5-6: Comparison between XRD results and thermodynamic predictions for samples 10, 11, 12 and 13 in Mg-Al<sub>2</sub>Ca-Mg<sub>2</sub>Ca phase field

Sample	Identified phases	Thermodynamic calculation [14]
10	(Mg) + Mg <sub>2</sub> Ca + Al <sub>2</sub> Ca(weak peak)	(Mg) + Mg <sub>2</sub> Ca + Al <sub>2</sub> Ca (little)
11	(Mg) + Mg <sub>2</sub> Ca + Al <sub>2</sub> Ca	(Mg) + Mg <sub>2</sub> Ca + Al <sub>2</sub> Ca
12	(Mg) + Mg <sub>2</sub> Ca + Al <sub>2</sub> Ca(weak peak)	(Mg) + Al <sub>2</sub> Ca + Mg <sub>2</sub> Ca
13	(Mg) + Mg <sub>2</sub> Ca + Al <sub>2</sub> Ca(weak peak)	(Mg) + Mg <sub>2</sub> Ca + Al <sub>2</sub> Ca (little)

The XRD pattern of sample 12 in Figure 5-57 indicates the presence of (Mg),  $\text{Al}_2\text{Ca}$ , and  $(\text{Mg}_2\text{Ca})$  phases. This is in agreement with the phase assemblage diagram in Figure 5-58. The micrograph in Figure 5-59 shows that the phase evolution is consistent with solidification process shown in the calculated vertical section in Figure 5-62. Coarse plate-like  $\text{Al}_2\text{Ca}$  is the primary phase and wrapped up with the white secondary phase (Mg) and secondary fine  $\text{Al}_2\text{Ca}$ . The lamellar structure is the product of the invariant reaction  $L \rightarrow \text{Al}_2\text{Ca} + (\text{Mg}) + (\text{Mg}_2\text{Ca})$ . Even the small amount of  $\text{Al}_2\text{Ca}$  appears clearly in the micrograph.

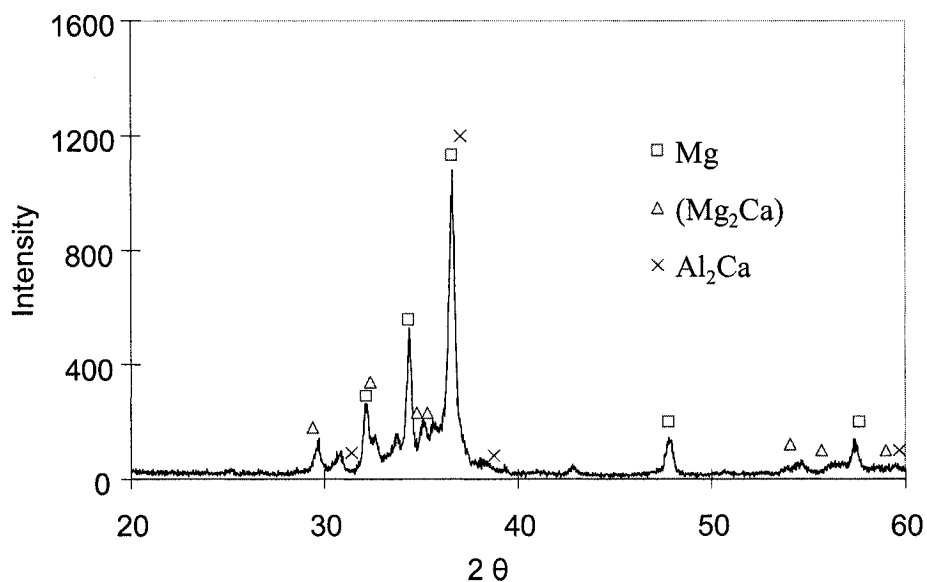


Figure 5-57: XRD pattern of sample 12 (19.32/62.65/18.04 Ca/Mg/Al wt%)

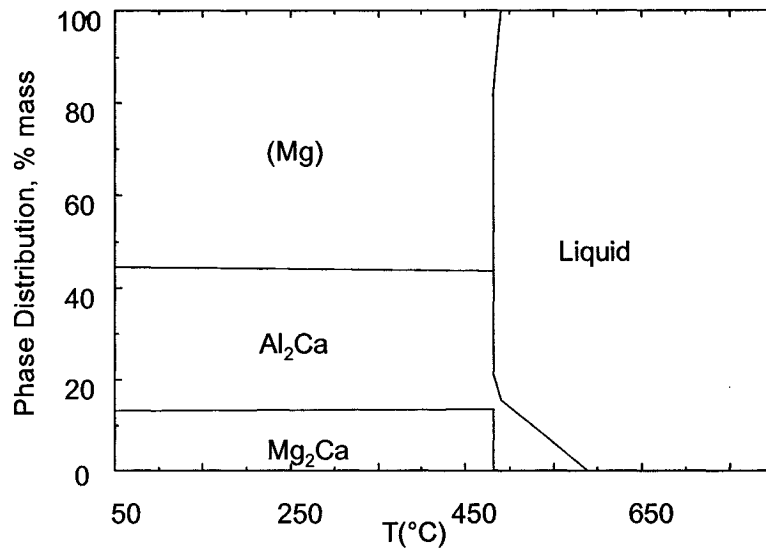


Figure 5-58: Phase assemblage of sample 12 (19.32/62.65/18.04 Ca/Mg/Al wt%)

There is no doubt to identify ( $Mg_2Ca$ ) with seven characteristic peaks in the XRD pattern, however, it is hard to see the distinct morphology in the micrograph. This is because ( $Mg_2Ca$ ) is embedded in interdendritic eutectic structure. A similar view point was also reported by Suzuki *et al.* [77]. The eutectic structure of sample 12 can be seen more clearly with higher magnification (1000X) micrograph shown in Figure 5-60.

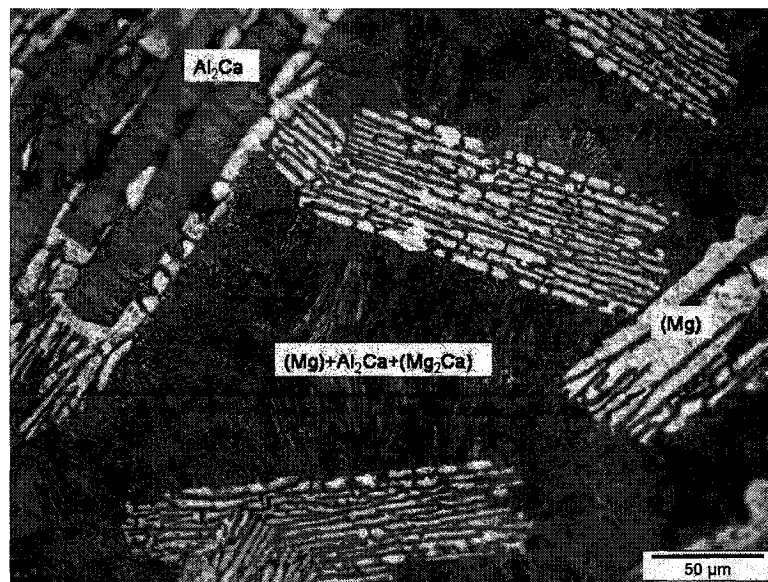


Figure 5-59: Optical microscope of sample 12, 500X (19.32/62.65/18.04 Ca/Mg/Al wt%)



Figure 5-60: Optical microscope of sample 12, 1000X  
(19.32/62.65/18.04 Ca/Mg/Al wt%)

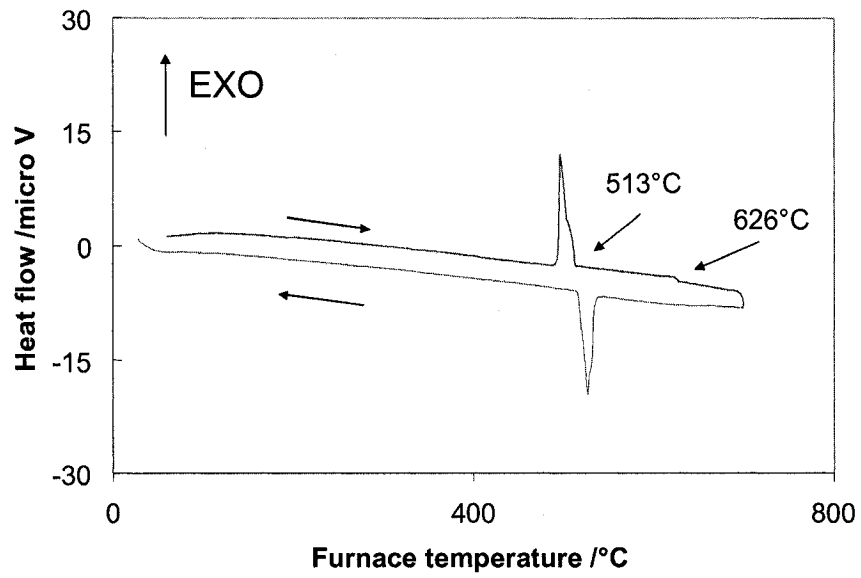


Figure 5-61: DSC spectra of sample 12 (19.32/62.65/18.04 Ca/Mg/Al  
wt%)

The simulated XRD pattern of ( $Mg_2Ca$ ) is prepared using the lattice parameters of  $Mg_2Ca$  with 22 at.% Al dissolution. It matches the experimental XRD pattern of sample 12 better than the simulated XRD pattern using parameters for pure  $Mg_2Ca$ . That means the  $Mg_2Ca$  dissolved approximately 22 at.% Al in this sample. The precise amount of Al dissolution can be determined by microprobe analysis in the future work.

Comparison of the phases found in sample 12 using XRD and the thermodynamic calculations is presented in Table 5-6 shown earlier.

The DSC spectra of sample 12 in Figure 5-61 show that the eutectic transformation occurs at  $513^\circ C$  which is characterized by a sharp, narrow and strong peak, respecting the infinite phase change rate principle, whereas the liquidus occurs at  $626^\circ C$  which is determined by the intersection of tailing and the baseline.

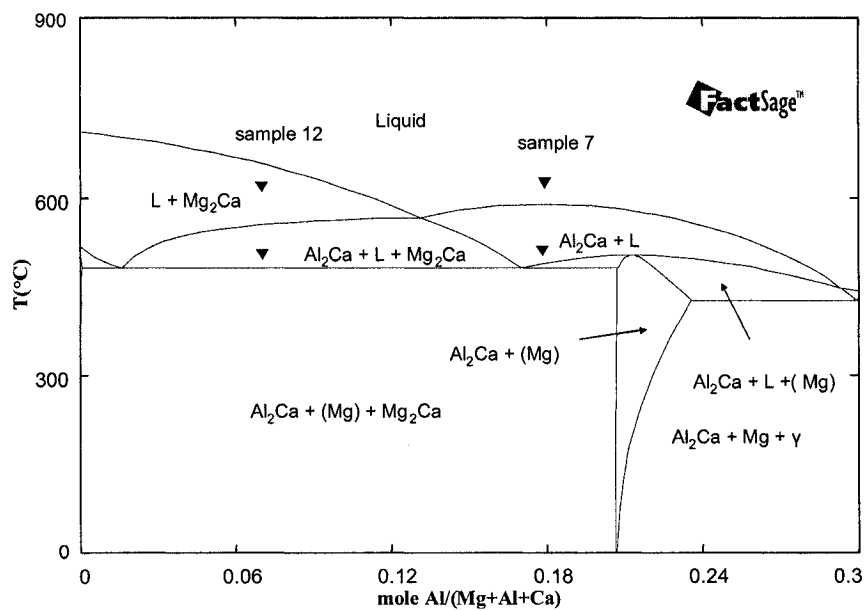


Figure 5-62: The calculated vertical section at constant 69 at.% Mg with DSC signals from cooling curve of sample 7 and 12

The experimental eutectic temperature is in accord with the adjacent sample 11 and the eutectic point represented by sample 10. Summary of these results is in Table 5-5. Furthermore, the measurement of the eutectic temperature is made certain by labeling the DSC results of samples 12 and 7 on the same vertical section in Figure 5-62. Both of them yield common eutectic transformation temperature.

The XRD pattern of sample 13 is shown in Figure 5-63. The identification of (Mg<sub>2</sub>Ca) phase is performed using the simulated XRD patterns for both pure Mg<sub>2</sub>Ca and the (Mg<sub>2</sub>Ca) with 22 at.% Al. It can be seen that the sample's peaks fall between these two patterns, marked as a triangle and diamond in the legend. This implies qualitatively that the phase (Mg<sub>2</sub>Ca) dissolves less than 22 at.% Al. The distortion of (Mg<sub>2</sub>Ca) lattice varies with the amount of Al dissolution. The peaks for Al<sub>2</sub>Ca are small, that is consistent with the small relative amount of Al<sub>2</sub>Ca shown in the phase assemblage diagram in Figure 5-64. Nevertheless, the peaks for (Mg) can be seen clearly in Figure 5-63.

The micrograph of sample 13 in Figure 5-65 shows stone-like primary phase (Mg<sub>2</sub>Ca) and eutectic lamellar structure. They are formed at the liquidus L/L + (Mg<sub>2</sub>Ca) and the eutectic transformation borderline (Mg<sub>2</sub>Ca) + (Mg) + L/(Mg) + Al<sub>2</sub>Ca + (Mg<sub>2</sub>Ca), respectively, as can be seen from the phase assemblage diagram shown in Figure 5-64 or the vertical section in Figure 5-55. The phases of (Mg) + (Mg<sub>2</sub>Ca) + Al<sub>2</sub>Ca in this sample are in agreement with the work of [79], who studied a sample with a close chemical composition.



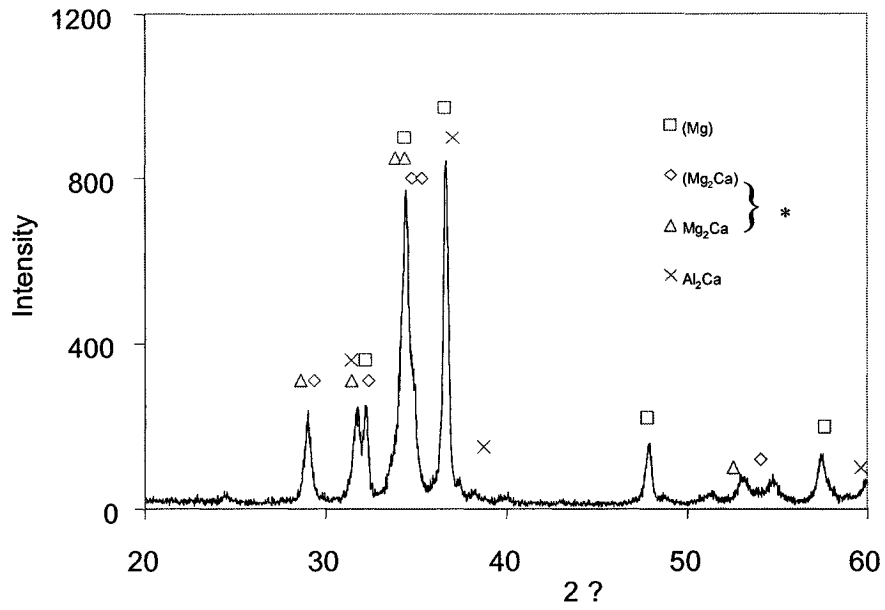


Figure 5-63: XRD pattern of sample 13 (21.69/75.38/2.94 Ca/Mg/Al wt%)  
 \* included in this diagram for comparison.

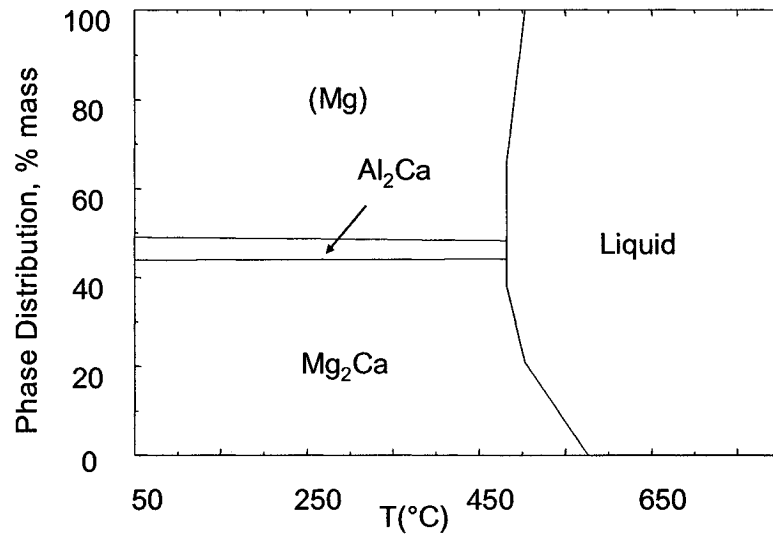


Figure 5-64: Phase Assemblage of sample 13 (21.69/75.38/2.94 Ca/Mg/Al wt%)

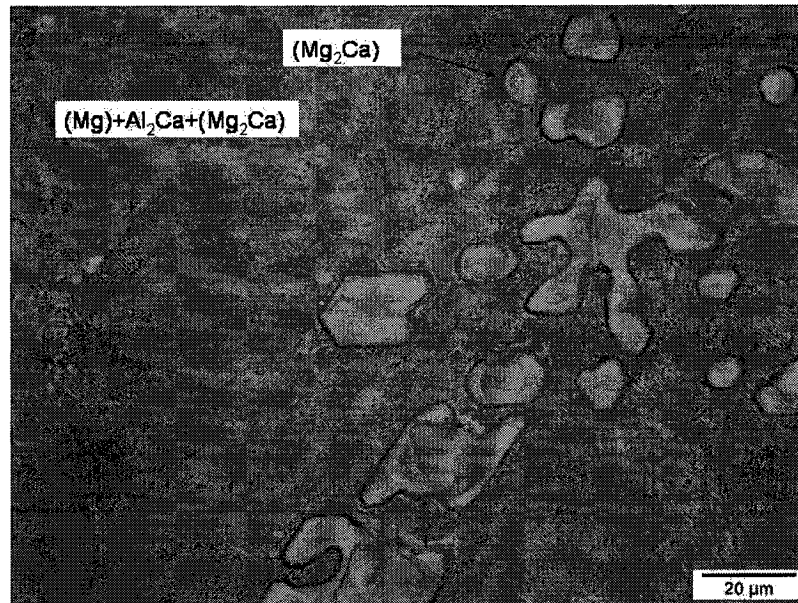


Figure 5-65: Optical microscope of sample 13, 1000X  
(21.69/75.38/2.94 Ca/Mg/Al wt%)

The DSC spectra of sample 13 are shown in Figure 5-66. The narrow sharp peak corresponds to the eutectic transformation at 513°C according to the infinite phase change rate principle, whereas, the small peak corresponds to the liquidus that occurs at 548°C. The DSC results labeled on the vertical section in Figure 5-55 and summarized in Table 5-5 are in accord with the results obtained for samples 11, 10 and 12.

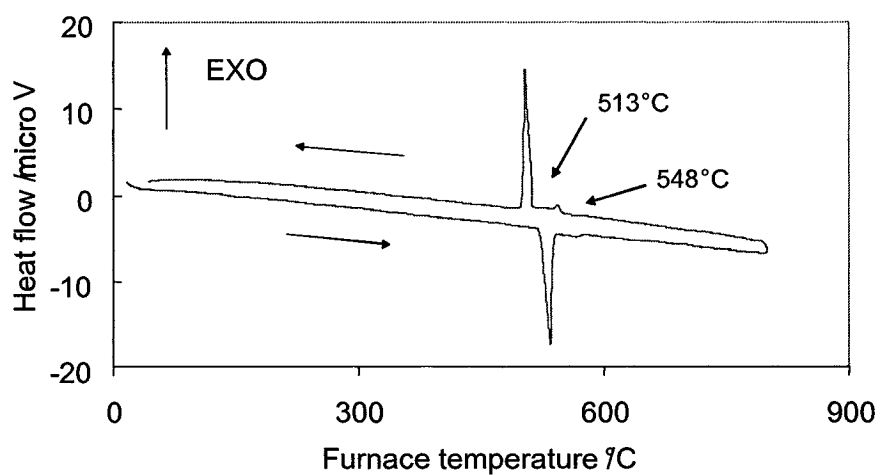


Figure 5-66: DSC spectra of sample 13 (21.69/75.38/2.94 Ca/Mg/Al wt%)

## 5.4 Samples in the $\text{Al}_2\text{Ca}$ - $\gamma$ -Al triangle

There are three phase borderlines in the  $\gamma$ - $\text{Al}_2\text{Ca}$ -Al triangle as can be seen in Figure 5-1. To validate the phase borderlines, four samples 14, 15, 16 and 17 are selected close to these lines.

Sample 14 and 15 are close to  $\beta$ - $\text{Al}_4\text{Ca}$  borderline as can be seen in Figure 5-1. The XRD patterns of both samples in Figures 5-67 and 5-68 show clearly peaks for (Al) and  $\text{Al}_2\text{Ca}$ . Sample 14 also contains weak peaks for  $\text{Al}_4\text{Ca}$  but no peaks for  $\beta$ , whereas sample 15 contains weak peaks for  $\beta$  but no peaks for  $\text{Al}_4\text{Ca}$ . This is not consistent with the thermodynamic modeling but can be due to the small relative amount of  $\beta$  and  $\text{Al}_4\text{Ca}$  in samples 14 and 15, respectively. Also, the phase assemblage diagram of sample 14 in Figure 5-69 shows 70 wt%  $\text{Al}_4\text{Ca}$  and that of sample 15 in Figure 5-70 contains 60 wt%  $\beta$ . While  $\text{Al}_4\text{Ca}$  and  $\beta$  were not displayed strongly in the XRD patterns, (Al) and  $\text{Al}_2\text{Ca}$  always have strong peaks. This could be due to lower thermal stability of  $\text{Al}_4\text{Ca}$  and  $\beta$ . In fact, as stated in the literature, the phases  $\text{Al}_4\text{Ca}$  and  $\beta$  have a lower melting temperature than  $\text{Al}_2\text{Ca}$  and Al. The  $\beta$  phase starts decomposing at 257°C and melts completely at 447°C and  $\text{Al}_4\text{Ca}$  starts melting at 610°C [62]. Whereas,  $\text{Al}_2\text{Ca}$  has higher congruent melting temperature at 1079°C and the Al melts at 659°C [62].

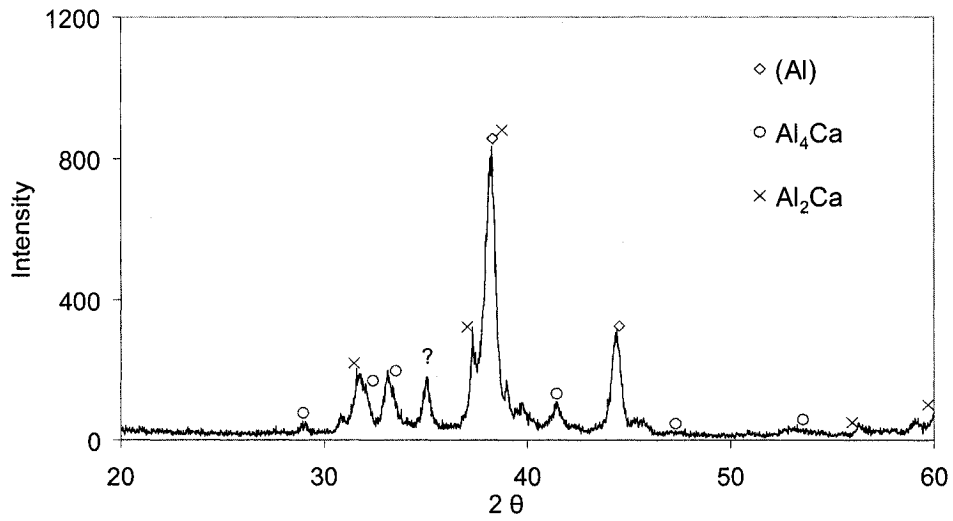


Figure 5-67: XRD pattern of sample 14 (19.12/7.91/72.97 Ca/Mg/Al wt%)

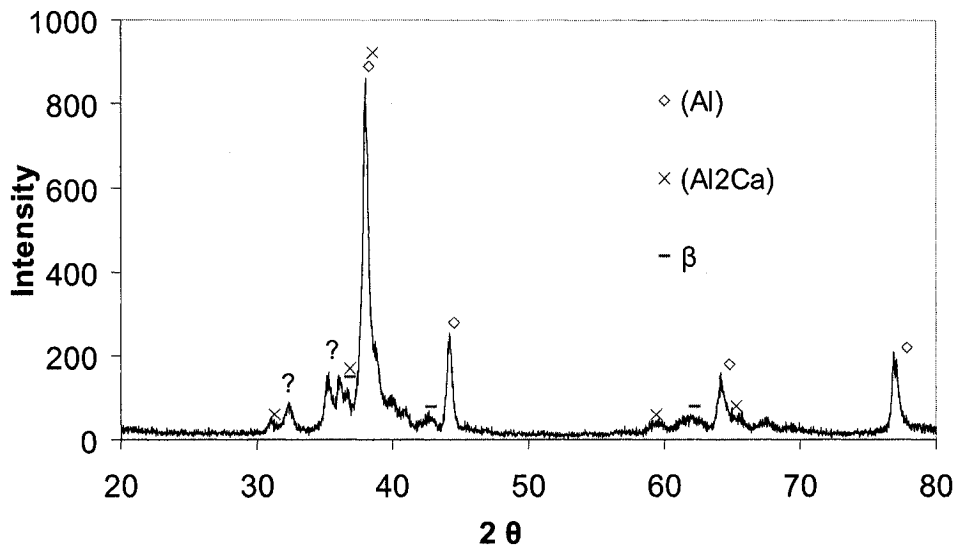


Figure 5-68: XRD pattern of sample 15 (11.67/22.04/66.29 Ca/Mg/Al wt%)

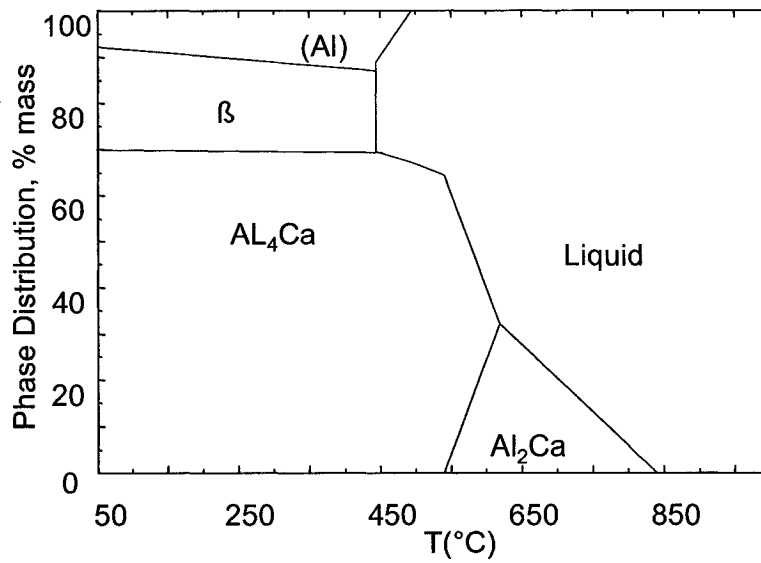


Figure 5-69: Phase assemblage of sample 14 (19.12/7.91/72.97 Ca/Mg/Al wt%)

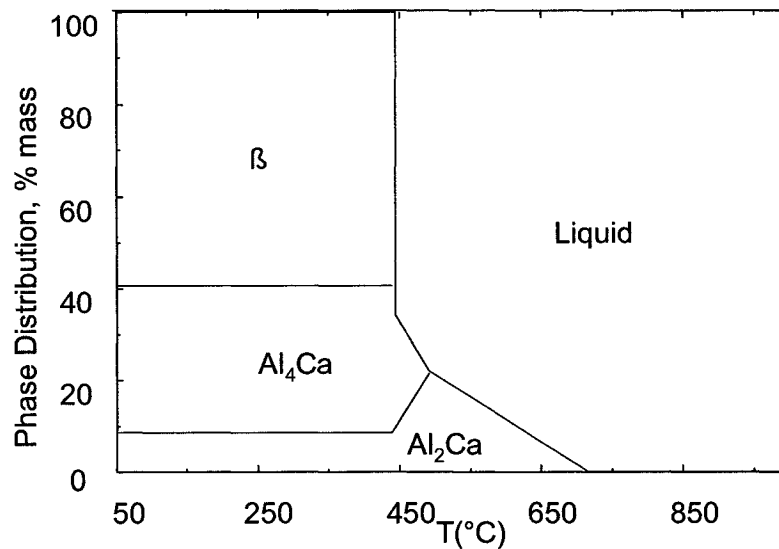


Figure 5-70: Phase assemblage of sample 15 (11.67/22.04/66.29 Ca/Mg/Al wt%)

The phase transformation temperatures of samples 14 and 15 are measured by the DSC spectra presented in Figures 5-71 and 5-72, which are labeled on the vertical sections shown in Figures 5-73 and 5-74. The DSC measurements and the

thermodynamic calculations for these samples are summarized in Table 5-7. To be noted that the peak of sample 14 at 542°C (Figure 5-71) seems to be linked to the formation of  $\beta$  according to the infinite phase change rate principle if it is inferred from the phase assemblage diagram solely. However,  $\beta$  was not detected in the XRD pattern shown in Figure 5-67. Therefore, the most possible transformation according to the phase amount involvement principle is  $L+Al_2Ca \rightarrow Al_4Ca$ .

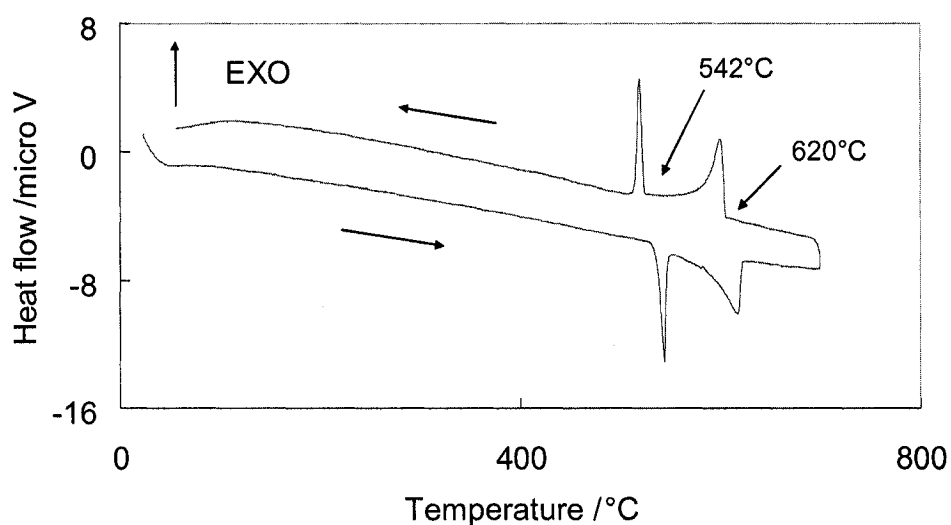


Figure 5-71: DSC spectra of sample 14 (19.12/7.91/72.97 Ca/Mg/Al wt%)

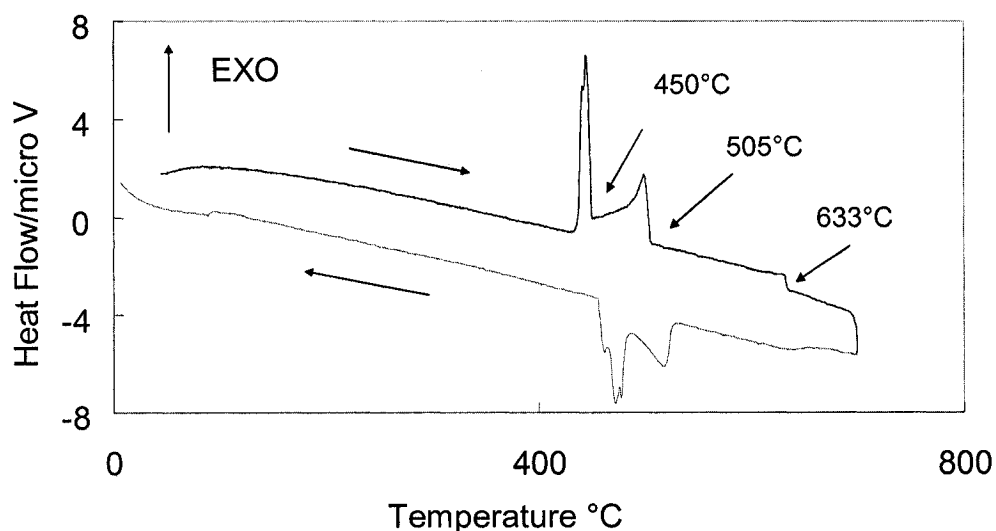


Figure 5-72: DSC spectra of sample 15 (11.67/22.04/66.29 Ca/Mg/Al wt%)

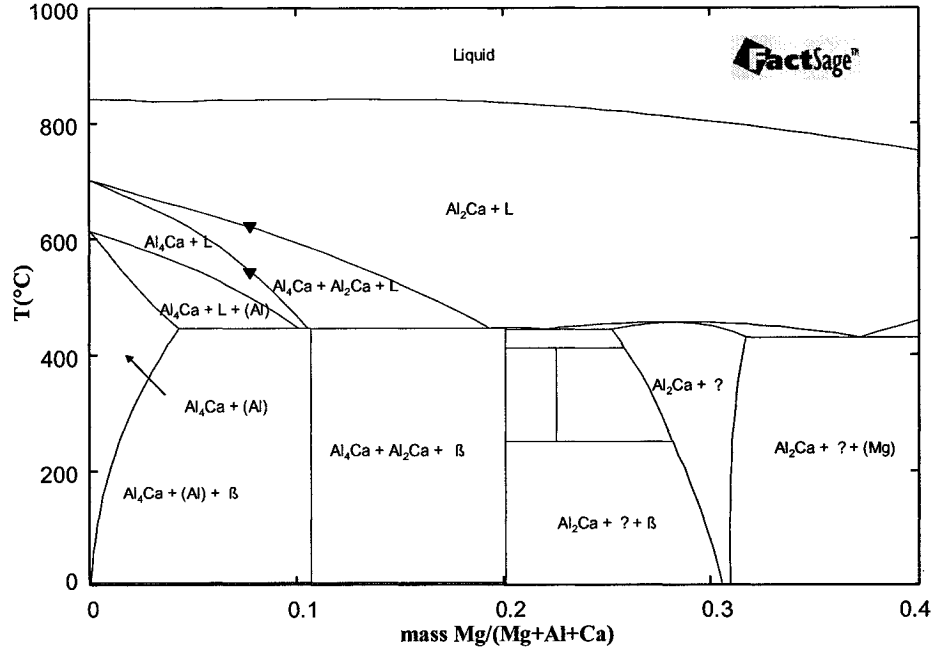


Figure 5-73: The calculated vertical section at constant 19.1 wt% Ca with DSC signals from cooling curve of sample 14

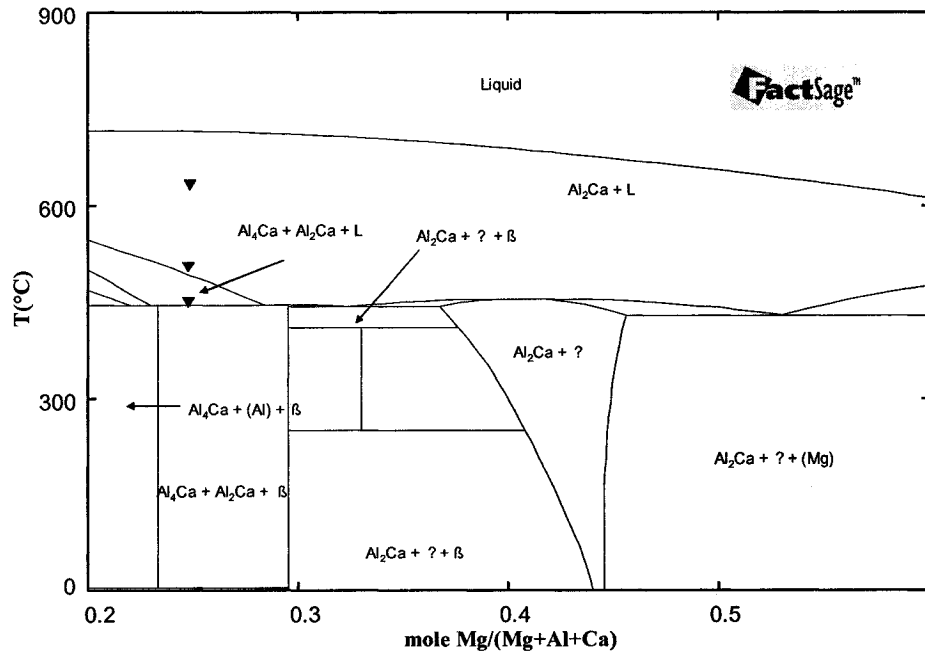


Figure 5-74: The calculated vertical section at constant 8 at.% Ca with DSC signals from cooling curve of sample 15

Table 5-7 The DSC measurements and calculated transformation temperature in  $Al_2Ca$ - $\gamma$ -Al region (h: denotes heating and c: denotes cooling)

Sample	DSC Thermal Signals ( $^{\circ}C$ )	Thermodynamic calculation based on the database reported in [14]	
		Temp. ( $^{\circ}C$ )	Reactions or phase boundary
14	-	444	$L + Al_4Ca + (Al) / Al_4Ca + (Al) + \beta$
	-	492	$Al_4Ca + L / L + Al_4Ca + (Al)$
	542c/548h	540	$Al_4Ca + Al_2Ca + L / Al_4Ca + L$
	620c/628h	618	$Al_2Ca + L / Al_4Ca + Al_2Ca + L$
	-	838	$L / Al_2Ca + L$
15	450c/456h	445	$L + Al_2Ca + Al_4Ca / Al_2Ca + Al_4Ca + \beta$
	505c/496h	491	$L + Al_2Ca / L + Al_2Ca + Al_4Ca$
	633c/640h	714	$L / L + Al_2Ca$
16	454c/464h	454	$L + Al_2Ca / Al_2Ca + \gamma$
	774c/783h	752	$L / L + Al_2Ca$
17	446c/452h	446	$Al_4Ca + Al_2Ca + L / Al_4Ca + Al_2Ca + \beta$
	488c/482h	469	$Al_2Ca + L / Al_4Ca + Al_2Ca + L$
	-	884	$L / Al_2Ca + L$

The DSC spectra of sample 16 in Figure 5-75 show sharp and narrow peak at  $454^{\circ}C$  in the cooling session. This relates to the invariant transformation on the borderline of  $L + Al_2Ca / Al_2Ca + \gamma$  as can be seen in the vertical section shown in Figure 5-76, according to the infinite phase change rate principle. Correspondingly, the tailing temperature at  $752^{\circ}C$  is the liquidus. Labeling the DSC signals on the vertical section in Figure 5-76 shows a good agreement with the solidus, but a small deviation from the liquidus.

The XRD pattern of sample 16 in Figure 5-77 shows the peaks of (Mg), (Al) and  $Al_2Ca$  phases. These results do not agree with the calculated phase assemblage diagram shown in Figure 5-78 which shows that this sample should contain  $\gamma$ ,  $Al_2Ca$  and  $\beta$  at room temperature. Although it is not expected to detect  $\beta$  due to its small relative amount indicated in the phase assemblage diagram, it is still not clear why  $\gamma$  was not detected, nevertheless, this is probably due to a nonequilibrium solidification which might have



occurred in this sample. Samples 16 and 17 also show some unknown peaks which do not belong to any known phases and any possible oxides. It needs more investigation around sample 16 to check the reproducibility of the unknown peaks and clarify whether these belong to a new phase or an inclusion.

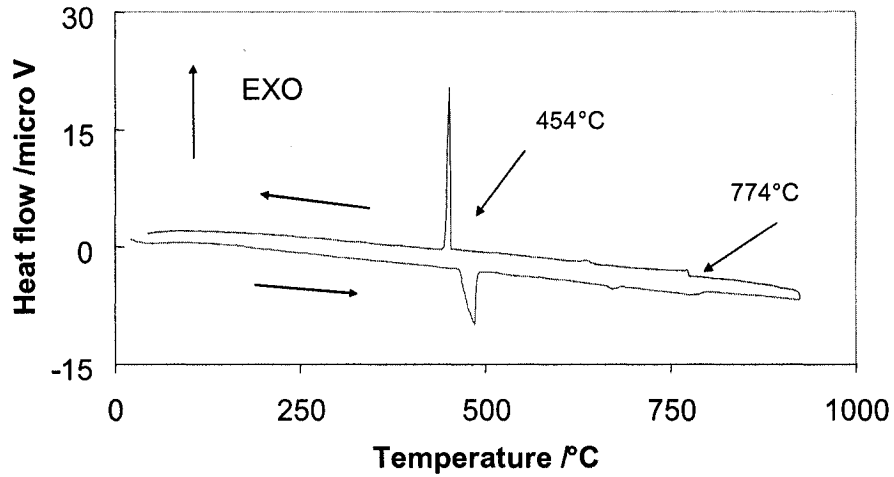


Figure 5-75: DSC spectra of sample 16 (15.68/33.28/51.04 Ca/Mg/Al wt%)

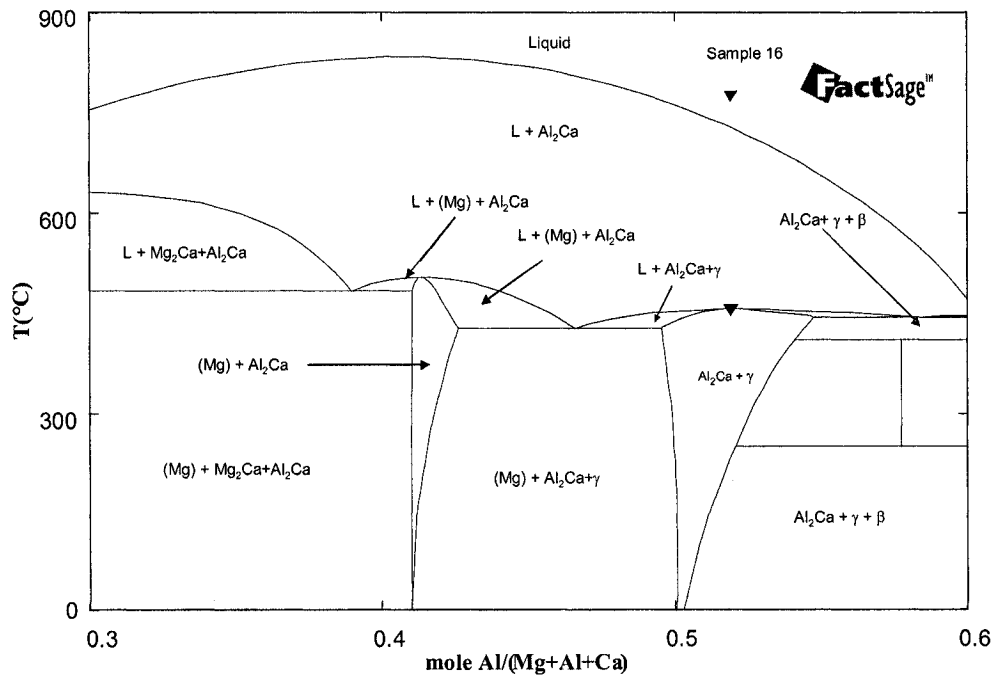


Figure 5-76: The calculated vertical section at constant 38.5 at.% Mg with DSC signals from cooling curve of sample 16

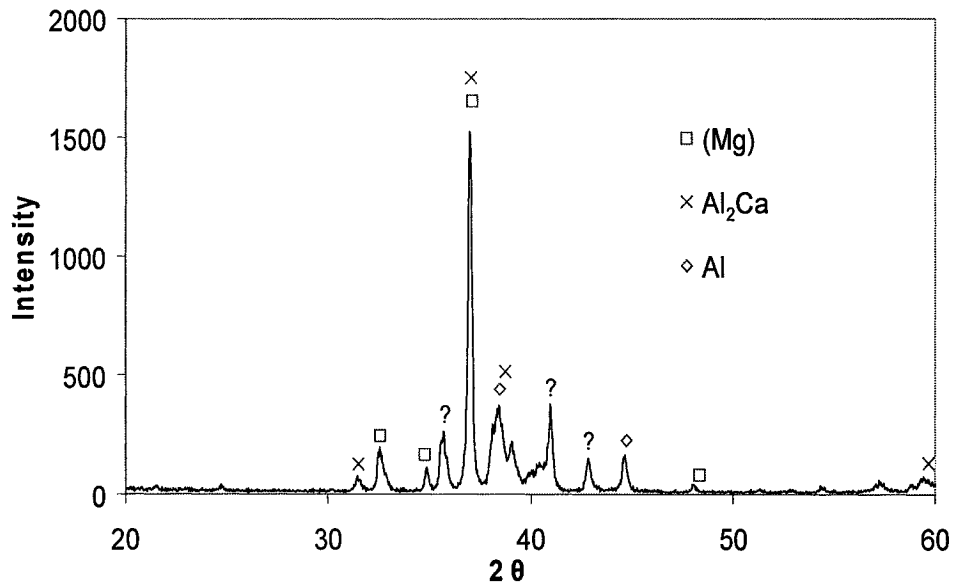


Figure 5-77: XRD pattern of sample 16 (15.68/33.28/51.04 Ca/Mg/Al wt%)

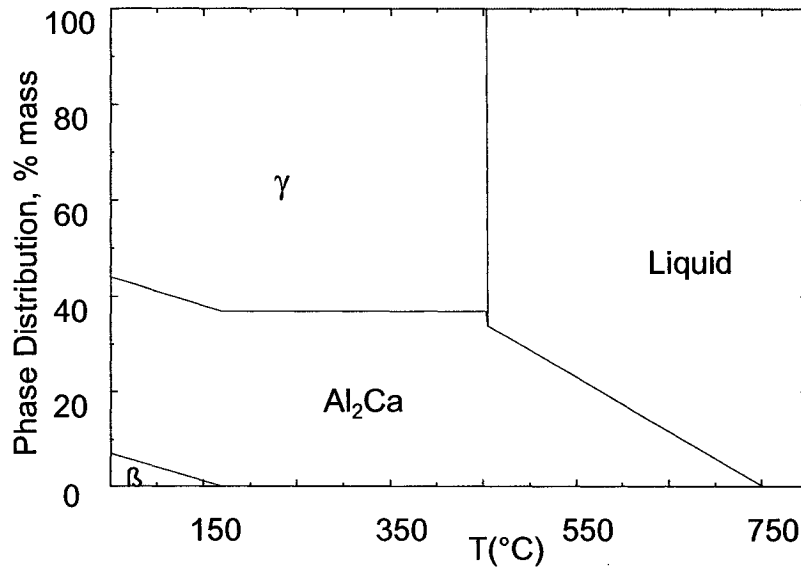


Figure 5-78: Phase assemblage of sample 16 (15.68/33.28/51.04 Ca/Mg/Al wt%)

Sample 17 is located close to  $\text{Al}_2\text{Ca}$ - $\beta$  borderline in the isothermal section in Figure 5-1. The XRD pattern in Figure 5-79 indicates the peaks for  $\text{Al}_2\text{Ca}$ ,  $\beta$  and ?, but no peaks for  $\text{Al}_4\text{Ca}$ . There is a discrepancy with the phase assemblage diagram in Figure 5-80, which predicts the formation of  $\text{Al}_4\text{Ca}$  but no ?. Probably the nonequilibrium

solidification leads to the precipitation of  $\gamma$ , and the small amount and the instability of  $\text{Al}_4\text{Ca}$  lead to no traces of  $\text{Al}_4\text{Ca}$  in the XRD pattern. Similarly, the XRD pattern of sample 15 (Figure 5-68) does not show the expected  $\text{Al}_4\text{Ca}$ , too.

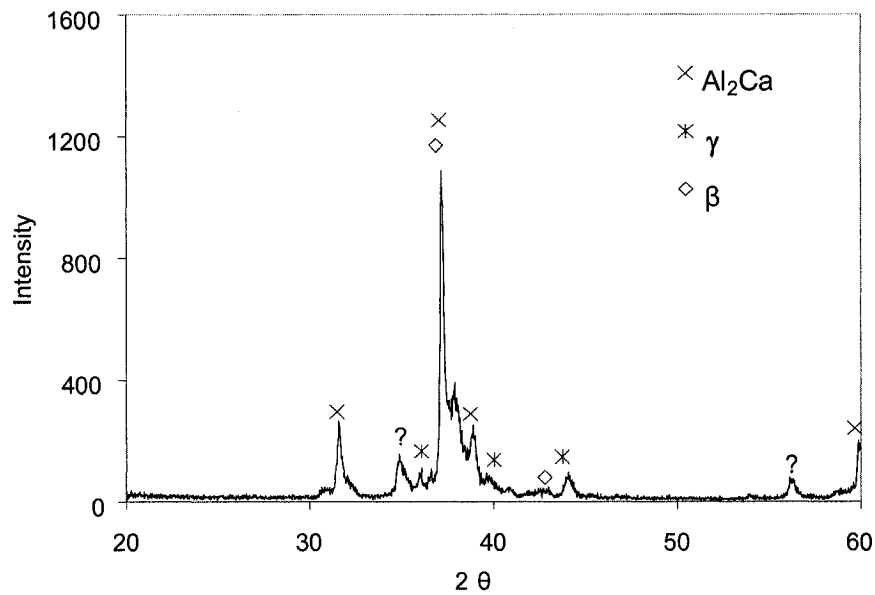


Figure 5-79: XRD pattern of sample 17 (22.81/15.31/61.88 Ca/Mg/Al wt%)

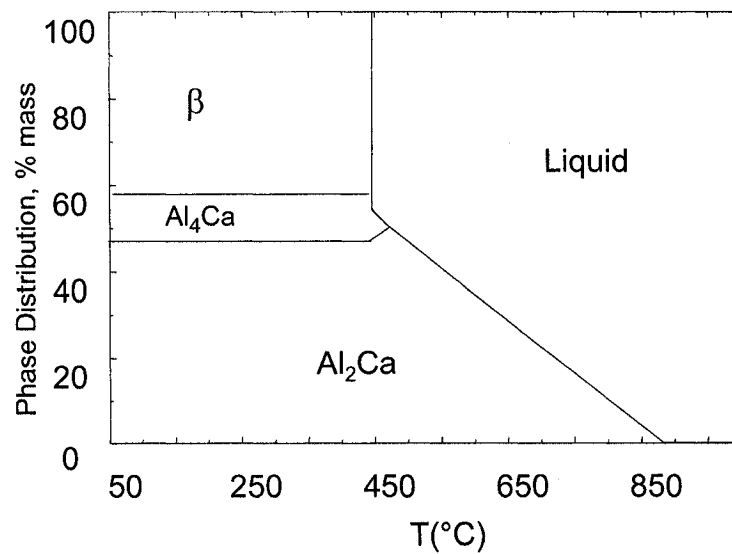


Figure 5-80: Phase assemblage diagram of sample 17 (22.81/15.31/61.88 Ca/Mg/Al wt%)

The DSC spectra of sample 17 in Figure 5-81 shows three peaks with onset temperatures at 669, 488.6 and 446°C, taken from the cooling cycle. These temperatures

labeled on the vertical section in Figure 5-82 show an agreement with the thermodynamic model in the solidus, but a discrepancy in the liquidus. The determination of the temperature of 446°C as being an invariant transformation obeys the infinite phase change rate principle by referring to the phase assemblage diagram in Figure 5-80.

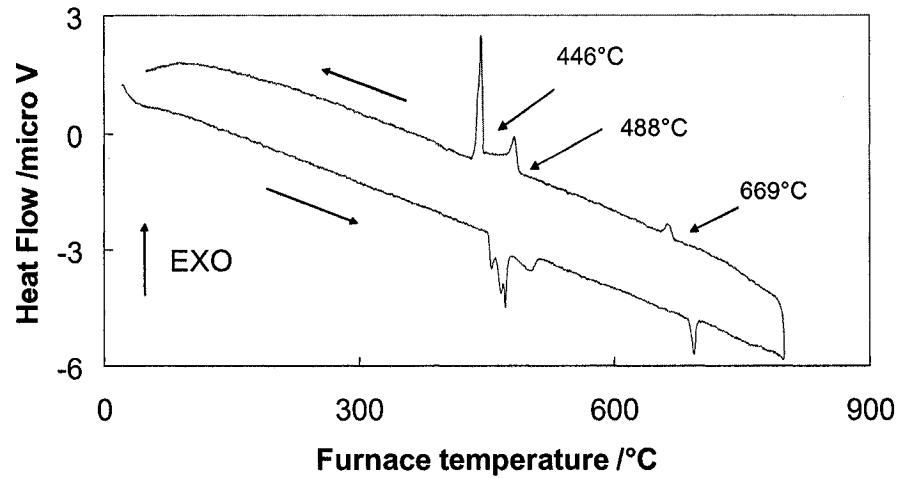


Figure 5-81: DSC spectra of sample 17 (22.81/15.31/61.88 Ca/Mg/Al wt%)

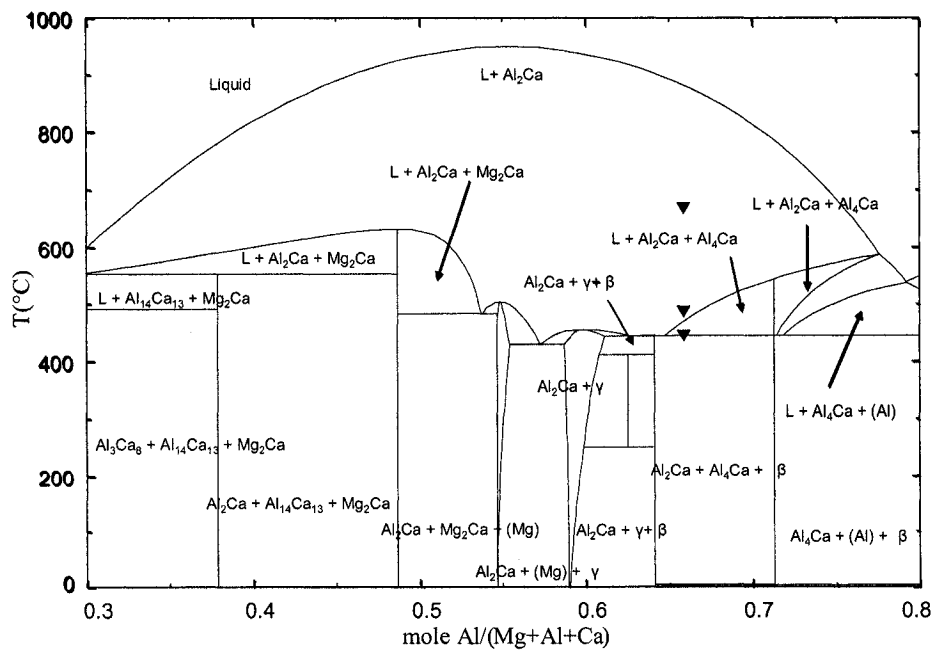


Figure 5-82: Calculated vertical section at constant 18 at.% Mg with DSC signals from cooling curve of sample 17

The DSC measurements and the calculated phase transformation temperatures of sample 14 to 16 are summarized in Table 5-7.

## **5.5 Samples in the $\text{Mg}_2\text{Ca-Al}_2\text{Ca-Al}_{14}\text{Ca}_{13}$ phase field**

Samples 18, 19 and 20 are selected in this phase field as shown in Figure 5-1. The XRD patterns of samples 18, 19 and 20 in Figures 5-83, 5-84 and 5-85 show the peaks for  $\text{Al}_2\text{Ca}$ ,  $\text{Mg}_2\text{Ca}$  and  $\text{Al}_{14}\text{Ca}_{13}$  phases. The peaks for  $\text{Al}_{14}\text{Ca}_{13}$  in sample 18 are weak because this sample is almost located on the  $\text{Mg}_2\text{Ca-Al}_2\text{Ca}$  borderline as seen in Figure 5-1. Sample 19 is a bit farther away from the  $\text{Mg}_2\text{Ca}$  corner and closer to the  $\text{Al}_{14}\text{Ca}_{13}$  corner than sample 20. Therefore, it ends up with stronger peaks for  $\text{Al}_{14}\text{Ca}_{13}$  and  $\text{Al}_2\text{Ca}$ , but with weaker peaks for  $\text{Mg}_2\text{Ca}$  than sample 20.

The XRD pattern of sample 18 indicates that the phase  $\text{Al}_2\text{Ca}$  with 5 wt% Mg matches the XRD pattern better than pure  $\text{Al}_2\text{Ca}$ . Hence, it is denoted by  $(\text{Al}_2\text{Ca})$  in the legend of Figure 5-83. Figure 5-83 and 5-84 show an unknown peak at  $37.6^\circ$ . It does not belong to any known phases and any possible oxides.

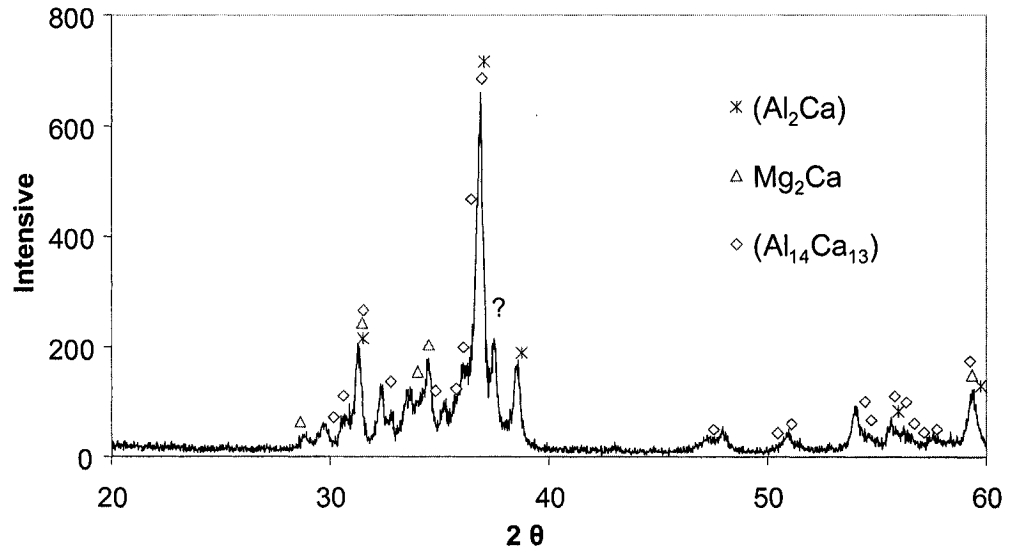


Figure 5-83: XRD pattern of sample 18 (44.30/23.76/31.94 Ca/Mg/Al wt%)

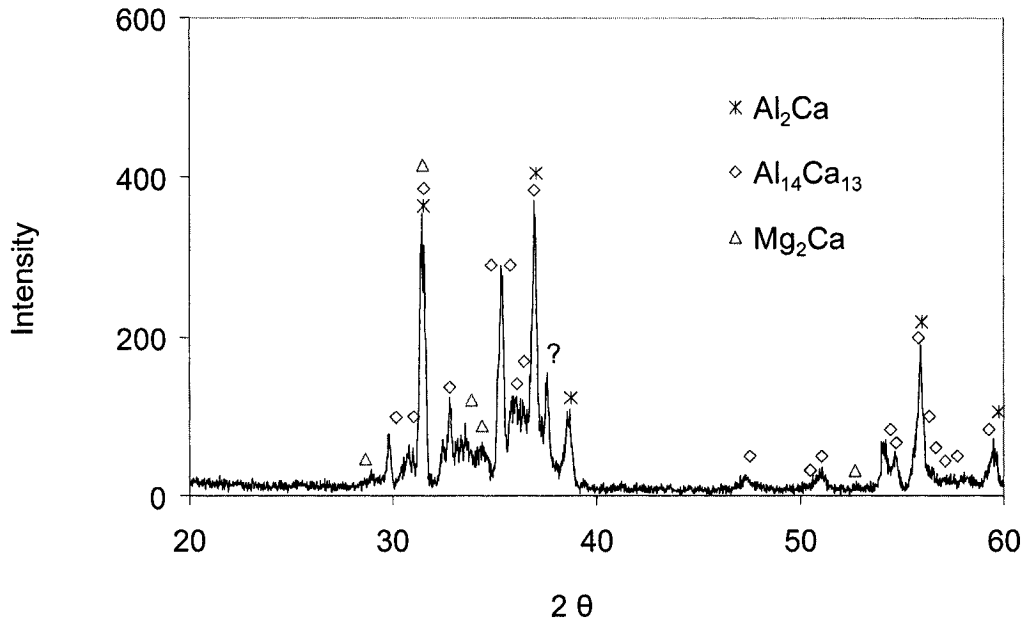


Figure 5-84: XRD pattern of sample 19 (46.73/13.00/40.27 Ca/Mg/Al wt%)

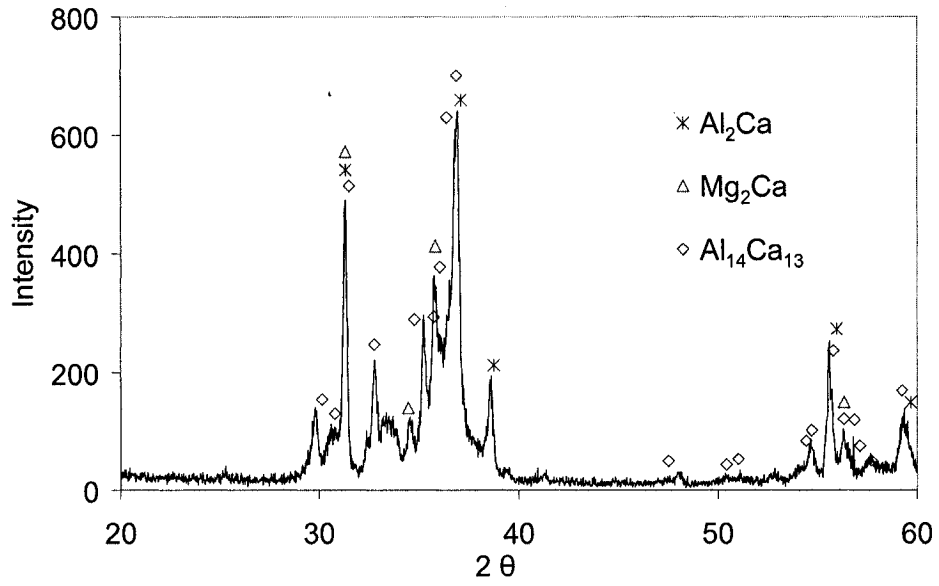


Figure 5-85: XRD pattern of sample 20 (47.47/22.42/30.11 Ca/Mg/Al wt%)

The XRD results of samples 18, 19 and 20 are in agreement with their phase assemblage diagrams shown in Figures 5-86, 5-87 and 5-88, respectively.

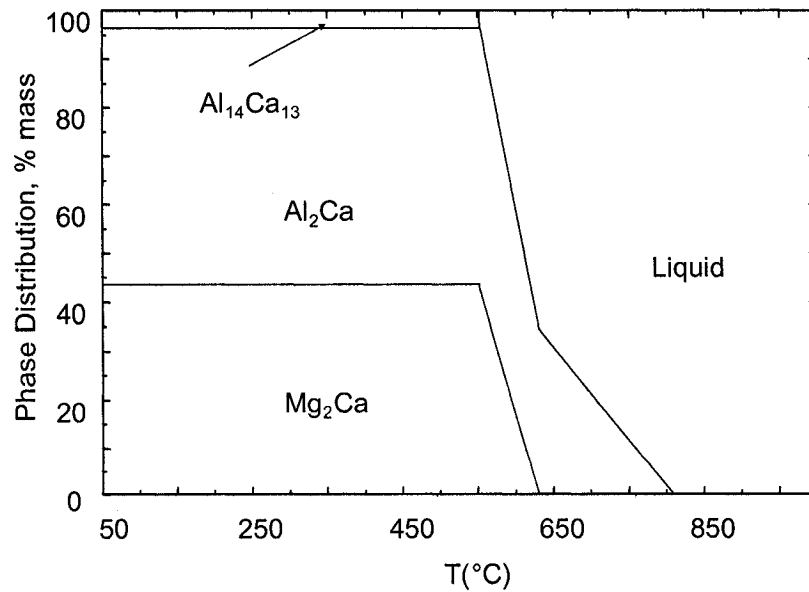


Figure 5-86: Phase assemblage of sample 18 (44.30/23.76/31.94 Ca/Mg/Al wt%)

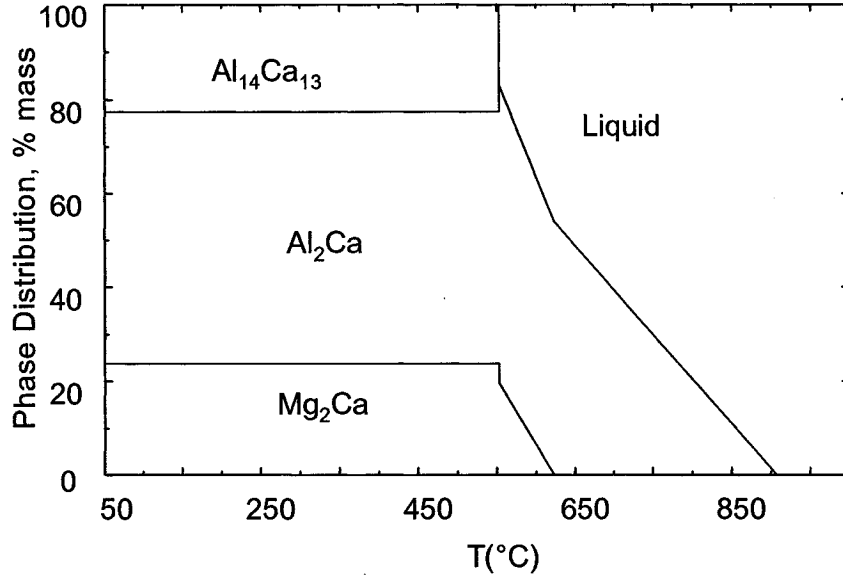


Figure 5-87: Phase assemblage of sample 19 (46.73/13.00/40.27 Ca/Mg/Al wt%)

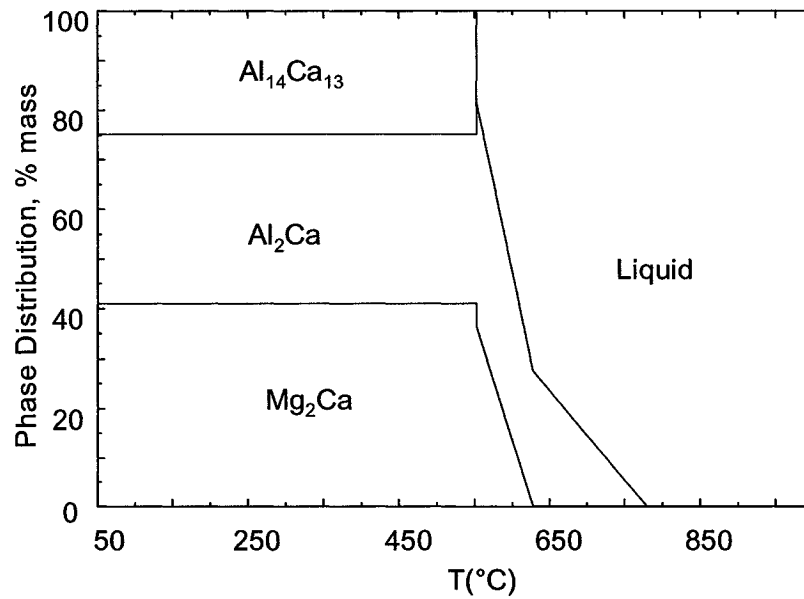


Figure 5-88: Phase assemblage of sample 20 (47.47/22.42/30.11 Ca/Mg/Al wt%)

The DSC spectra of samples 20, 19 and 18 in Figures 5-89, 5-90 and 5-91 show a single peak all at 506°C. This temperature corresponds to the invariant transformation in



the phase assemblage diagrams respecting the infinite phase change rate principle. The DSC spectra of sample 19 in Figure 5-91 show a weak signal and did not reveal a usual pattern. The sample is so brittle and became fine powder spontaneously.

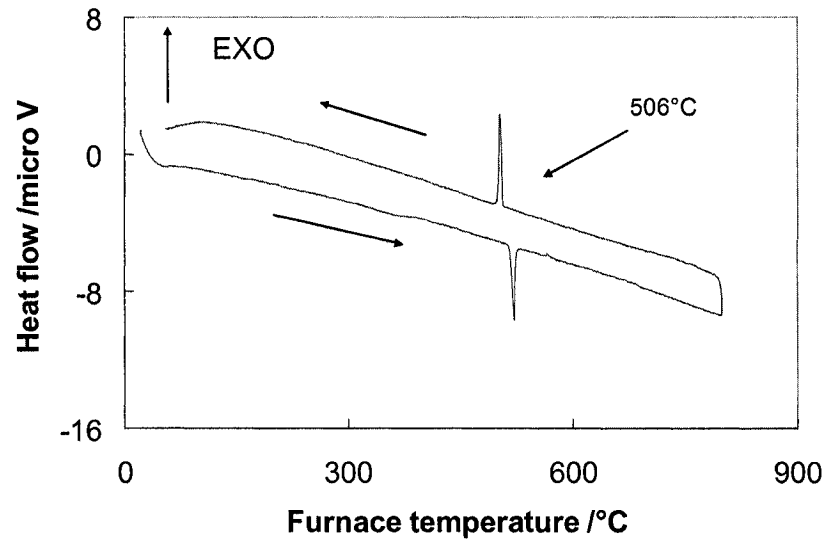


Figure 5-89: DSC spectra of sample 20 (47.47/22.42/30.11 Ca/Mg/Al wt%)

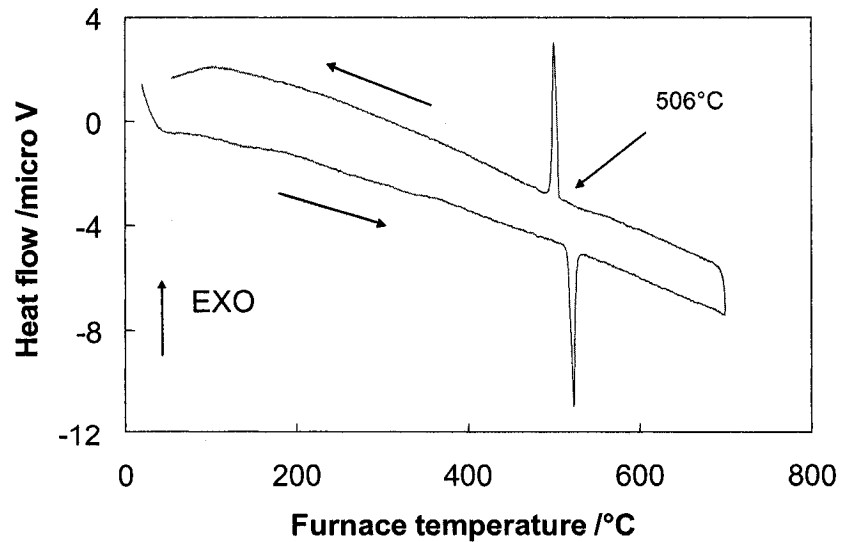


Figure 5-90: DSC spectra of sample 18 (44.30/23.76/31.94 Ca/Mg/Al wt%)

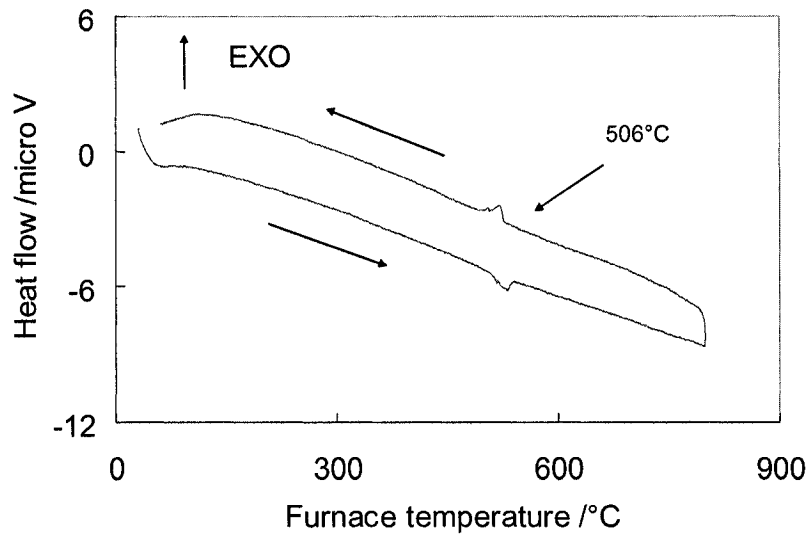


Figure 5-91: DSC spectra of sample 19 (46.73/13.00/40.27 Ca/Mg/Al wt%)

The DSC measurements are labeled on the vertical section in Figures 5-92 and 5-93. These diagrams show consistent experimental results, but discrepancy with the calculated phase diagrams.

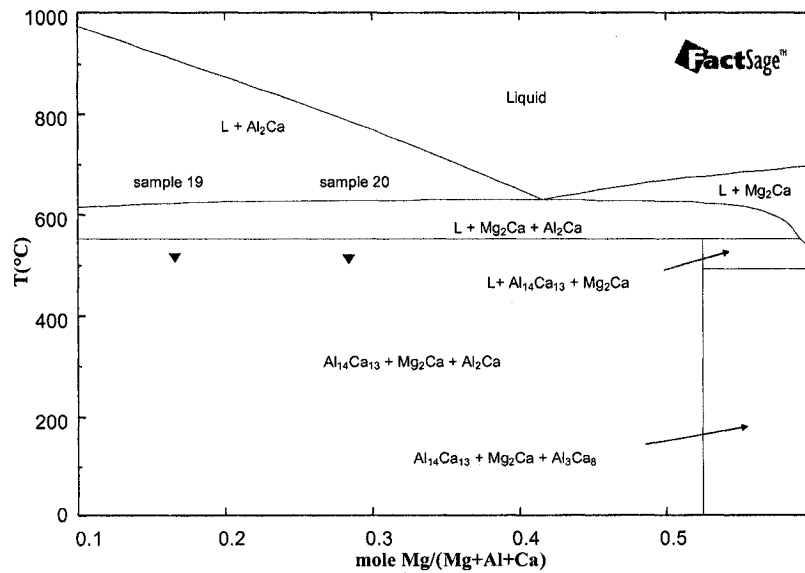


Figure 5-92: The calculated vertical section at constant 36.5 at.% Ca with DSC signals from cooling curve of sample 19 and 20

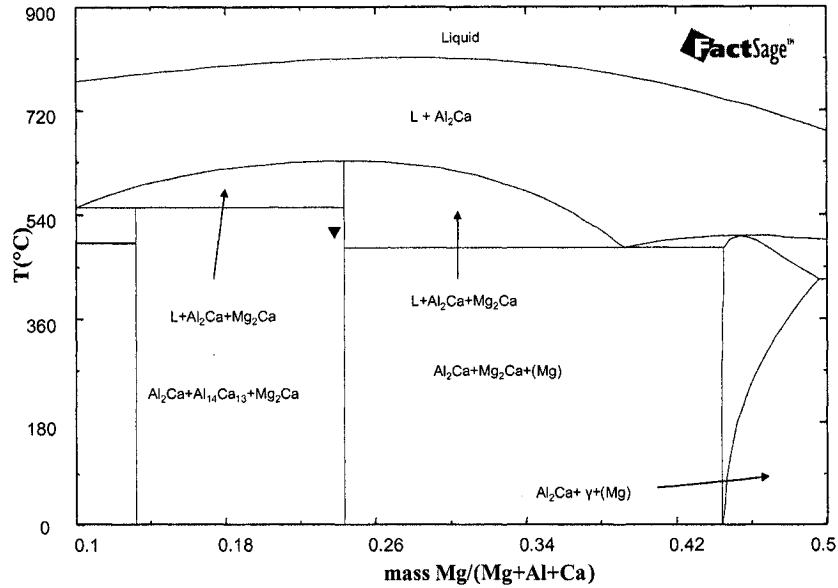


Figure 5-93: The calculated vertical section at constant 31.9 wt% Al with the DSC signals from cooling curve of sample 18

The DSC measurements in the  $Mg_2Ca$ - $Al_2Ca$ - $Al_{14}Ca_{13}$  phase field are summarized in Table 5-8. The samples in this field could not be melted due to the high temperature required which might have caused oxidation of the samples.

Table 5-8 The DSC measurements with thermodynamic analysis in the  $Mg_2Ca$ - $Al_2Ca$ - $Al_{14}Ca_{13}$  phase field

Sample	DSC Thermal Signals (°C)	Thermodynamic calculation based on the database reported in [14]	
		Temp. °C	Reactions or phase boundary
18	506c/512h	550	$L + Al_2Ca + Mg_2Ca / Al_2Ca + Mg_2Ca + Al_{14}Ca_{13}$
	-	631	$L + Al_2Ca / L + Al_2Ca + Mg_2Ca$
	-	810	$L / L + Al_2Ca$
19	506c/520h	550	$L + Al_2Ca + Mg_2Ca / Al_2Ca + Mg_2Ca + Al_{14}Ca_{13}$
	-	620	$L + Al_2Ca + Mg_2Ca / L + Al_2Ca$
	-	909	$L + Al_2Ca / L$
20	506c/514h	550	$L + Al_2Ca + Mg_2Ca / Al_2Ca + Mg_2Ca + Al_{14}Ca_{13}$
	-	627	$L + Al_2Ca + Mg_2Ca / L + Al_2Ca$
	-	785	$L + Al_2Ca / L$

## 5.6 Sample in the $\text{Mg}_2\text{Ca}-\text{Al}_{14}\text{Ca}_{13}-\text{Al}_3\text{Ca}_8$ phase field

Sample 21 was prepared in this phase field. The DSC spectra of this sample in Figure 5-94 show a peak at  $507^\circ\text{C}$ . This corresponds to either the invariant transformation at phase borderline  $\text{L} + \text{Al}_2\text{Ca} + \text{Mg}_2\text{Ca} / \text{L} + \text{Mg}_2\text{Ca} + \text{Al}_{14}\text{Ca}_{13}$  at  $550^\circ\text{C}$  or at the phase borderline  $\text{L} + \text{Mg}_2\text{Ca} + \text{Al}_{14}\text{Ca}_{13}/\text{Al}_3\text{Ca}_8 + \text{Mg}_2\text{Ca} + \text{Al}_{14}\text{Ca}_{13}$  at  $491^\circ\text{C}$  because both of the cases obey the infinite phase change rate principle by referring to the phase assemblage in Figure 5-95. However, when sample 18, 19 and 20 are taken into account, it might be better to correlate the peak temperature to the first reaction at  $550^\circ\text{C}$  in order to be consistent with the other samples in this region. The DSC results are summarized in Table 5-9 and labeled with solid triangle on the vertical section shown in Figure 5-96.

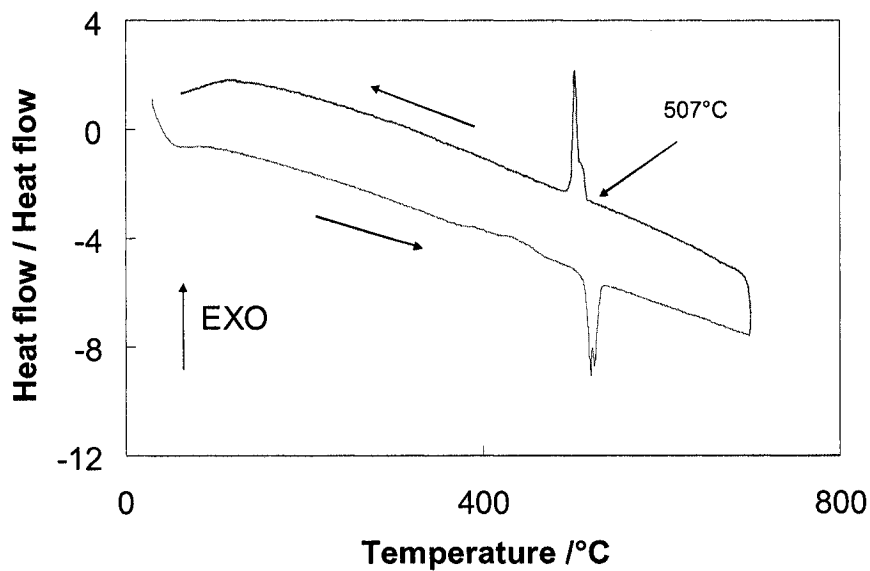


Figure 5-94: DSC spectra of sample 21 (59.39/15.78/24.83 Ca/Mg/Al wt%)

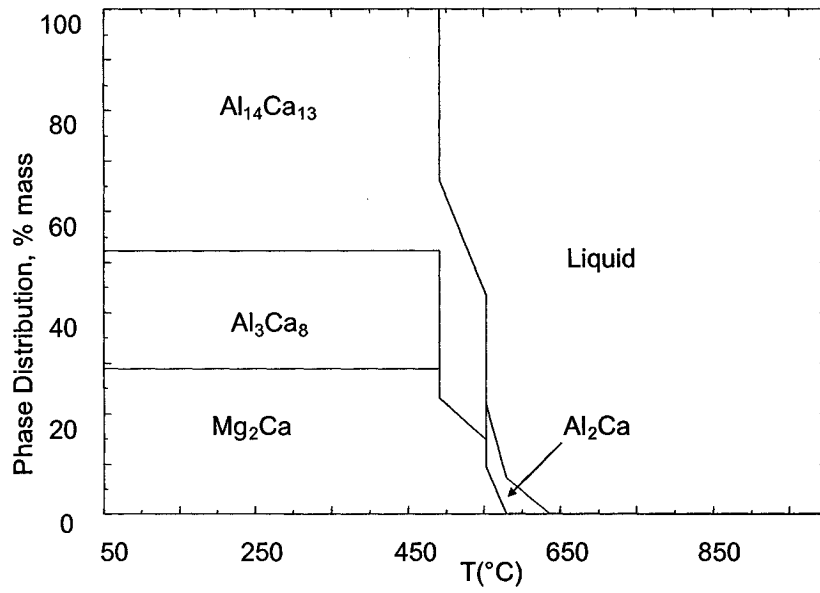


Figure 5-95: Phase assemblage of sample 21 (59.39/15.78/24.83 Ca/Mg/Al wt%)

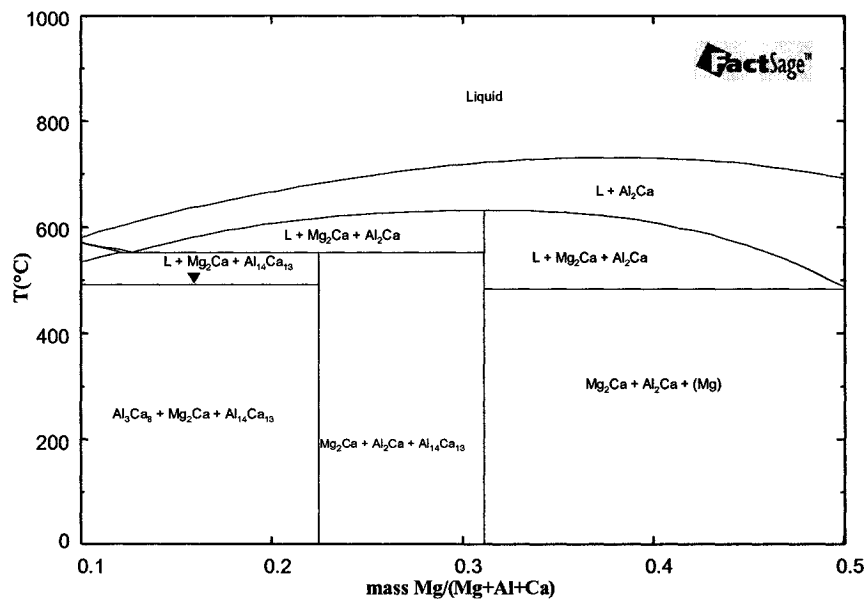


Figure 5-96: Calculated vertical section at constant 24.8 wt% Al with DSC signals from cooling curve of sample 21

*Table 5-9: DSC measurements with thermodynamic analysis of  
in Mg<sub>2</sub>Ca-Al<sub>14</sub>Ca<sub>13</sub>-Al<sub>3</sub>Ca<sub>8</sub> phase field phase field*

Sample	DSC Thermal Signals (°C)	Thermodynamic calculation based on the database reported in [14]	
		Temp.(°C)	Reactions or phase boundary
21	-	633	L/L + Al <sub>2</sub> Ca
	-	577	L + Al <sub>2</sub> Ca/ L + Al <sub>2</sub> Ca + Mg <sub>2</sub> Ca
	512h/507c	550	L + Al <sub>2</sub> Ca + Mg <sub>2</sub> Ca / L + Mg <sub>2</sub> Ca + Al <sub>14</sub> Ca <sub>13</sub>
	-	491	L + Mg <sub>2</sub> Ca + Al <sub>14</sub> Ca <sub>13</sub> /Al <sub>3</sub> Ca <sub>8</sub> + Mg <sub>2</sub> Ca + Al <sub>14</sub> Ca <sub>13</sub>

# CHAPTER 6

## *Summary, Contributions and Suggestions*

---

### **6.1 Summary**

A thorough understanding of the Mg-Al-Ca system has been built through extensive experimental work and overall analysis coupled with thermodynamic calculation.

The phase transformation temperatures detected by the DSC were compared with the pertinent vertical section calculated based on the current thermodynamic modeling. Many samples match perfectly with the thermodynamic findings, such as samples 1 to 5 and 15 to 17. A considerable discrepancy in the transformation temperature was detected in samples 6 to 13 and 18 to 21. However, the experimental results are not scattered, but rather consistent with each other. Also a few samples show a large discrepancy with the liquidus temperature compared with the calculated values, such as samples 15 and 17. This suggests that the Mg-Al-Ca system model should be reoptimized using the experimental results obtained in this work.

A ternary eutectic point in the Mg-rich corner was verified in this work. The typical eutectic features were observed with all the techniques used in this research such as DSC, XRD, microscopy and thermodynamic calculation. A lamellar structure was obtained in the micrograph. The eutectic temperature is determined at 512°C. The eutectic composition is close to 10.8 at.% Ca, 79.5 at.% Mg and 9.7 at.% Al (sample 10).

This result is in agreement with the report of Portnoi and Spektorova [75], the Dow Chemical Co. [76] and the results of Tkachenko *et al.*[17]. Another five samples: 6, 8, 11, 12 and 13 around sample 10 were used to further support this finding because they too undergo this eutectic transformation at later stages of their solidifications.

The phases predicted from current thermodynamic modeling [14] agree with the XRD and metallographic results in the phase field Mg-Mg<sub>2</sub>Ca-Al<sub>2</sub>Ca and Mg-Al<sub>2</sub>Ca- $\gamma$ . However, the phases predicted do not agree with the XRD results in the phase field  $\gamma$ -Al<sub>2</sub>Ca-Al due to the unstable nature of Al<sub>4</sub>Ca. This is also due to the fact that the samples are selected on the phase borderline, which has higher chance to go into nonequilibrium state.

The morphology of the Al<sub>2</sub>Ca,  $\gamma$ , (Mg) was recognized through analysis of many samples. The morphology of Mg<sub>2</sub>Ca was observed but still needs more samples to make further verification.

Sample 6, the composition of which closely resembles one of Gröbner's [5] samples, has been identified with the phases Al<sub>2</sub>Ca, Mg and Mg<sub>2</sub>Ca by XRD and metallography. It shows similar micrograph to that of Gröbner. This partially supports the methodology used in this work.

A new phase was found close to the Mg-Al side by the XRD. The morphology of the new phase was tentatively linked to dark dots embedded in the  $\gamma$  phase.

The Mg<sub>2</sub>Ca was found to exist as a solid solution with a certain amount of Al dissolution by XRD, named as (Mg<sub>2</sub>Ca). Also, Mg and Al form solid solutions and were named (Mg) and (Al).



## 6.2 Contribution to the knowledge

1. A systematic and consistent way of interpreting the DSC results is presented in this thesis. It was found that the cooling rather than the heating spectrum is reasonable and practical to be used in extracting the transformation temperature, unlike what was noted in the literature where they were using sometimes heating curve and in other instances they used the cooling curve. Further, on the cooling spectrum, the onset rather than the offset or the peak maximum point which were used randomly by other researchers should be chosen in determining the phase transformation temperature. Supercooling effect on the cooling spectrum can be settled by calibration of DSC instrument. Setting the onset of the peak of pure Mg as the known melting point at 650°C seems to eliminate the supercooling effect of pure Mg, and therefore minimizing the surpercooling effect of other Mg alloys in this work.

2. The presence and the absence of the DSC peaks for the transformation can be predicted with the aid of the vertical section. The relationship between the phase borderline slope and the shape of the DSC peak was clarified. However, it was found out that the relation between phase borderline in the phase assemblage diagram and the shape of the DSC peak is more practical in correlating DSC peaks to the phase transformation.

To simplify the description and the reason of correlating each of the DSC peaks to the exact phase transformation, two principles were followed. First: the sharpness of the DSC peaks for the transformation is related to the slope of the borderline in the phase assemblage diagram. Therefore, the sharpest peak of the DSC spectrum is always related

to the vertical borderline in the phase assemblage which corresponds to the invariant transformation. This finding is named as infinite phase change rate principle. Second: the intensity of the DSC peaks is dependent on the phase amount involved in the transformation. When there is large amount, more nucleation and energy accumulation take place which results in higher heat flux flowing between the DSC's crucibles causing stronger peak. This finding is named as the phase amount involvement principle.

3. The phase morphologies of  $\text{Al}_2\text{Ca}$ ,  $\gamma$ , and (Mg) were observed by metallography and reported in this study.

4. The eutectic point in the Mg-rich corner was verified in this work.

5. A new phase region was found and its composition limits were put forward.

### **6.3 Suggestion for future work**

1. Mg-Al-Ca system should be re-optimized taking the current experimental findings into consideration.

2. Further experiments should be conducted to verify all the invariant transformations in this system.

3. It is recommended to further study the solubility of Al in  $\text{Mg}_2\text{Ca}$  using the microprobe technique and to further investigate the microstructure of  $\text{Mg}_2\text{Ca}$ -containing samples by the SEM.

4. The crystal structure and composition of the new phase should be determined by combining the XRD and SEM/EDX techniques.

## REFERENCES

- [1] Humble, P., Towards a Cheap Creep Resistant Magnesium Alloy, *Materials Forum*, 21, pp.45-56, 1997.
- [2] Greenfield, P., *Magnesium*, Mills and Boo Limited, London, pp.7-19, 1972.
- [3] Mordike, B.L., Ebert, T., Magnesium Properties-Application-Potential, *Material Science and Engineering*, A 302(1), pp.37-45, 2001.
- [4] Luo, A.A., Magnesium: Current and Potential Automotive Applications. *JOM* 54(2), pp.42-48, 2002.
- [5] Gröbner J., Kevorkov D., Chumak I., Schmic-Fetzer R., Experimental investigation and thermodynamic calculation of ternary Al-Ca-Mg phase equilibria, *Zeitschrift fuer Metallkunde*, 94(9), pp.976-982, 2003.
- [6] Mordike, B.L., Creep-Resistant Magnesium alloys. *Material Science and Engineering*, A324(1), pp.103-112, 2002.
- [7] Ninomiya, R., Ojiro, T. and Kubota, K., Improved Heat-Resistance of Mg-Al Alloys By the Ca Addition. *Acta Metallurgica Materialia*, 43(2), pp.669-674, 1995.
- [8] Maruyama, K., Suzuki, M. and Sato, H., Creep Strength of Magnesium-Based Alloys. *Metallurgical Transactions*, 33(3), pp.875-882, 2002.
- [9] Pekguleryuz, M.O. and Baril, E. Creep Resistant Magnesium Diecasting Alloys Based on Alkaline Earth Elements, *Materials Transactions*, 42(7), pp.1258-1267, 2001.
- [10] Luo, A.A., Balogh., M.P Powell, B.R: Creep and Microstructure of Magnesium-Aluminum-Calcium Based Alloy, *Metallurgical and Materials Transactions*, 33, pp.567-574, 2002.
- [11] Blum. W, Zhang, P., Watzinger, B., Grossmann, B.V., Lipowski, H. and

- Haldenwanger, H.G., Creep Resistance of Die-cast Mg-Al-base Alloys, *Material Science Forum*, 350-351 (Magnesium Alloys), pp.141-150, 2000.
- [12] Blum, W., Zhang, P., Watzinger, B., Grossmann, B.V. and Haldenwanger, H.G., Comparative Study of Creep of the Die Cast Mg-alloys AZ91, AS21, AS41, AM60 and AE42, *Material Science and Engineering*, A319-321, pp.735-740, 2001.
- [13] Ozturk, K., Zhong, Y. and Liu, Z. K., Computational Thermodynamics and Experimental Investigation of Mg-Al-Ca alloys, *Magnesium Technology, Proceedings of the Symposium held during the TMS Annual Meeting, New Orleans, LA, United States*, pp.113-117, 2001
- [14] Islam, F., Thermodynamic Modeling of Mg-Al-Ca System, MASC thesis, Concordia University, Montreal, Quebec, Canada, 2004.
- [15] Kraus, W. and Nolze, G., PowderCell for Windows, Federal Institute for Materials Research and Testing Berlin, Version 2.3, 1999.
- [16] Gröbner, J., Schmid-Fetzer, R. and Kevorkov, D., The Al-Li-Si System: Experimental Study and Thermodynamic Calculation of the Polythermal, *Journal of Solid State Chemistry*, 156(2), pp.506-511, 2001.
- [17] Tkachenko, V.G., Khoruzhaya, V.G., Meleshevich, K.A., Karpets, M.V., and Frizel, V.V., Phase Equilibria in Mg-Al-Ca System, *Powder Metallurgy and Metal Ceramics*, 42(5-6), pp.268-273, 2003.
- [18] Schlesinger, M.E. and Jacob, S., Advances in High-Temperature Calorimetry: A Comparison, *Journal of the Minerals Metals and Materials Society (JOM)*, 57(12), pp.37-40, 2004.
- [19] Graham, D.A., and Yao, J.Y., A DSC and TEM Study of Precipitation in T1 and T4 Treated Al-Mg-Si Alloys, *Materials Science Forum*, 331-337(part 2), pp.1083-1088, 2000.
- [20] Inoue, A., Nishiyama, N., Hatakeyama, K. and Masumoto, T., New amorphous Al-Ca and Al-Ca-M (M = Mg or Zn) alloys. *Materials Transactions*, 35(4),

pp.282-287, 1994.

- [21] Mahendran, K.H., Nagaraj, S., Sridharan, R. and Gnanasekaran, T. , Differential Scanning Calorimetric Studies on the Phase Diagram of the Binary LiCl-CaCl<sub>2</sub> System, Journal of Alloys and Compounds, 325(1-2), pp.78-83, 2001.
- [22] Kubaschewski, O., Alcock, C.B. and Spencer, P.J., Materials Thermochemistry, 6<sup>th</sup> ed., Oxford: Pergamon Press, pp.70-83, 1993.
- [23] Cezairliyan, A., Pulse Calorimetry, Specific Heat of Solids, New York: Hemisphere Publishing, pp.323-353, 1988.
- [24] Richardson, M.J., Quantitative Aspects of Differential Scanning Calorimetry, Thermochemica Acta, 300(1-2), pp.15-28, 1997.
- [25] Nevriya, M. Sedmidubsky, D. and Leitner, J., Calibration of the Setaram High Temperature Calorimeter for Determination of High Capacity of Phases in the Sr-Cu-O System, Thermochemica Acta, 347(1-2), pp.123-128, 2000.
- [26] Su, H.N., Introduction to TG/DTA/DSC, [http://tptc.iit.edu/Center/research/Phase Diagram /Content/presentation//DSC.pdf](http://tptc.iit.edu/Center/research/Phase%20Diagram/Content/presentation//DSC.pdf)
- [27] Hohne, G.W.H., Hemminger, W.F. and Flammersheim, H.J., Differential Scanning Calorimetry, Springer-verlag Berlin Heidelberg New York, 2003.
- [28] Prince A., Aluminum – Calcium – Magnesium, in Ternary alloys: a comprehensive compendium of evaluated constitutional data and phase diagram, 3, pp.611-614, 1988.
- [29] Dow Chemical Co., Liquidus Determination of Polynary Magnesium Alloys, Reports, Michigan, USA, 31, pp.335, 1959.
- [30] Ozturk, K. Investigation in Mg-Al-Ca-Sr System by Computational Thermodynamics Approach Coupled with First-Principles Energetics and Experiments, PhD thesis, the Pennsylvania State University, Pennsylvania, USA, 2003.
- [31] Kurnakov, N.S. and Micheeva, V.I., Transformations in the Middle Portion of the System Al-Mg, Ann.Secteur anal. Phys-chim. Inst.Chim. Gen.(U.S.S.R), 13,

pp.209-224, 1940.

- [32] Makarkvo, E.S., Crystal Structure of the Gamma Phase of the System Al-Mg and Tl-Bi. Doklady Akademil Nauk SSSR, 74(5), pp.935-938, 1950.
- [33] Samson, S., The Crystal Structure of the Phase Beta  $Mg_2Al_3$ , Acta Crystallographica, 19(3), pp.401-413, 1965.
- [34] Bandyopadhyay, J. and Gupta, K.P., Phase Relationship and Structural Transformations in Al-Mg System in the Composition Range 39 to 56 at Per Cent Mg, Transaction of Indian Institute of the metals, 23(4), pp.65-70, 1970.
- [35] Brown, J.A. and Pratt, J.N., The Thermodynamic Properties of Solid Al-Mg Alloys. Metallurgical Transactions, 1(10), pp.2743-2750, 1970.
- [36] Schurmann, E and Fischer, A., Melting Equilibria in the Ternary System of Aluminum-Magnesium-Silicon: I. Binary System of Aluminum-Magnesium; II. Binary System of Magnesium-Silicon, Giessereiforschung, 29(3), pp.107-113, 1977.
- [37] Schurmann,E. and H.J.Voss, Melting Equiliria of the Binary System of Magnesium-Aluminum, Giessereiforschung, 33(2), pp.43-46, 1981.
- [38] Samson, S. and Gordon, E.K., The Crystal Structure of Epsilon- $Mg_{23}Al_{30}$  Acta Crystallographica, 24(8), pp.1004-1013, 1968
- [39] Schobinger-Papamantellos, P. and Fischer, P., Neutron Diffraction Study of  $Mg_{17}Al_{12}$ , Naturwissenschaften, 57(3), pp.128-129, 1970.
- [40] Laves, F. and Moeller, K., Contribution to the Understanding of the Aluminum-Magnesium System, Zeitschrift fuer Metallkunde, 30(7), pp.232-235, 1938.
- [41] Hansen, M.and Anderko, K., Constitution of Binary Alloys, 2<sup>nd</sup> ed. 1958, New York, USA, McGraw-Hill.
- [42] Eickhoff, K. and Vosskuhler, H., The Phase Diagram of Al-Mg, A Critical Evaluation, Zeitschrift fuer Metallkunde, 44, pp.223-231, 1953.
- [43] Murray, J.L., The Al-Mg (Aluminum-Magnesium) System, Bulletin Alloy Phase

- Diagrams, 3(1), pp.60-74, 1982.
- [44] Saunders, N.: A Review and Thermodynamics Assessment of the Al-Mg and Mg-Li Systems, *Calphad*, 14(1), pp.61-70, 1990.
- [45] Schuermann, E., Geissler, I.K., Phase equilibriums in the solid condition of the aluminum-rsp. The Magnesium-rich Corner of the Ternary System of Aluminum-Lithium-Magnesium. Part 3. Phase Equilibriums in the Solid Condition of the Binary System of Aluminum-Magnesium, *Giessereiforschung*, 32(4), pp.167-170, 1980.
- [46] Liang, P., Su, H.L., Donnadiou, P., Harmelin, M.G., Quivy, A., Ochin, P., Effenberg, G., Seifert, H.J., Lukas, H.L. and Aldinger, F., Experimental Investigation and Thermodynamic Calculation of the Central Part of the Mg-Al Phase Diagram, *Zeitschrift fuer Metallkunde*, 89(8), pp.536-540, 1998.
- [47] Baar, N., On the alloys of Molybdenum with Nickel, Manganese with Thallium, and Calcium with Magnesium, Thallium, Lead, Copper, and Silver, *Zeitschrift fuer Anorganische und Allgemeine Chemie*, 70, pp.362-366, 1911.
- [48] Paries, R., Contribution on the Ternary Alloys, *Publications Scientifiques et Techniques, Ministere de L'Air*, 45, pp.39-41, 1934
- [49] Vosskuhler. H, The Phase Diagram of Magnesium Rich Mg-Ca Alloys, *Zeitschrift fuer Metallkunde*, 29, pp.236-237. 1937
- [50] Klemm, W. and Dinkelacher, F., On the Behavior of Magnesium with Calcium, Stronium, and Barium, *Zeitschrift fuer Anorganische und Allgemeine Chemie*, 255, pp.2-12, 1947.
- [51] Haughton, J.L., Alloys of Magnesium, Part VI.-The Constitution of the magnesium-rich Alloys of Magnesium and Calcium, *Journal of the Institute of Metals*, 61, pp.241-246, 1937.
- [52] Nayeb-Hashemi, A.A. and Clark, J.B., The Ca-Mg (Calcium-Magnesium) System, *Bulletin of Alloy Phase Diagrams*, 8(1), pp.58-65, 1987.
- [53] Nowotny, H., Wormnes, E. and Mohrheim, A., Investigation on the Al-Ca, Mg-

- Ca, Mg-Zr Systems, Zeitschrift fuer Metallkunde, 32, pp.39-42, 1940.
- [54] Witte, H., The Crystal Structure of Mg<sub>2</sub>Ca, Naturwissenschaften, 25, pp.795, 1937.
- [55] Agarwal, R., Lee, J.J., Lukes, H.L, and Sommer, F., Calorimetric Measurements and Thermodynamic Optimization of the Ca-Mg System. Z. Metallkd., 86(2), pp.103-108, 1995.
- [56] Klemm, W. and Dinkelacher, F., The Behavior of Magnesium with Calcium, Strontium, and Barium, Zeitschrift fuer Anorganische und Allgemeine Chemie, 255, pp.2-12, 1947.
- [57] Kremann, R., Wostall, H. and Schopfer, H., The EMF Behavior of Binary Alloys, Forschungsarb Metallkunde, 5(1), pp.1-20, 1922.
- [58] Bulian, W. and Fahrenhorst, E.: The Solid Solubility of Calcium in Magnesium, Metallforschung, 1(3), pp.70, 1946.
- [59] Burke, E.C., Solid Solubility of Calcium in Magnesium, Transactions American Institute of Mining, Metallurgical, and Petroleum Engineers, Metallurgical Society, 203, pp285-286, 1955.
- [60] Donski, L., Alloys of Ca with Zn, Al, Tl, Pb, Sn and Cu, Zeitschrift fuer Anorganische und Allgemeine Chemie, 57, pp.201-205. 1908.
- [61] Bozza, G. and Sonnino, C., The Al-Ca System, Giorn. Chem. Ind. Appl., 10, pp.443-449, 1928.
- [62] Matsuyama, K., The Equilibrium diagram of the Aluminum-Calcium System. Science Reports of the Tohoku Imperial University, Series 1: Mathematics, Physics, Chemistry, 17(4), pp783-789, 1928.
- [63] Kevorkov, D. and Schmid-Fetzer, R., The Al-CA system, Part 1: Experimental Investigation of Phase Equilibria and Crystal Structures, Zeitschrift fuer Metallkunde, 92(8), pp946-952, 2001.
- [64] Huang, B.Q. and Corbett, J. D., Two New Binary Calcium-Aluminum Compounds: Ca<sub>13</sub>Al<sub>14</sub>, with a Novel Two-Dimensional Aluminum Network, and



- $\text{Ca}_8\text{Al}_{13}$ , an  $\text{Fe}_3\text{Al}$ -Type Analogue, *Inorganic Chemistry*, 37(22), pp. 5827-5834, 1998.
- [65] Ozturk K., Chen L-Q, Liu Z-K, Thermodynamic Assessment of the Al-Ca Binary System Using Random Solution and Associate Models, *Journal of Alloys and Compounds*, 340(1-2), pp.199-206, 2002.
- [66] Kevorkov, D., Schmid-Fetzer, R., Pisch A., Hodaj F., Colinet C., The Al-Ca system, Part 2: Calorimetric Measurements and Thermodynamic Assessment, *Zeitschrift fuer Metallkunde*, 92(8), pp.953-958, 2001.
- [67] Itkin V.P., Alcock C.B., Ekeren Van P.J., Oonk H.A.J, The Al-Ca (aluminum-calcium) system, *Bulletin of Alloy Phase Diagrams*, 9(8), pp.652-657, 1988.
- [68] *Metals Handbook*, ASM International, Ohio, 1985.
- [69] Landelli, A., Crystallographic studies of the systems  $\text{MAl}_2\text{-MGa}_2$  (M=Yb, Ca, Eu, Sr).” *Journal of the Less-Common Metals*, 135(2), pp.195-198., 1987.
- [70] Rivillo, T. and Wallace, W.E., Magnetism and Phase Relations of the  $\text{PrAl}_2\text{-CaAl}_2$ ,  $\text{GdAl}_2\text{-CaAl}_2$  Systems.” *Journal of Solid State Chemistry*, 33(2), pp.309-315, 1980.
- [71] Villiars, P. and Calvert, L.D., *Pearson’s Handbook of Crystallographic Data for Intermetallic Phases*, ASM International, Materials Park. Ohio, 1991.
- [72] F. Islam and M. Medraj, Thermodynamic Modeling of the Mg-Al-Ca System, *Journal of Canadian Metallurgical Quarterly*, 44(3), accepted, 2005.
- [73] FactSage 5.3, 2003, Thermfact(Center for Research in computational Thermochemistry), Montreal, Quebec, Canada.
- [74] Ozturk, K. Investigation in Mg-Al-Ca-Sr System by Computational Thermodynamics Approach Coupled with First-Principles Energetics and Experiments, PhD thesis, the Pennsylvania State University, Pennsylvania, USA, 2003.
- [75] Portnoi, K.I. and Spektorova, S.I., *Express Information*, B19, pp.5, 1948.

- [76] Dow Chemical Co. Midland, MI, Dow Chemical Co. Report 15004, U.S. Government Reports, 31, pp.355, 1959.
- [77] Suzuki, A., Saddock, N.D., Jones, J.W. and Pollock, T.M., Structure and Transition of Eutectic (Mg,Al)<sub>2</sub> Ca Laves Phase Die-Cast Mg-Al-Ca Base Alloy, Scripta Materialia, 51(10), pp.1005-1010, 2004.
- [78] Pekguleryuz, M.O., and Kaya, A.A., Magnesium Alloys and Their Applications, Advanced Engineering Materials, 5(12), pp.866-878, 2003.
- [79] Catterall. J.A and Pleasance.R.J, Constitution of Magnesium-Rich Magnesium-Aluminum-Calcium Alloys, Journal of the Institute of Metals, 86(4), pp.189-92, 1957.
- [80] Villars, P., Calvert, L.D., Pearson's Handbook of Crystallographic Data for Intermetallic Phases, ASM International, Materials Park, Ohio, 1991.

# APPENDIX A

## *XRD Patterns Simulation*

---

### A-1 XRD pattern calculation of $Al_2Ca$

Table A-1: The crystal structure data of  $Al_2Ca$  [69-71]

Structure	$Cu_2Mg$		
Spacegroup	Fd-3m		
Space number	227		
Lattice parameter(nm)	a	b	c
	0.8040	0.8040	0.8040
Angles	$\alpha$	$\beta$	$\gamma$
	90°	90°	90°
Atoms in unit cell	24		

Table A-2: Atoms positions in the unit cell of  $Al_2Ca$  [69-71]

Atom	Wyckoff position	x	y	z
Ca	8a	0	0	0
Al	16d	5/8	5/8	5/8

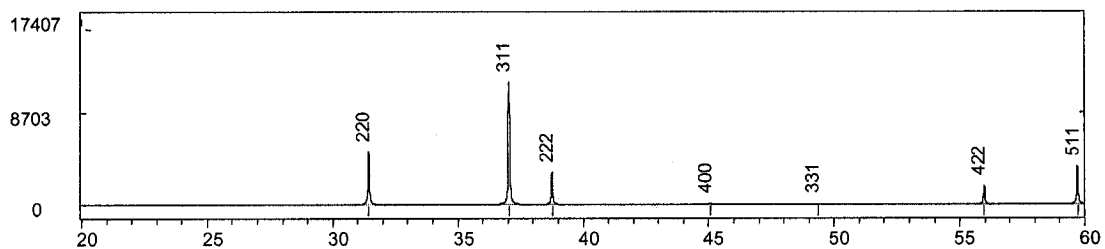


Figure A-1: Calculated XRD diffraction pattern for  $Al_2Ca$

## A-2 XRD pattern calculation of Mg<sub>2</sub>Ca

Table A-3: Crystal Structure Data of Mg<sub>2</sub>Ca [71]

Structure	MgZn <sub>2</sub>		
Space group	P6 <sub>3</sub> /mmc		
Space number	194		
Lattice parameter(nm)	a	b	c
	0.6225nm		1.018nm
Angles	$\alpha$	$\beta$	$\gamma$
	-	-	120°
Atoms in unit cell	12		

Table A-4: Atoms Positions in the Unit Cell of Mg<sub>2</sub>Ca [71]

Atom	Wyckoff position	x	y	z
Mg1	2a	0	0	0
Ca	4f	1/3	2/3	0.062
Mg2	6h	0.830	0.660	1/4

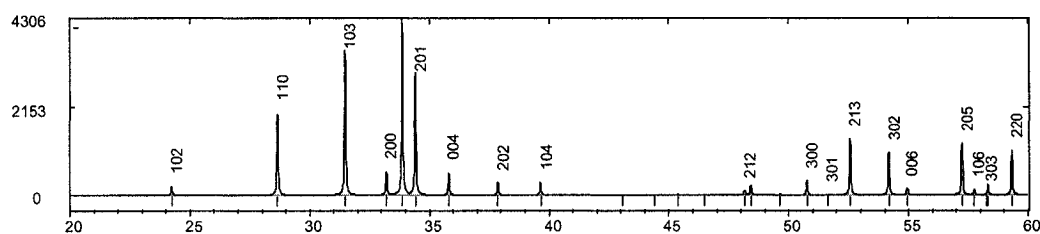


Figure A-2: Calculated XRD diffraction pattern for Mg<sub>2</sub>Ca

## A-3 XRD pattern calculation of $\gamma$

Table A-5: Crystal Structure data of  $\gamma$  [71].

Structure	Cubic		
Spacegroup	I43m		
Spacegroup number	217		
Lattice parameter (Å)	a	b	c
	10.55(3)	10.55(3)	10.55(3)
Angles	$\alpha$	$\beta$	$\gamma$
	90.00	90.00	120.00
Atoms in unit cell	58		

Table A-6: Atoms positions in the unit cell of  $\gamma$  [71]

Atom	Wyckoff position	x	y	z
Mg1	2a	0	0	0
Mg2	8c	0.3240	0.3240	0.3240
Mg3	24g	0.3582	0.3582	0.0393
Al	24g	0.0954	0.0954	0.2725

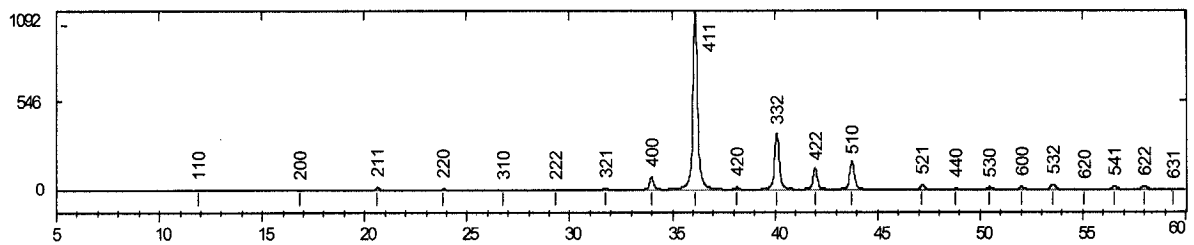


Figure A-3: Calculated XRD diffraction pattern for  $\gamma$ .

## A-4 XRD pattern calculation of $Al_4Ca$

Table A-7: The crystal structure data of  $Al_4Ca$  [53, 71]

Structure type	$Al_4Ca$		
Spacegroup	I4/mmm		
Space number	139		
Lattice parameter(nm)	a	b	c
	0.4353nm		1.070nm
Angles	$\alpha$	$\beta$	$\gamma$
	90°	90°	90°
Atoms in unit cell	18		

Table A-8: Atoms positions in the unit cell of  $Al_4Ca$  [53, 71]

Atom	Wyckoff position	x	y	z
Ca	2a	0	0	0
Al	4e	0	0	0.38000

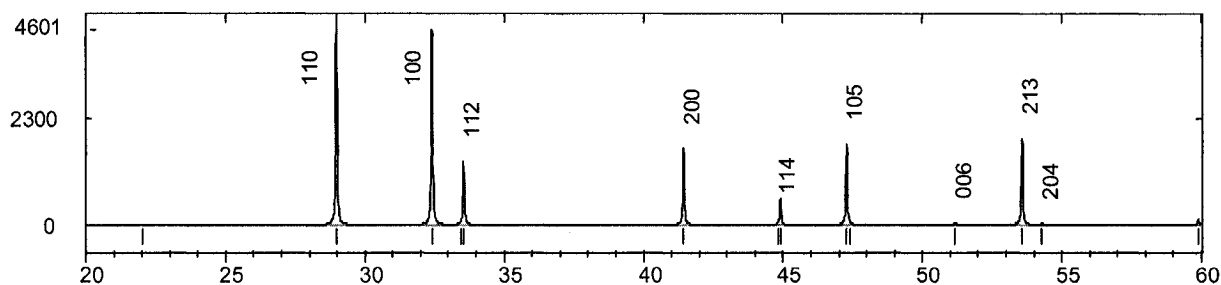


Figure A-4: Calculated XRD diffraction pattern for  $Al_4Ca$ .

## A-5 XRD pattern calculation of $\text{Al}_3\text{Ca}_8$

Table A-9: The crystal structure data of  $\text{Al}_3\text{Ca}_8$  [63]

Structure	triclinic		
Structure type	$\text{Ca}_8\text{In}_3$		
Spacegroup	P-1		
Space number	2		
Lattice parameter(nm)	a	b	c
	0.94950(8)nm	0.95922(8)	0.96704(7)
Angles	$\alpha$	$\beta$	$\gamma$
	99.057(6)	101.152(7)	119.613(8) $^\circ$
Atoms in unit cell	22		

Table A-10: Atoms positions in the unit cell of  $\text{Al}_3\text{Ca}_8$  [63]

Atom	Wyckoff position	x	y	z
Al1	1a	0	0	0
Al2	1h	1/2	1/2	1/2
Al3	2i	0.679(5)	0.348(5)	0.037(4)
Al4	2i	0.828(5)	.163(5)	.490(4)
Ca1	2i	.027(3)	.434(4)	.315(3)
Ca2	2i	.058(3)	.701(4)	.108(4)
Ca3	2i	.120(3)	.108(4)	.341(3)
Ca4	2i	.262(3)	.342(3)	.695(3)
Ca5	2i	.688(4)	-0.003(4)	.121(3)
Ca6	2i	.342(3)	.369(5)	.116(3)
Ca7	2i	.532(3)	.211(4)	.654(3)
Ca8	2i	.557(3)	.211(3)	.344(3)

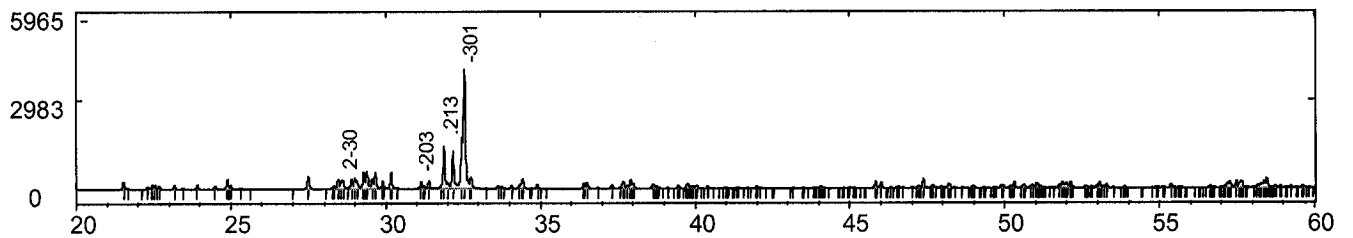


Figure A-5: Calculated XRD diffraction pattern for  $\text{Al}_3\text{Ca}_8$ .

## A-6 XRD pattern calculation of $Al_{14}Ca_{13}$

Table A-11: The crystal structure data of  $Al_{14}Ca_{13}$  [64, 71]

Structure type	Monoclinic symmetry		
Spacegroup	C2/m		
Space number	12		
Lattice parameter(nm)	a	b	c
	15.551(4) nm	9.873920	9.726 (2)nm
Angles	$\alpha$	$\beta$	$\gamma$
	90°	108.09°	90°
Atoms in unit cell	54		

Table A-12: Atoms positions in the unit cell of  $Al_{14}Ca_{13}$  [64, 71]

Atom	x	y	z
Ca1	0.14628(7)	0.2027(1)	0.3659(1)
Ca2	0.36159(7)	0.2819(1)	0.2275(1)
Ca3	0.1969(1)	0	0.0851(2)
Ca4	0.5036(1)	0	0.2024(2)
Ca5	0	0	0.5
Al1	0.1581(1)	0.3653(2)	0.0827(2)
Al2	0.0013(2)	0	0.1578(3)
Al3	0.2586(2)	0	0.6548(3)
Al4	0.3398(2)	0	0.4311(3)
Al5	0	0.3542(2)	0.5
Al6	0	0.2249(2)	0

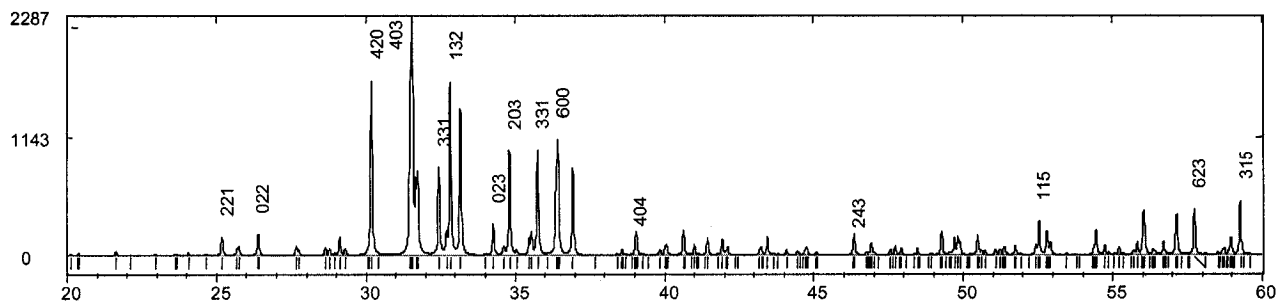


Figure A-6: Calculated XRD diffraction pattern for  $Al_{14}Ca_{13}$



## A-7 XRD pattern calculation of $\beta$

Table A-13: The crystal structure data of  $\beta$  [49, 71]

Structure			
Structure type	Cu		
Spacegroup	Fm-3m		
Space number	225		
Lattice parameter(nm)	a	b	c
	0.42155nm	-	-
Angles	$\alpha$	$\beta$	$\gamma$
	90°	90°	90°
Atoms in unit cell	4		

Table A-14: Atoms positions in the unit cell of  $\beta$  [49, 71]

Atom	Wyckoff position	x	y	z
M	4a	0	0	0

M = Al, Mg

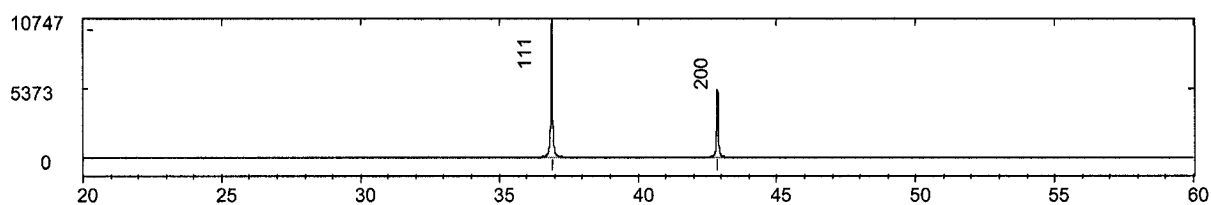


Figure A-7: Calculated XRD diffraction pattern for  $\beta$

## A-8 XRD pattern calculation of Al

Table A-15: The crystal structure data of Al [50, 71]

Structure type	Cu		
Spacegroup	Fm-3m		
Space number	225		
Lattice parameter(nm)	a	b	c
	0.404950nm	0.404950nm	0.404950nm
Angles	$\alpha$	$\beta$	$\gamma$
	90°	90°	90°
Atoms in unit cell	4		

Table A-16: Atoms positions in the unit cell of Al [50, 71]

Atom	Wyckoff position	x	y	z
Al	4a	0	0	0

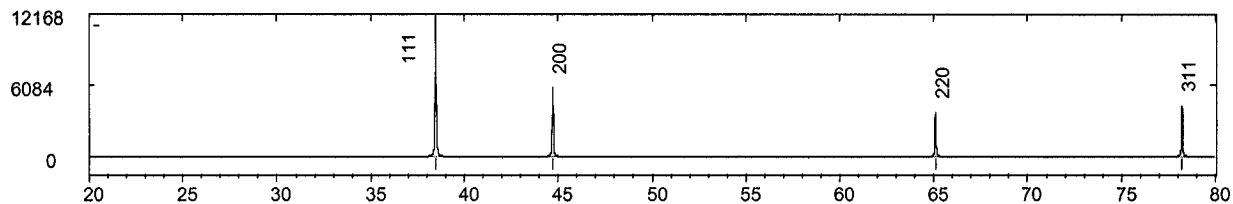


Figure A-8: Calculated XRD diffraction pattern for Al

## A-9 XRD pattern calculation of Mg

Table A-17: The crystal structure data of pure Magnesium [71]

Structure			
Structure type	Mg		
Spacegroup	P63/mmc		
Space number	194		
Lattice parameter(nm)	a	b	c
	0.3210nm	-	0.5212nm
Angles	$\alpha$	$\beta$	$\gamma$
	-	-	120°
Atoms in unit cell	2		

Table A-18: Atoms positions in the unit cell of pure Mg [71]

Atom	Wyckoff position	x	y	z
Mg	2c	1/3	2/3	1/4

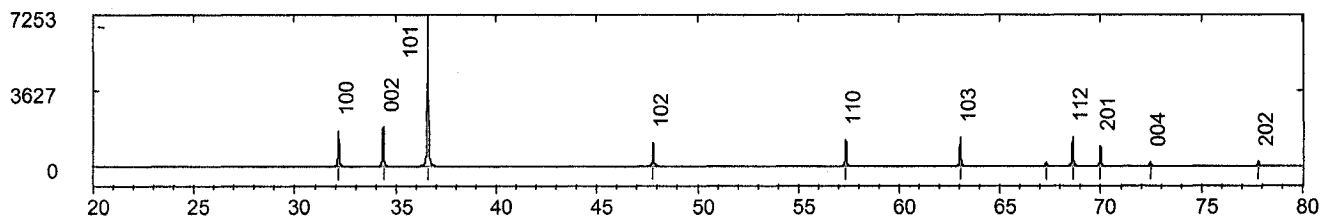


Figure A-9: Calculated XRD diffraction pattern for Mg

Table A-19: Solid phases lattice parameter comparison

Phase	Pearson symbol prototype	Lattice parameter (nm)	Phase composition	Reference
Al <sub>2</sub> Ca <1086°C	cF24 MgCu <sub>2</sub>	a = 0.8038	At 0 at.% Mg	[80]
		a = 0.807	At 5 at.% Mg (Al, Mg) <sub>2</sub> Ca	[5]
Al <sub>3</sub> Ca <sub>8</sub> , <579°C	aP22 Ca <sub>8</sub> In <sub>3</sub>	A = 0.9495, α = 99.057 B = 0.95922, β = 101.152 C = 0.96704, γ = 119.613	At 0 at.% Mg	[63]
		A = 0.926, α = 99.48 B = 0.9466, β = 99.42 C = 0.978, γ = 119.89	At 10 at.% Mg Al <sub>3</sub> (Ca, Mg) <sub>8</sub>	[5]
CaMg <sub>2</sub> <715°C	hP12 MgZn <sub>2</sub>	A = 0.623 C = 1.015	At 0 at.% Al	[80]
		A = 0.607 C = 0.973	At 22 at.% Al	[5]

## APPENDIX B

### *Metallographic technique*

---

1. Grinding: Mechanically grind through series SiC abrasive paper (240, 320, 400, 600 grit) using light pressure. Grind only long enough to remove previous scratches. Rinse the sample well in water and dry with methanol and a blast of hot air. In the progressing from one grit size to the next, the specimen should be turned 90°. It should be cleaned with a cloth saturated with a water soluble solvent, such as industrial ethanol, to prevent coarse abrasive particles from being carried to disks with fine particles. Greater pressure is applied to the trailing side of the specimen than the leading side, to keep the surface parallel and flat.

2. Mechanical polishing is done in two stages:

a. Rough Polishing: Removes the major part of the disturbed metal remaining after the final grinding step, using 1200 grit abrasive paper with alcohol for approximately 6 minutes. Mounts should be cleaned well with diluted soapy water and cotton, rinse in water and dry with methanol and a blast of hot air.

b. Refining Polishing: Removes the superficial scratches that remain after rough polishing using 0.3 microns alumina powder on cloth Anamet 621. Polish in 5 min by rotating mount clockwise under medium pressure (polishing time should be twice as long as is needed to remove the scratches from the final grinding operation). The suspension should be made with distilled water using the ratio of 10 grams of alumina per 500 ml of water. The cloth should be kept just moist enough to prevent seizure of the

specimen. The specimen should be reciprocated across the face of the wheel and rotated counter to the wheel rotation to change the contact point between that specimen and the wheel and distribute the abrasive. During the last 5 seconds scratches can be reduced to a minimum by flooding the wheel with the abrasive suspension and using light pressure on the specimen. Finally, mounts should be rinsed in water and cleaned with a cotton swab then dried with methanol and a blast of hot air.

3. Chemical polishing: etching using Nital solution (1 ml volume of  $\text{HNO}_3$  in 100 ml ethanol). The specimen is swabbed for 4 to 10 seconds. Light scratches and cold worked surface metal on the polished specimen can be removed by alternate light etching and light repolishing. If soap was used in the polishing slurry, it must be thoroughly rinsed away, because it can cause considerable staining.

4. Steps 2 and 3 were repeated until all scratches and deformation have been removed.

5. For faster drying, a hand-held dryer should be used. It is worth mentioning that Ca rich alloys reacted fast with oxygen and immediately showed corroded surfaces when dried.